

THE INTERFERON STIMULATED GENE PRODUCT LYMPHOCYTE
ANTIGEN 6 COMPLEX, LOCUS E PROMOTES ENTRY
OF A SUBSET OF DIVERSE RNA VIRUSES
AND INHIBITS INFECTION BY
CORONAVIRUSES

APPROVED BY SUPERVISORY COMMITTEE

Lora Hooper, Chair

Neal Alto

Sandra Schmid

John Schoggins

DEDICATION

I dedicate my dissertation to my late father, Alexander Shuisun Mar, for teaching me the importance of integrity and hard work. During his life, he prioritized my education and cultivated my interest in the biological sciences. I know that it was his dream for me to become a Doctor of Medicine. Hopefully becoming a Doctor of Philosophy will suffice.

I would like to thank my mother for her unrelenting support and encouragement all the way from Olympia, Washington. I would also like to thank my brother and sister for their support. Their love made it possible for me to succeed so far away from home.

I would like to thank my significant other for his love, and for his commitment to keeping graduate school fun while still pushing me to be my best.

I would like to thank John for his patience, guidance, and encouragement, and for the inspiration to develop as an independent scientist and well-networked professional.

I would like to thank my dissertation committee for their guidance, support, and encouragement, and for accepting snacks as bribery throughout the years.

I would like to thank all my scientific mentors, whether PI, post-doc, graduate student, or technician, who imparted much of the knowledge needed to survive this profession.

I would like to thank the many friends that I have met in and before graduate school for helping me maintain a balanced and healthy social life, which undoubtedly also made me a better, harder-working student... maybe.

Finally, I would like to thank my cats for putting up with me interrupting their nap time and taking hundreds of pictures of them cuddling while I have stayed home to write.

THE INTERFERON STIMULATED GENE PRODUCT LYMPHOCYTE
ANTIGEN 6 COMPLEX, LOCUS E PROMOTES ENTRY
OF A SUBSET OF DIVERSE RNA VIRUSES
AND INHIBITS INFECTION BY
CORONAVIRUSES

by

KATRINA BOCKYING MAR

DISSERTATION

Presented to the Faculty of the Graduate School of Biomedical Sciences

The University of Texas Southwestern Medical Center at Dallas

In Partial Fulfillment of the Requirements

For the Degree of

DOCTOR OF PHILOSOPHY

The University of Texas Southwestern Medical Center at Dallas

Dallas, Texas

Degree Conferral May, 2019

Copyright

by

Katrina Bocking Mar, 2019

All Rights Reserved

THE INTERFERON STIMULATED GENE PRODUCT LYMPHOCYTE
ANTIGEN 6 COMPLEX, LOCUS E PROMOTES ENTRY
OF A SUBSET OF DIVERSE RNA VIRUSES
AND INHIBITS INFECTION BY
CORONAVIRUSES

Katrina Bockying Mar, Ph. D.

The University of Texas Southwestern Medical Center at Dallas, 2019

Supervising Professor: John W. Schoggins, Ph. D.

PREFACE

Interferons (IFNs) contribute to cell-intrinsic antiviral immunity by inducing hundreds of IFN-stimulated genes (ISG). In a screen to identify novel antiviral factors, the Schoggins lab unexpectedly uncovered a subset of genes that enhanced viral infection. Here, I describe my personal efforts to study lymphocyte antigen 6, locus E (LY6E), a protein which was identified in the screen to enhance the infection of viruses from *Flaviviridae*,

Orthomyxoviridae, *Retroviridae*, and *Alphaviridae* viral families. In my studies, I confirmed that LY6E promotes viral infection of viruses from the same families, as demonstrated by both ectopic overexpression and endogenous knockout approaches. Using influenza A virus (IAV) as a model, I narrowed the enhancing effect of LY6E specifically to the entry step of uncoating, which precedes release of the viral genome into the cytoplasm and is required for viral replication. I also observed that the viral enhancement phenotype is conserved across evolution, as orthologs from bat, rhesus macaque, and mouse exerted a similar effect. To understand the physiological relevance of viral enhancement at the cellular level, I generated Ly6e conditional knockout mice and crossed them to multiple Cre recombinase transgenic mouse strains. As a result, I obtained mice with specific ablation of Ly6e in distinct immune cell compartments. From both *ex vivo* and *in vivo* studies using the Ly6e knockout mice, I concluded that Ly6e in alveolar macrophages is important for optimal defense against IAV infection. Finally, in collaboration with the postdoctoral fellow Stephanie Pfaender, I have shown that LY6E also possesses potent antiviral activity against a distinct subset of enveloped RNA viruses. Cumulatively, my work has uncovered three unique ways by which the ISG LY6E may contribute to the antiviral immune response. This work also provides insight regarding the multi-faceted ways a single ISG can provide broad protection against infection by viruses from diverse viral families.

TABLE OF CONTENTS

PREFACE.....	v
TABLE OF CONTENTS	vii
PRIOR PUBLICATIONS	xiii
LIST OF FIGURES	xiv
LIST OF APPENDICES	xv
LIST OF DEFINITIONS	xvi
CHAPTER ONE: Review of the literature	1
THE ANTIVIRAL INTERFERON RESPONSE.....	1
Pattern recognition initiates the immune response to pathogenic infection	1
Recognition of viral infection by pathogen recognition receptors results in interferon production	1
The interferon response reinforces antiviral defenses	4
Inborn errors in the interferon pathway reveal an essential role for antiviral immunity in humans	5
Evolution highlights the importance of redundancy in effector-driven antiviral defenses	7
High-throughput screening for function-based discovery of antiviral effectors	9
Genome-wide RNA interference screens have uncovered important host factors and pathways.....	9
CRISPR as an improved technique for genome-wide loss-of-function studies..	14
Unbiased gain-of-function screening by CRISPR identifies an influenza A virus	

restriction factor	16
Targeted screening for antiviral factors by ectopic overexpression	17
LY6E IS A SMALL, MULTI-TASKING PROTEIN	20
LY6E belongs to the Ly6/uPAR superfamily.....	20
Genomic organization of Ly6/uPAR gene family in mice and men	21
Examples of Ly6/uPAR family members and their diverse functions	23
The identification of Ly6e/Sca-2/Tsa-1/9804	27
Identification and characterization of murine Ly6e and human LY6E.....	28
LY6E has a complicated naming history	30
LY6E is associated with diverse cellular processes.....	31
Murine Ly6e/Tsa-1 modulates TCR signaling to regulate thymocyte development	32
LY6E modulates signaling on B cells, osteoclasts, and monocytes.....	35
LY6E is required for embryonic development in mice	37
LY6E may be involved in the antiviral immune response	39
LY6E promotes viral infection	40
CHAPTER TWO: LY6E mediates an evolutionarily conserved enhancement of virus infection by targeting a late entry step.....	42
ABSTRACT	42
INTRODUCTION	42
RESULTS	44
LY6E enhances a subset of enveloped RNA viruses.....	44

LY6E enhances infectivity of monocytic and fibroblast cells	47
A related LY6/uPAR family member enhances YFV infection	49
Loss of endogenous LY6E reduces viral susceptibility	51
LY6E does not regulate interferon-mediated gene expression	55
LY6E enhances yellow fever virus entry	58
LY6E enhances influenza A virus uncoating.....	61
Viral enhancement by LY6E is conserved across evolution	67
Leucine 36 is essential for viral enhancement by LY6E	71
DISCUSSION	76
METHODOLOGY	79
Cell lines	79
Viruses	80
In vitro transcription of viral and replicon RNA	81
Pseudoparticle generation	81
Transductions, infections, and plaque assays	81
LY6E antibody staining	84
Western blotting.....	84
siRNA-mediated gene silencing	85
RNA isolation and RT-qPCR.....	86
IFN α IC ₅₀ assay.....	86
YFV cold-bind assay.....	87
YFV replicon assay.....	88

YFV electroporation assay.....	88
YFV bafilomycin A1 entry time course.....	89
IAV cold-bind assay	89
IAV minigenome assay.....	89
IAV internalization assay.....	90
IAV endosomal escape assay.....	91
IAV acid bypass assay	91
IAV uncoating assay.....	92
IAV NP/nucleus co-localization by ImageStream.....	92
Transferrin uptake assay	93
Cholera toxin uptake assay	93
Dextran uptake assay	94
Molecular phylogenetics analysis.....	94
LY6E ortholog molecular phylogenetic analysis.....	95
Determining amino acid sequence identity and similarity.....	95
Alignment of LY6E orthologs to determine conserved residues for alanine mutagenesis.....	96
Structural prediction using SWISS-MODEL.....	96
Immunofluorescence.....	96
Statistical analyses	96
Cloning.....	97
CHAPTER THREE: Ly6e in alveolar macrophages contributes to the antiviral response..	98

ABSTRACT.....	98
INTRODUCTION	98
RESULTS	101
Generation of Ly6e conditional knockout mice.....	101
Loss of Ly6e in AMs renders mice more susceptible to sub-lethal IAV infection.	103
DISCUSSION	106
METHODOLOGY	107
Mice	107
Propagation and titering of viral stocks	108
IAV infections in vivo	109
Alveolar macrophage harvest and ex vivo infection.....	109
RT-qPCR to analyze Ly6e and IAV gene expression	110
CHAPTER FOUR: LY6E inhibits infection by the <i>Coronaviridae</i> family.....	111
ABSTRACT.....	111
INTRODUCTION	111
RESULTS	113
LY6E inhibits infection by a human coronavirus	113
Loss of endogenous LY6E increases susceptibility to HCoV-OC43	114
LY6E-mediated inhibition of coronavirus is evolutionarily conserved.....	116
Loss of LY6E in murine macrophages increases coronavirus susceptibility	116
DISCUSSION	118
METHODOLOGY	120

Cells	120
Virus.....	121
Transductions and infections	121
Mice	121
Production and infection of BMDM	122
Isolation and infection of AM.....	122
CHAPTER FIVE: Conclusions and Recommendations	124
CONCLUSIONS	124
The ISG LY6E mediates evolutionarily conserved enhancement of viral entry	124
Ly6e expression in AM is important for surviving sub-lethal IAV infection.....	125
LY6E restricts infection by <i>Coronaviridae</i> family viruses.....	128
RECOMMENDATIONS	129
Unraveling the molecular mechanism for viral enhancement and inhibition	129
Untangling the importance of LY6E to the antiviral IFN response.....	131
APPENDIX A	132
BIBLIOGRAPHY	137

PRIOR PUBLICATIONS

- Liu, Z. L., **Mar, K. B.**, Hanners, N. W., Perelman, S. S., Kanchwala, M., Chao, X., Schoggins, J. W., Alto, N. M. (2019) “A NIK-SIX gene regulatory circuit suppresses inflammation and apoptosis in response to non-canonical NF- κ B activation.” Nature
- Richardson, R. B., Ohlsen, M. B., Eitson, J. L., Kumar, A., McDougal, M. B., Boys, I. N., **Mar, K. B.**, De La Cruz-Rivera, P. C., Douglas, C., Konopka, G., Xing, C., Schoggins, J. W. (2018) “A CRISPR screen identifies IFI6 as an ER-resident interferon effector that blocks flavivirus replication.” Nature Microbiology
- Mar, K. B.**, Rinkenberger, N. R., Boys, I. N., Eitson, J. L., McDougal, M. B., Richardson, R. B., and Schoggins, J. W. (2018) “LY6E mediates an evolutionarily conserved enhancement of virus infection by targeting a late entry step.” Nature Communications
- Mar, K. B.** & Schoggins, J. W. (2016) “NLRX1 helps HIV avoid a STING operation.” Cell Host Microbe Preview
- Schoggins, J. W., MacDuff, D. A., Imanaka, N., Gainey, M. D., Shrestha, B., Eitson, J. L., **Mar, K. B.**, Richardson, R. B., Ratushny, A. V., Litvak, V., Daebelic, R., Manicassamy, B., Aitchison, J. D., Aderem, A., Alliot, R. M., García-Sastre, A., Racaniello, V., Snijder, E. J., Yokoyama, W. M., Diamond, M. S., Virgin, H. W., Rice, C. M. (2014) “Pan-viral specificity of IFN-induced genes reveals new roles for cGAS in innate immunity.” Nature
- Jhingran, A., **Mar, K. B.**, Kumasaka, D. K., Knoblaugh, S. E., Ngo, L. Y., Segal, B. H., Iwakura, Y., Lowell, C. A., Hamerman, J. A., Lin, X., Hohl, T. M. (2012) “Tracing conidial fate and measuring host cell antifungal activity using a reporter of microbial viability in the lung.” Cell Reports

LIST OF FIGURES

FIGURE 1. LY6E enhances infection by a subset of enveloped RNA viruses	46
FIGURE 2. LY6E-mediated enhancement is dependent on cell type	48
FIGURE 3. A related LY6/uPAR protein enhances yellow fever virus infection	50
FIGURE 4. Loss of LY6E reduces but does not abrogate viral infection	52
FIGURE 5. Genotype of LY6E KO cell line and LY6E knockdown studies.....	54
FIGURE 6. LY6E does not affect the global transcriptome or IFN signaling	57
FIGURE 7. LY6E enhances entry of yellow fever virus	60
FIGURE 8. LY6E enhances entry of influenza A virus at the step of uncoating.....	66
FIGURE 9. Phylogenetic analysis of LY6E orthologs	69
FIGURE 10. LY6E-mediated viral enhancement is conserved across mammals species	70
FIGURE 11. A conserved amino acid is essential for viral enhancement by human LY6E	73
FIGURE 12. Site-directed mutagenesis of LY6E.....	75
FIGURE 13. Generation and validation of Ly6e KO mice	103
FIGURE 14. Loss of <i>Ly6e</i> in AMs increases susceptibility to IAV infection <i>in vivo</i>	105
FIGURE 15. LY6E is antiviral against HCoV-229E (data from Stephanie Pfaender).....	113
FIGURE 16. Ectopic overexpression of LY6E inhibits HCoV-OC43	114
FIGURE 17. Knockout of endogenous LY6E increase HCoV-OC43 infectivity	115
FIGURE 18. Murine <i>Ly6e</i> is antiviral against <i>Coronaviridae</i> viruses.....	117

LIST OF APPENDICES

APPENDIX A: Primers used for cloning plasmids used in Chapter 2	132
---	-----

LIST OF DEFINITIONS

AC – accessory cells

ADAR1 – adenosine deaminases acting on ribonucleic acids 1

APOBEC3G - Apolipoprotein B messenger ribonucleic acid-editing enzyme catalytic polypeptide-like 3G

AMP – adenosine monophosphate

APCs – antigen-presenting cells

APL – acute promyelocytic leukemia

ASC – apoptosis-associated speck like protein containing caspase activation and recruitment domain

ATRA – all-trans-retinoic acid

BCG - bacillus Calmette-Guerin

BMDC – bone marrow derived dendritic cells

BMDM – bone marrow derived macrophages

BST2 – bone marrow stromal antigen 2

C9 – complement component 9

CARD – caspase activation and recruitment domain

cGAS – cyclic-guanosine monophosphate-adenosine monophosphate synthase

CHIKV – Chikungunya virus

CoV – coronaviruses

Cre – Cre recombinase

CRISPR – clustered regularly interspaced short palindrome repeats

CRISPR SAM - clustered regularly interspaced short palindrome repeats synergistic activation mediator

CTCF – CCCTC-binding factor

DAI – deoxyribonucleic acid-dependent activator of interferon regulatory factor

DAMP – damage-associated molecular pattern

DC – dendritic cell

DENV – dengue virus

DNA – deoxyribonucleic acid

dNTP – deoxynucleotide triphosphates

DSB – double strand break

dsRNA – double-stranded ribonucleic acids

ds-vRNA – double-stranded viral ribonucleic acids

EB3 - end-binding 3

EMSA – electrophoretic mobility shift assays

ER – endoplasmic reticulum

ERAD – endoplasmic reticulum-associated degradation

ES – embryonic stem

EST – expressed sequence tags

EUCOMM - European Conditional Mouse Mutagenesis

FISH – fluorescence in situ hybridization

FLPe - FLP1 recombinase

FRT – FLP recombination site

GalNAc - N-acetylgalactosamine

GAS – interferon gamma activated sites

Gas6 – growth arrest-specific 6

GFP – green fluorescent protein

GML - glycosylphosphatidylinositol anchored molecule like

GMP – guanosine monophosphate

GPI - glycosylphosphatidylinositol

GPIHBP1 - glycosylphosphatidylinositol anchored high density lipoprotein-binding protein 1

HCoV - human coronavirus

HCV – hepatitis C virus

HEK – human embryonic kidney

HIV-1 – human immunodeficiency virus-1

HPSE - heparanase

HSF1 – heat shock factor 1

HSV-1 – herpes simplex virus-1

IAV – influenza A virus

IDO1 – indoleamine 2,3-dioxygenase

IFI – interferon inducible protein

IFITM – interferon induced transmembrane

IFN – interferon

IFNAR – interferon alpha and beta receptor

IFNLR – interferon lambda receptor

IKKs – inhibitor of nuclear factor kappa-light-chain-enhancer of activated B cells kinases

IL10RB – interleukin 1- receptor subunit beta

IRF – interferon regulatory factor

ISG – interferon-stimulated gene

ISGF3 – interferon-stimulated gene factor 3

ISRE – interferon-stimulated response element

JAK1 – Janus kinase 1

LAT – linker for activation of T cells

LGP2 - laboratory of genetics and physiology 2

lncRNA – long non-coding ribonucleic acid

LPL – lipoprotein lipase

LPS - lipopolysaccharides

LU or Ly6/uPAR - lymphocyte antigen 6/urokinase-type plasminogen activator receptor

Ly6 – lymphocyte antigen 6

LY6E – lymphocyte antigen 6 complex, locus E

LYNX – Ly6/neurotixin

LYPD – Ly6/plasminogen activator, urokinase receptor domain containing

mAb – monoclonal antibody

Mapk14 - Mitogen-activated protein kinase kinase kinase 14

MAV-1 – mouse adenovirus type 1

MAVS – mitochondrial antiviral-signaling protein

MCOLN2 – mucolipin 2

MDA5 – melanoma differentiation association gene 5

MDV – Marek’s disease virus

MERS-CoV - Middle East Respiratory Syndrome Coronavirus

Mga – MAX gene-associated protein

MHC I - major histocompatibility complex class I

MHV – mouse hepatitis virus

miR – micro ribonucleic acid

MOI – multiplicity of infection

MMR – measles, mumps, and rubella

MyD88 - myeloid differentiation primary response 88

nAChR – nicotinic acetylcholine receptor

NF- κ B – nuclear factor kappa-light-chain enhancer of activated B cells

NLR – nucleotide-binding oligomerization domain-like receptor

NOD – nucleotide-binding oligomerization domain

OIP-1 – osteoclast inhibitory peptide 1

ONNV – O’nyong nyong virus

OVA – ovalbumin

ORF – open reading frame

OST - oligosaccharyltransferase

PAMP – pathogen-associated molecular pattern

PBL – peripheral blood lymphocytes

PKR – protein kinase R

PLAUR – plasminogen activator, urokinase receptor

PLC – phospholipase C

PMA - phorbol 12-myristate 13-acetate

Pparg – peroxisome proliferator-actiated receptor gamma

PRR – pattern recognition receptor

PSCA – prostate stem cell antigen

RARE – retinoic acid response element

RIG-E – retinoic acid-inducible gene-E

RIG-I – retinoic acid-inducible gene-I

RLR- retinoic acid-inducible gene-I-like receptor

RNAi – ribonucleic acid interference

RT – reverse transcriptase

RTP4 – receptor transporting protein 4

RyDEN - repressor of yield of dengue

SAMHD1 – sterile alpha motif and HD-containing protein 1

SARS-CoV - Severe Acute Respiratory Syndrome Coronavirus

Sca – stem cell antigen

SLE – systemic lupus erythematosus

SLURP – secreted Ly6/plasminogen activator, urokinase receptor domain containing

sgRNA – single guide ribonucleic acid

SH2 – Src homology 2

siRNA – small interfering ribonucleic acid

shRNA – short hairpin ribonucleic acid

SNP – single nucleotide polymorphism

SOCS – suppressor of cytokine signaling

SPCS – signal peptidase complex

SSS – synthetic serum substitute

ss-vDNA - single-stranded viral deoxyribonucleic acid

ss-vRNA – single-stranded viral ribonucleic acids

STAT – signal transducer and activator of transcription

STING – stimulator of interferon genes

SynA – syncytin A

T1AEC – type I alveolar epithelial cells

TAP – tandem affinity purification

TBK-1 – TANK-binding kinase 1

TCR – T cell receptor

TFP – three-finger protein

TIR – Toll-interleukin receptor

TLRs – Toll-like receptors

TNF – tumor necrosis factor

TRAF – tumor necrosis factor receptor-associated factor

TRIF – Toll-interleukin receptor-containing adapter inducing interferon beta

T_{RM} – resident memory CD8⁺ T cell

Tsa-1 – thymic shared antigen 1

TYK2 – tyrosine kinase 2

uPA – urokinase-type plasminogen activator

uPAR – urokinase-type plasminogen activator receptor

USP18 – ubiquitin specific peptidase 18

UTR – untranslated region

vDNA – viral deoxyribionucleic acids

vMIA – viral mitochondrial inhibitor of apoptosis

WNV – West Nile virus

YFV – yellow fever virus

Zfx – Zing finger protein X

ZIKV – Zika virus

CHAPTER ONE

Review of the Literature

THE ANTIVIRAL INTERFERON RESPONSE

Pattern recognition initiates the immune response to pathogenic infection

The ability to distinguish self from non-self is the core feature of vertebrate immunity. Detection of conserved pathogen-associated molecular patterns (PAMPs) and damage-associated molecular patterns (DAMPs) by pattern recognition receptors (PRRs) is the first step in the innate immune response to infection. Pathogen sensing triggers the production of cytokines and chemokines that respectively activate and recruit innate immune cells, including antigen-presenting cells (APCs). Migration of APCs to peripheral lymphoid organs to interact with T and B lymphocytes elicits a pathogen-specific, adaptive immune program. Depending on the combined effectiveness of innate and adaptive immune arms, this cellular response results in successful clearance of pathogen burden and can provide a ‘blueprint’ for responding to future infections.

Recognition of viral infection by PRRs results in interferon production

Viral nucleic acids are the major PAMP detected by cytosolic and endosomal PRRs (Yan and Chen 2012; Sparrer and Gack 2015). Non-self nucleic acids contain distinct structural moieties that prevent PRRs from inadvertently binding self, or host cell, nucleic acids. Cytosolic double-stranded viral ribonucleic acids (ds-vRNA) are primarily detected by the retinoic acid-inducible gene-I (RIG-I)-like receptor (RLR) family, which includes RIG-I,

melanoma differentiation association gene 5 (MDA5), and laboratory of genetics and physiology 2 (LGP2) (Chow, Gale, and Loo 2018). Several members of the nucleotide-binding oligomerization domain (NOD)-like receptor (NLR) family can also detect vRNA indirectly via interaction with DEAD/H-box proteins (Li et al. 2015; Wang et al. 2015; Zhu et al. 2017) or directly (Hong, Yoon, and Wilson 2012). Viral deoxyribonucleic acids (vDNA) are detected by multiple cytosolic receptors, including the enzyme cyclic-guanosine monophosphate (GMP)-adenosine monophosphate (AMP)-synthase (cGAS) (Sun et al. 2013; Wu et al. 2013), deoxyribonucleic acid (DNA)-dependent activator of interferon (IFN) regulatory factor (DAI) (Takaoka et al. 2007), and IFN-inducible protein 16 (IFI16) (Unterholzner et al. 2010). In the endosomal lumen, a subfamily of Toll-like receptors (TLRs) that includes TLR3, TLR7/8, and TLR9 can respectively detect ds-vRNA, single-stranded vRNA (ss-vRNA), and vDNA from incoming virus (Yan and Chen 2012).

Upon engagement with viral nucleic acids, PRRs interact with adaptor proteins that bridge pathogen sensing with molecular signaling pathways. RLR family members RIG-I and MDA5 both possess caspase activation and recruitment domains (CARDs) at the N terminus that can associate with the CARD domain of mitochondrial antiviral-signaling protein (MAVS). MAVS assembles into prion-like aggregates that scaffold with several tumor necrosis factor (TNF) receptor-associated factors (TRAFs) with TANK-binding kinase 1 (TBK-1) and inhibitor of nuclear factor kappa-light-chain-enhancer of activated B cells (NF- κ B) kinases (IKKs) to activate transcription factors IFN regulatory factor 3 (IRF3), IRF7, and NF- κ B (Cai et al. 2014; Chow, Gale, and Loo 2018; Hou et al. 2011; Liu et al. 2013). NLRs are more heterogenous in terms of downstream signaling pathways, with several members

engaging the canonical apoptosis-associated speck like protein containing CARD (ASC)-caspase-1 pathway to cleave pro-cytokines and others interacting with MAVS-dependent signaling (Wang et al. 2015; Zhu et al. 2017; Li et al. 2015; Allen et al. 2011). Endosomal PRR TLR3 engages the adapter molecule Toll-interleukin receptor (TIR)-containing adapter-inducing IFN β (TRIF) to activate NF- κ B, IRF3, and IRF7. In contrast, TLR7/8/9 depend on Myeloid differentiation primary response 88 (MYD88) to activate NF- κ B. DNA sensors such as DAI, cGAS, and IFI16 require stimulator of IFN genes (STING) to also activate both NF- κ B and IRF3 (Sparrer and Gack 2015).

Activated canonical NF- κ B and IRF3/7 enter the nucleus and induce the expression of type I IFNs, type III IFNs, and other pro-inflammatory cytokines. In humans, the type I IFN proteins are encoded by a single IFN β , 13 partially homologous IFN α subtypes, and several other poorly understood IFN genes. The human type III IFNs include IFN λ 1, IFN λ 2, IFN λ 3, and IFN λ 4. The type I IFNs IFN β and all IFN α bind the heterodimeric, transmembrane cell surface receptor that is composed of IFN alpha and beta receptor subunit 1 (IFNAR1) and IFN alpha and beta receptor subunit 2 (IFNAR2). The four type III IFNs bind the IFN λ receptor complex which is composed of IFN lambda receptor chain 1 (IFNLR1) and interleukin 10 receptor subunit beta (IL10RB). Engagement of either IFNAR1/IFNAR2 or IFNLR1/IL10RB complexes leads to activation of the receptor-associated kinases Janus kinase 1 (JAK1) and tyrosine kinase 2 (TYK2), which then phosphorylate tyrosines on the cytosolic portion of the receptor. This phosphorylation event generates a docking site for signal transducer and activator of transcription 1 (STAT1) and STAT2 molecules, resulting in their recruitment and phosphorylation by JAK1/TYK2. Phosphorylation of STAT1 and

STAT2 leads to their dimerization and subsequent association with IRF9 to form the IFN-stimulated gene factor 3 (ISGF3) complex that enters the nucleus and binds IFN-stimulated response elements (ISREs) in the promoters of IFN-stimulated genes (ISGs). While type I and type III IFNs induce overlapping ISG transcriptional profiles, differential expression of the cognate receptors restricts the effects of these cytokines to distinct tissues (Wack, Terczynska-Dyla, and Hartmann 2015; McNab et al. 2015).

The interferon response reinforces antiviral defenses

Secreted IFNs act in an autocrine and paracrine manner to activate a well-characterized transcriptional response to viral infection. Cell-intrinsic host factors such as the IFN induced transmembrane (IFITM) family of proteins are expressed basally and can constrain low levels of viral infection; however, additional layers of cell-intrinsic and extrinsic defense rendered by ISGs are required to control higher levels of viral replication.

IFN induces hundreds of ISGs that bolster pre-existing antiviral defenses at multiple levels (Yan and Chen 2012). IFNs improve cellular sensitivity to infection by increasing expression of PRRs such as RIG-I and cGAS. Expression of PRRs alone is insufficient to induce additional IFN in the absence of PAMPs, which minimizes the risk of aberrant inflammation. IFN also increases the expression of pro-inflammatory cytokines and chemokines and their cognate receptors, which results in the activation and recruitment of innate immune cells (Tang et al. 2005; Tobler et al. 2008; Wandrer et al. 2016). The magnitude and extent of IFN signaling is restrained by ISGs that negatively regulate IFN signaling, such as suppressor of cytokine signaling (SOCS) family proteins and ubiquitin

specific peptidase 18 (USP18) (Schneider, Chevillotte, and Rice 2014). IFNs can also induce the expression of long non-coding RNAs (lncRNAs), a novel class of RNAs that do not encode for proteins and can be longer than 200 nucleotides in length (Qiu et al. 2018). Some lncRNAs can reduce IFN production, such as lnc-Lsm3b which competitively binds RIG-I (Jiang et al. 2018). Other lncRNAs can also promote IFN production, such as NEAT1 which can stimulate RIG-I and cGAS signaling pathways (Ma et al. 2017; Morchikh et al. 2017). A subset of ISGs encode for effector proteins, several of which have been described to function as antiviral factors (Schneider, Chevillotte, and Rice 2014).

Inborn errors in the IFN pathway reveal an essential role for antiviral immunity in humans

Congenital loss of intact IFN signaling due to deleterious genetic mutations results in broad susceptibility to viral infection (Sancho-Shimizu, Perez de Diego, Jouanguy, et al. 2011). Using dermal fibroblasts from a previously healthy 13-month-old infant who succumbed to fatal encephalitis as a complication of measles, mumps, and rubella (MMR) vaccine, Duncan and colleagues found that these cells were insensitive to exogenous IFN treatment as measured by susceptibility to viral infection and lack of antiviral gene induction. Sequencing of patient cDNA revealed homozygosity for a single base pair deletion in exon 5 of *IFNAR2* (c.A311del). This deletion causes a frameshift mutation that generates a downstream premature stop codon in all three protein isoforms of *IFNAR2*, resulting in defective IFN signaling. The researchers found that reconstitution of patient fibroblasts with exogenous *IFNAR2* expression by lentiviral transduction restored responsiveness to IFN and subsequently control of *in vitro* infection with the attenuated viruses found in the MMR

vaccine (Duncan et al. 2015). This data suggests that the immune system of the previously healthy child was unable to mount an appropriate IFN response to the live attenuated viruses in the MMR vaccine, which likely resulted in her death.

Genetic deficiency in signaling molecules downstream of IFNAR2 also results in heightened susceptibility to viral infection, further demonstrating the importance of an intact IFN pathway. In 2003, Dupuis and colleagues reported on two unrelated infants with distinct homozygous mutations in *STAT1*. Sequencing of *STAT1* in the first mutant revealed a two nucleotide deletion in exon 20 (1757-1758delAG) resulting in a premature stop codon at amino acid 603, whereas the second infant was found to have a substitution of a proline at amino acid 600 to leucine. The deletion in *STAT1* from the first infant was predicted to result in a truncated protein lacking a Src homology 2 (SH2) domain. The substitution in the second infant's genome occurred in a highly conserved residue, also in the SH2 domain. Epstein-Barr virus (EBV)-transformed B cells from both infant patients were impaired in responsiveness to IFN and ability to control viral infection. While both children had developed an infection from the bacillus Calmette-Guerin (BCG) vaccine due to the requirement of STAT1 downstream of anti-bacterial IFN γ signaling, successful antibiotic treatment kept the bacterial disease in remission at the time of death by disseminated viral infection (Dupuis et al. 2003).

Inborn mutations in other molecules associated with pathogen-sensing and IFN signaling manifest in relatively minor phenotypes when compared to loss of IFNAR2 and STAT1, due to redundant roles of these proteins in the antiviral immune response (Sancho-Shimizu, Perez de Diego, Jouanguy, et al. 2011). For example, a young child from a

nonconsanguineous family with two distinct null mutations in IRF7 was shown to be highly susceptible to severe infection with influenza A virus (IAV). Further study of cells from the patient showed that her null mutations in IRF7 resulted in an inability to induce type I IFN production after *ex vivo* infection with IAV or herpes simplex virus-1 (HSV-1). However, stimulation of these cells with synthetic double-stranded RNA (dsRNA) triggered IFN production, as dsRNA is sensed by TLR3 which activates IRF3-dependent signaling. Due to IRF7-independent mechanisms, the patient was still able to develop protective immunity against IAV with annual IAV vaccination (Ciancanelli et al. 2015). The narrow role of IRF7 in antiviral immunity is mirrored in patients deficient in TLR3 signaling pathways, who have impaired IFN-mediated responses to viral infection but are otherwise resistant to severe disease as other antiviral signaling pathways are still intact (Zhang et al. 2007; Casrouge et al. 2006; Sancho-Shimizu, Perez de Diego, Lorenzo, et al. 2011). Cumulatively, studies of patients with genetic deficiencies in molecules required for the IFN signaling pathway demonstrate an indispensable role for host antiviral immunity.

Evolution highlights the importance of redundancy in effector-driven antiviral defenses

At the level of a single cell, defense against viral infection is executed by intrinsic antiviral restriction factors with assistance from additional effectors encoded by ISGs. These host proteins directly limit viral infectivity by targeting specific stages of the viral life cycle. The ability of both basal and induced effector proteins to target different viruses at distinct and sometimes redundant stages of replication demonstrate an evolutionary strategy by the host to defend against an ever-adapting foe (Chemudupati et al. 2018).

The existence of viral antagonists of host antiviral factors support the necessity of a multifactorial defense. One of the best studied examples of the host-virus arms race is human immunodeficiency virus 1 (HIV-1), which brandishes accessory proteins Vif, Vpu, and Vpx/Vpr to target and dismantle specific host effectors. Apolipoprotein B mRNA-editing enzyme catalytic polypeptide-like 3G (APOBEC3G) converts cytosine to uracil which results in hypermutation of single-stranded vDNA (ss-vDNA), an essential intermediate of retroviral replication (Lecossier et al. 2003; Zhang et al. 2003). APOBEC3G also prevents viral reverse transcription in a deaminase-independent manner by binding ss-vDNA to physically block reverse transcriptase (RT) (Iwatani et al. 2007; Chaurasiya et al. 2014). To counteract this potent host defense, Vif binds both APOBEC3G and the Cullin5-ElonginB/C ubiquitin ligase complex to mediate proteasomal degradation of APOBEC3G (Kobayashi et al. 2005; Yu et al. 2003). Bone marrow stromal antigen 2 (BST2) was initially implicated to have antiviral activity when it was identified as a target of Vpu. BST2 was renamed tetherin when it was found to tether budding virions to the cell surface (Neil, Zang, and Bieniasz 2008). Vpu was found to remove BST2 and shuttle it for degradation by endosomal trafficking (Van Damme et al. 2008; Mitchell et al. 2009). Human sterile alpha motif and HD-domain containing protein 1 (SAMHD1) is an enzyme that hydrolyzes deoxynucleotide triphosphates (dNTPs) into deoxynucleoside and inorganic triphosphate, resulting in depletion of a building block required for reverse transcription (Goldstone et al. 2011). Interestingly, SAMHD1 activity is regulated by cell cycle progression as it is inactive during S phase, which is when high dNTP levels are needed for host DNA replication (Franzolin et al. 2013). Vpx/Vpr antagonizes SAMHD1 by binding and redirecting it for proteasomal degradation via association with the

Cullin4-based E3 ubiquitin ligase complex (Laguetta et al. 2011; Hrecka et al. 2011). The ability of HIV-1 to evade multiple antiviral restriction factors by developing counteractive accessory proteins highlights a need by the host to maximally utilize diverse defense mechanisms.

High-throughput screening for function-based discovery of antiviral effectors

Over the past two decades, advances in molecular high-throughput screening platforms have led to a rapid increase in the identification and characterization of novel antiviral ISG effectors. Function-based discovery screens have allowed for comparative analysis of hundreds of ISGs at a time. Application of different molecular techniques, host backgrounds, and viruses has led to a diverse dataset. Furthermore, variation in screening approaches has resulted in the discovery of distinct effector ‘hits,’ suggesting that the complexity of the IFN response cannot be unraveled with only a single method.

Genome-wide RNA interference screens have uncovered important host factors and pathways

In 1998, Andrew Fire and Craig Mello discovered that delivery of specific sequences of dsRNA into *Caenorhabditis elegans* resulted in targeted depletion of mRNA encoding for a gene of interest and consequently the protein of interest (Fire et al. 1998; Zamore 2006). This Nobel prize-winning discovery of RNA interference (RNAi) was eventually expanded to use in mammalian cells, resulting in unprecedented deep dissection of biological pathways through powerful loss-of-function screens (Aza-Blanc et al. 2003; Berns et al. 2004; Pelkmans et al. 2005). Difficulties in delivering small interfering RNA (siRNA) to

transfection-resistant cells was circumvented by development of short hairpin RNA (shRNA) that can be delivered and integrated into the host genome via lentiviral vectors (Silva et al. 2005; Paddison et al. 2004; Moffat et al. 2006).

Screening for human host cofactors involved in viral replication began with small, targeted libraries. Using siRNAs designed to target 62 genes that encode proteins known to interact with hepatitis C virus (HCV) RNA or proteins, the researchers identified 26 host genes that modulate HCV replication (Randall et al. 2007). In addition, by knocking down Dicer, an integral component of the RNAi pathway, they discovered that HCV replication is dependent on microRNA-122 (miR-122) expression. This pioneering research led to study of miR-122 in primate models (Lanford et al. 2010) and development of a novel therapeutic to treat chronic HCV infection (van der Ree et al. 2017).

The commercialization of genome-scale siRNA libraries led to the rapid increase in identification of novel host factors involved in viral infection. By combining RNAi with microscope-based image quantification, Krishnan and colleagues identified hundreds of factors relevant for West Nile virus (WNV) and dengue virus (DENV) entry (Krishnan et al. 2008). Furthermore, their study established novel roles for ubiquitin and endoplasmic reticulum (ER)-associated degradation (ERAD) pathways in viral infection, further demonstrating methods by which viruses unexpectedly hijack host pathways (Neufeldt et al. 2018).

Multiple groups employed RNAi screening in lung epithelial cell lines to identify host factors required for IAV infection (Konig et al. 2010; Karlas et al. 2010), highlighting the importance of kinases and components of the endosomal pathway in viral entry. Using an

osteosarcoma cell line, Brass and colleagues similarly screened a siRNA library and identified IFITM3 as an inhibitor of IAV, WNV, and DENV entry (Brass et al. 2009). More recently, meta-analysis was subsequently performed on eight published RNAi screens against IAV, leading to the discovery of the E3 ubiquitin-protein ligase UBR4 as essential for IAV replication through direct interaction with viral proteins (Tripathi et al. 2015).

RNAi screening has also been performed *in vivo* by using replication-competent RNA viruses to deliver siRNA by infection (Varble et al. 2013; Benitez et al. 2015). In the initial 2013 study by Varble and colleagues, a library of Sindbis-based viruses was engineered to be identical at the protein level, but to also contain a unique siRNA designed to target the expression of one of 10,000 different host genes. Viruses containing siRNA that knocked down expression of genes that limited viral replication gained a competitive advantage over other viruses, leading to enriched representation in the overall library. This strategy led to identification of Zinc finger protein X (Zfx) and MAX gene-associated protein (Mga) which both encode for transcription factors that support transcriptional activation of antiviral genes.

In a sister study using IAV, the virus library was modified to encode siRNA that targeted genes encoding known or putative host restriction factors (Benitez et al. 2015). Additionally, the IAV-based library was engineered on the background of a mutant virus lacking functional NS1, rendering it unable to block PAMP detection and evade the IFN-mediated host antiviral defense (Donelan, Basler, and Garcia-Sastre 2003). Surprisingly, a virus encoding siRNA to silence the PRR MDA5 became enriched across four replicate screens. As RIG-I had previously been considered the primary PRR responsible for the IFN-mediated response against IAV, the researchers investigated further using *in vitro* model

systems. While loss of RIG-I in vitro completely blunted *Ifnb* expression induced by infection with NS1-mutant IAV, genetic deficiency in MDA5 only resulted in a partial loss. Interestingly, loss of MDA5 led to a 20-fold reduction in *Irf7* induction by IAV infection, suggesting that MDA5 is required for amplification of the antiviral response downstream of RIG-I-mediated induction of IFN.

The advent of RNAi screening rapidly improved identification of host pathways and factors that are associated with viral infection, including an antiviral effector that has since been demonstrated to have clinical significance. While many screens focused on understanding pathways required for viral replication, a subset of RNAi screens contributed to our understanding of antiviral factors (Brass et al. 2009; Varble et al. 2013; Benitez et al. 2015; Li et al. 2013; Subramanian et al. 2018; Fusco et al. 2013; Zhao et al. 2012). The use of RNAi to identify IFITM3 as a novel antiviral factor was further complemented by studies demonstrating an integral role in protecting mice against primary viral infection (Everitt et al. 2012). IFITM3 was also found to be selectively expressed by murine lung resident memory CD8⁺ T cells (T_{RM}) after primary IAV infection (Wakim et al. 2013). Adoptive transfer of IFITM3-depleted T_{RM} from transgenic OT-I mice, which express a singular T cell receptor (TCR) specific for ovalbumin (OVA) peptide OVA₂₅₇₋₂₆₄, into recipient mice infected with IAV-OVA led to greater host susceptibility to viral infection when compared to recipient mice that had received IFITM3-replete T_{RM}. The increased host resistance was associated with the ability of IFITM3-replete T_{RM} to persist in the lung tissue in the presence of cytopathic IAV infection, which successfully eliminated IAV-susceptible IFITM3-depleted T_{RM}. Analysis of single nucleotide polymorphisms (SNPs) led to identification of the SNP

rs12252-C in *IFITM3*, which reduces antiviral function and is associated with increased hospitalization for severe pandemic H1N1/09 IAV infection (Everitt et al. 2012; Zhang et al. 2013). More recently, SNPs in rs34481144 were identified in the 5' untranslated region (UTR) of *IFITM3* (Allen et al. 2017). While risk alleles A/G or A/A at this locus were associated with lower mRNA expression and increased susceptibility to severe IAV infection, the protective allele G/G was associated with increased *IFITM3* expression and resistance to severe viral disease. Mechanistic studies using electrophoretic mobility shift assays (EMSA) indicated that the rs34481144 risk allele decreased binding of the transcription factor IRF3 and increased binding of the transcriptional repressor CCCTC-binding factor (CTCF). This SNP was associated with increased methylation in effector memory T_{EM} CD8⁺ T cells but not in patient-derived epithelial cells or monocytes, suggested a cell type specific role for *IFITM3* expression. In corroboration with murine studies, the researchers found that nasal washes from IAV-infected individuals with the genotype A/G contained significantly fewer CD8⁺ T cells when compared to washes from patients with the G/G genotype, which may explain the increased susceptibility of patients with the rs34481144 risk allele to severe IAV infection.

Overall, the leap from research bench to clinic with miR-122 and *IFITM3* demonstrate a few of the major contributions that RNAi technology has had on our understanding of antiviral immunity. However, meta-analyses of genome-wide RNAi screens performed with the same virus have uncovered a striking lack of reproducibility between published studies: less than 7% across 3 RNAi screens using HIV-1 and 7.1% for 8 RNAi screens using IAV (Bushman et al. 2009; Tripathi et al. 2015). While differences in

experimental design are highly influential in the degree of reproducibility, off target effects and incomplete ablation of expression remain a major hindrance for genome-wide RNAi screens (Pache, Konig, and Chanda 2011; Barrows et al. 2010).

CRISPR as an improved technique for genome-wide loss-of-function studies

In 2014, the lab of Feng Zhang published on the use of clustered regularly interspaced short palindrome repeats (CRISPR) for genome-wide loss-of-function screening in human cell lines (Shalem et al. 2014; Sanjana, Shalem, and Zhang 2014). CRISPR genome editing is most commonly mediated by the *Streptococcus pyogenes* nuclease Cas9, which uses gene-specific single guide RNA (sgRNA) to generate a double strand break (DSB). When targeted to the coding region of a gene, the DSB can create a frame shift that leads to a loss-of-function allele at the genomic level. By making their toolset available to the public, the Zhang lab provided a tractable alternative to RNAi technology that results in complete ablation rather than a reduction in gene expression. Furthermore, CRISPR was also demonstrated to be a viable tool for complementary *in vivo* loss-of-function studies, whether it be through one-step generation of mutant mice (Wang et al. 2013) or transgenic Cas9-knockin adult mice (Platt et al. 2014).

Genome-wide CRISPR screening has since been used by multiple groups to identify important host factors for flavivirus replication (Marceau et al. 2016; Ma et al. 2015; Zhang et al. 2016; Savidis et al. 2016). In one of the earliest studies, Ma and colleagues used a lentiviral sgRNA library transduced into human embryonic kidney (HEK293FT) cells to identify host genes that are required for cell death caused by WNV infection (Ma et al. 2015).

Their study led to identification of seven genes in the ERAD pathway that were required for WNV-induced cell death, but not replication. In an independent study by the Jan Carette lab, researchers employed CRISPR screening in a human hepatoma cell line (Huh7.5.1) in parallel with insertional mutagenesis in haploid cells (HAP1) to identify host factors with a role in DENV infection (Marceau et al. 2016). Their screen also identified genes in the ERAD pathway, as well as oligosaccharyltransferase (OST) complex genes involved in N-linked glycosylation. Mechanistic studies revealed that OST complex proteins associate with flavivirus non-structural proteins and play a critical role in viral RNA replication, but not translation or entry. Furthermore, many of the ER-associated genes identified in their screen were found to also be important for Zika virus (ZIKV) infection, but not for HCV. In another WNV-induced cell death CRISPR screen, Zhang and colleagues also identified ER-associated genes as essential for flavivirus infection, including genes belonging to the signal peptidase complex (SPCS) that were found to be required for processing of flavivirus structural proteins (Zhang et al. 2016). Cumulatively, these papers independently and redundantly identified ER-associated proteins as required for flavivirus replication, demonstrating the remarkable reproducibility of CRISPR screening technology.

Recently, genome-wide loss-of-function CRISPR screening has also been applied to IAV infection, specifically in the context of infection by a human isolate of the avian H5N1 strain (Han et al. 2018). Han and colleagues identified genes involved in sialic acid biosynthesis and glycosylation as IAV host factors. The transporter solute carrier family 35 member A1 (*SLC35A1*), which is required for sialylation of cell surface proteins, was found to be an essential host factor for IAV entry. In the same study, capicua (*CIC*) was identified

as a novel negative regulator of antiviral gene expression. While these loss-of-function screens have improved our understanding of host factors required for viral infection, CRISPR-mediated knockout has more recently been used for the identification of antiviral host factors involved in the IFN response (Richardson et al. 2018; OhAinle et al. 2018).

Unbiased gain-of-function screening by CRISPR identifies an IAV restriction factor

CRISPR technology has also been adapted to overexpress endogenous genes by fusing a catalytically dead Cas9 (D10A, H840A) to a C-terminal VP64 transactivation domain, termed CRISPR synergistic activation mediator (CRISPR SAM). The resulting protein (dCas9-VP64) can be expressed in the presence of a promoter-specific sgRNA to drive expression of endogenous genes (Perez-Pinera et al. 2013; Konermann et al. 2015). More efficient targeting can be achieved by also expressing a chimeric fusion protein (MS2-p65-HSF1) composed of transactivation domains from MS2 bacteriophage coat proteins, the NF- κ B subunit p65, and human heat-shock factor 1 (HSF1).

In order to identify genes that completely block IAV infection, Heaton and colleagues combined dCas9 with an ultra-sensitive method to detect viral infection (Heaton et al. 2017). They generated a cell line containing an integrated Cre recombinase reporter construct, which results in expression of the fluorescent protein ZsGreen when cells are infected with a transgenic IAV carrying Cre recombinase. Across three biological replicates, 25 repeated hits were observed with only 9 displaying reproducible inhibition of IAV infection. The researchers focused on the glycosyltransferase B4GALNT2, which has been shown to mediate transfer of N-acetylgalactosamine (GalNAc) to the sub-terminal galactose of a

carbohydrate containing a terminal sialic acid-galactose moiety. Mechanistically, B4GALNT2 was found to inhibit viral binding to the cell surface by modifying cellular glycans that avian IAV strains utilize for attachment. While this unbiased genome-wide screening approach identified a novel antiviral factor, it failed to uncover known IAV restriction factors such as IFITM3, likely due to poor gene induction per cell by the CRISPR-SAM system.

Targeted screening for antiviral factors by ectopic overexpression

For high-throughput identification of host factors that inhibit viral infection, researchers have relied on a gain-of-function approach using cDNA expression screens. The least biased variation of this approach utilized a cDNA library generated from IFN-treated cells, which contains putative antiviral genes that cumulatively make up the inhibitory effects of IFN (Suzuki et al. 2016). Alternatively, cDNA libraries of known ISGs have also been synthesized based on published microarray datasets from IFN-treated cells and screened for antiviral function (Schoggins et al. 2011; Schoggins et al. 2014; Kane et al. 2016; Dittmann et al. 2015; Liu et al. 2012; Schoggins et al. 2012).

To identify ISGs that inhibit DENV infection, Suzuki and colleagues generated a cDNA library from human epithelial cells (HeLa) that had been treated with type I IFN (Suzuki et al. 2016). The cDNA library was then packaged into lentiviral vectors and used to transduce the human hepatoma cell line (Huh7.5). Infection of the transduced cells with a high multiplicity of infection (MOI) of DENV resulted in elimination of most cells due to cytopathic effects. The surviving cells were selected and grown as clonal populations that

were further validated for resistance to DENV and subsequently analyzed by sequencing to determine the identity of the cDNA conferring viral resistance. Most clones that were analyzed contained cDNA encoding the uncharacterized ISG C19orf66, which the authors renamed as repressor of yield of DENV (RyDEN). Subsequent analyses of RyDEN revealed a broad inhibitory effect against multiple RNA viruses and specific inhibition of viral translation mediated by interaction of RyDEN with viral RNA and cellular mRNA-binding proteins. While this approach led to identification and characterization of a novel ISG, the strict requirement for blocking virus-induced cytopathic effects likely limited the discovery of additional antiviral genes.

When combined with viruses expressing fluorescent reporters and high-throughput readouts such as flow cytometry, screening by ectopic overexpression has been a powerful approach for identification of novel antiviral ISGs. Schoggins and colleagues performed one of the broadest gain-of-function screens, evaluating the antiviral activity of cDNA encoding 389 known ISGs against a panel of 18 medically-relevant viruses (Schoggins et al. 2011; Schoggins et al. 2014; Schoggins et al. 2012). To generate the cDNA library, researchers compiled microarray datasets from cell lines and tissues treated with type I IFN and selected genes of interest based on fold induction and other inclusion criteria (Schoggins et al. 2011). The cDNAs encoding ISGs of interest were commercially synthesized and cloned into a lentiviral plasmid backbone. Lentiviral pseudoparticles were used to express the ISG library in *STAT1*^{-/-} human fibroblasts that have an impaired response to type I IFNs (Dupuis et al. 2003). The transduced cells were then infected with viruses from different families, including *Flaviviridae*, *Togaviridae*, *Retroviridae*, *Picornaviridae*, *Arteriviridae*, *Orthomyxoviridae*,

Paramyxoviridae, and *Bunyaviridae* (Schoggins et al. 2011; Schoggins et al. 2012; Schoggins et al. 2014).

By testing the contributions of individual ISGs against multiple viruses, Schoggins and colleagues characterized the antiviral activities of both known and unknown ISGs. Ectopic overexpression of several ISGs, such as C6orf150 (later characterized as cGAS), heparanase (HPSE), IRF1, IFITM3, and RIG-I were found to broadly inhibit multiple viruses. Other ISGs were demonstrated to have more narrow inhibitory effects against single viral families, such as IFN alpha inducible protein 6 (IFI6) and receptor-transporting protein 4 (RTP4). Hierarchical clustering analyses to group viruses and broadly inhibitory ISGs revealed a division in ISG-mediated inhibition between positive-sense and negative sense single strand RNA viruses (+ssRNA and -ssRNA) (Schoggins et al. 2014). Overall, the screens revealed that the IFN response is composed of diverse effectors that function redundantly to orchestrate universal inhibition of viral infection.

Surprisingly, the ectopic overexpression approach also revealed a subset of ISGs that enhanced infection by certain viruses. While ISGs like SOCS1 can promote infection by inhibiting IFN signaling, viral enhancement by these ISGs was observed in a STAT1-deficient cellular background which suggests that the phenotype is independent of IFN signaling (Schneider, Chevillotte, and Rice 2014). Several ISGs, such as adenosine deaminases acting on RNA1 (ADAR1), APOBEC3A, mucolipin 2 (MCOLN2), indoleamine 2,3-dioxygenase (IDO1), and lymphocyte antigen 6 complex, locus E (LY6E) promoted infection by multiple viruses representing distinct families when ectopically expressed. APOBEC3A and IDO1 have since been described to inhibit viral infection (Kane et al. 2016;

Mao et al. 2011; Lepiller et al. 2015; Sharma et al. 2015). ADAR1 has been shown to negatively regulate MDA5-dependent IFN production and the antiviral ISG protein kinase R (PKR) activation by editing host and viral genomes and making them undetectable by MDA5 and PKR (Chung et al. 2018; Liddicoat et al. 2015; Pujantell et al. 2017; Pfaller et al. 2018). MCOLN2 has been shown to promote trafficking of endocytosed IAV through endosomes (Rinkenberger and Schoggins 2018). Several antiviral ISGs have previously been shown to enhance specific viruses via ‘viral hijacking’, such as IFITM3 promoting entry by human coronavirus, strain OC43 (HCoV-OC43) (Zhao et al. 2014). However, it is unclear whether viral enhancement by MCOLN2 and LY6E is a result of viral hijacking or if the two ISGs can contribute to the overall antiviral immune response.

LY6E IS A SMALL, MULTI-TASKING PROTEIN

LY6E belongs to the Ly6/uPAR superfamily

The ISG *LY6E* encodes for a 131 amino acid protein, which is further processed upon translation to the mature 81 amino acid form. Like other proteins that localize to the cell surface by glycosylphosphatidylinositol (GPI) anchor, LY6E contains both amino and carboxyl signal peptides. The amino signal peptide mediates translocation through the ER and is cleaved by a signal peptidase. The carboxyl terminal is cleaved with concomitant attachment of the GPI moiety in a transamidation reaction (Ferguson, Hart, and Kinoshita 2015). The tertiary structure of LY6E is shaped by disulfide bonding between highly-conserved cysteines that form three beta-sheet structural loops (‘fingers’) around a

hydrophobic core (Tsetlin 2015). In the center of this core is a strictly conserved asparagine residue that occurs after the last cysteine to form the CN sequence motif. Analysis of three-dimensional structures from other proteins with a similar ‘three-fingered protein’ (TFP) topology indicate that the asparagine residue is oriented towards the interior of the domain where it establishes the hydrophobic core through hydrogen bond interactions with the beta-sheet fingers (Galat et al. 2008). This unique, phalange-like structure is the determining feature of the lymphocyte antigen-6 (Ly6)/urokinase-type plasminogen activator receptor (uPAR) LU domain that distinguishes the Ly6/uPAR superfamily of proteins.

Genomic organization of Ly6/uPAR gene family in mice and men

The first Ly6 family proteins were described as lymphocyte differentiation antigens in mice (McKenzie et al. 1977). Complete annotation of the human and mouse genomes respectively revealed 35 and 61 Ly6/uPAR family members. The human Ly6/uPAR family is distributed in gene clusters across chromosomes 1, 2, 6, 8, 11, and 19 while the mouse family is localized to chromosomes 1, 2, 7, 9, 11, 15, 17, and 19. The Ly6 gene clusters on human chromosomes 8, 19, 11, and 6 are respectively syntenic to murine chromosomes 15, 7, 9, and 17, which suggests that these loci originated from a common ancestor. Human *LY6E* is located near the center of a short 500 kilobase cluster on chromosome 8 (8q24) that also contains prostate stem cell antigen (*PSCA*), *LY6K*, secreted Ly6/Plasminogen activator, urokinase receptor (*PLAUR*) domain containing 1 (*SLURP1*), Ly6/*PLAUR* domain containing 2 (*LYPD2*), Ly6/neurotoxin 1 (*LYNX1*), *SLURP2*, *LY6D*, glycosylphosphatidylinositol anchored molecule like (*GML*), *LY6L*, *LY6H*, and

glycosylphosphatidylinositol anchored high density lipoprotein-binding protein 1 (*GPIHBP1*). The syntenic region in mouse is located on chromosome 15 (15D3-15E1), with murine *Ly6e* in the center of a cluster that also contains *Psca*, *Slurp1*, *Lypd2*, *Slurp2*, *Lynx1*, *Ly6d*, *Ly6g6g*, *Ly6k*, *Gml*, *Gml2*, *Ly6m*, *Ly6i*, *Ly6a*, *Ly6c1*, *Ly6c2*, *Ly6a2*, *Ly6g*, *Ly6g2*, *Ly6f*, *Ly6l*, *Ly6h*, and *Gpihbp1*. The lack of human orthologs for several of the murine Ly6 genes, such as notable myeloid markers *Ly6g* and *Ly6c*, suggests that these genes arose through gene duplication events that occurred after evolutionary divergence of the two species. While most of the Ly6/uPAR family members encode proteins that are tethered to the cell surface by GPI anchor, a few family members, such as *SLURP1*, encode proteins that lack a GPI anchor and are thus secreted (Loughner et al. 2016).

The typical arrangement of a Ly6/uPAR family gene consists of three exons and two introns, although some gene members contain as many as 14 exons. Nearly all genes encode for a single LU domain with exceptions in both human and murine versions of *CDI77*, *LYPD3*, and *uPAR*, which contain 2 to 4 domains. The organization of all Ly6/uPAR members is similar, with the signal peptide for targeting to the ER encoded by a separate, earlier exon while the remaining polypeptide is contained within the remaining two exons (Loughner et al. 2016). Gene family members that are expressed at the cell surface also contain the GPI-anchor domain in the last exon. Human *LY6E* has two transcript variants with 4 exons each that encode an identical protein. Murine *Ly6e* has 6 transcript variants with 4 to 5 exons that all encode the same protein. The last three exons of both human *LY6E* and mouse *Ly6e* encode the precursor protein (Maglott et al. 2011).

Examples of Ly6/uPAR family members and their diverse functions

Variations in the flexible TFP domain allow each Ly6/uPAR family member to interact with functionally distinct protein partners, resulting in diverse biological roles. In the absence of a cytoplasmic tail, the GPI-anchored Ly6/uPAR proteins are unable to participate directly in intracellular signaling without a transmembrane partner. One of the best studied examples is Lynx1, a Ly6 protein that was originally identified in the brain of mice. Named for membership in the Ly6 family ('ly') and structural similarity to snake neurotoxins ('nx'), which also contain TFP domains, Lynx1 was found to associate with several nicotinic acetylcholine receptor (nAChR) subunits (Ibanez-Tallon et al. 2002). Like snake neurotoxins, Lynx1 interaction with nAChR modulates acetylcholine-induced currents in neurons (Miwa et al. 1999; Ibanez-Tallon et al. 2004). In the mouse brain, Lynx1 is expressed in neurons in the hippocampus, cortex, and cerebellum, specifically localizing to the soma and proximal dendrites. Deletion of Lynx1 in a murine model led to increased sensitivity for nicotine and decreased nAChR desensitization (Miwa et al. 2006). As a result, *Lynx1*^{-/-} mice have improved performance in learning and memory tests at the cost of enhanced neurodegeneration due to hyperactivation of nAChRs. Null mutations in nAChRs remedied neurodegeneration in aged *Lynx*^{-/-} mice, demonstrating the importance of Lynx1 in mediating the balance between activity and survival in the brain.

Several other Ly6 proteins have also been shown to interact with neuronal ion channels to modulate behavior. Knocking out the Lynx1 homolog, Lynx2, led to increased anxiety in mice due to accelerated desensitization of the $\alpha 4\beta 2$ nAChR (Tekinay et al. 2009). Ly6 protein-mediated modulation of neuronal signaling is conserved in *Drosophila*

melanogaster, as the protein SLEEPLESS or synthetic serum substitute (SSS) has been shown to interact with the potassium channel Shaker. SSS reduces neuronal excitability by increasing the open probability of Shaker (Wu et al. 2010; Koh et al. 2008). As a result, ectopic overexpression of SSS in *Drosophila* induced sleeping and loss of SSS reduced sleeping. Interestingly, SSS has also been shown to interact with fly nAChRs and heterologous expression of murine Lynx1 in flies partially rescues sleep in *sss* mutants, demonstrating conserved ability of Ly6 proteins to modulate neuronal activity across species (Wu, Robinson, and Joiner 2014).

A more recent study by Wu and colleagues used ectopic overexpression to screen for the ability of murine Ly6 family proteins to modulate nAChR activity (Wu et al. 2015). The researchers were specifically interested in examining interactions that may contribute to nicotine addiction, and thus co-expressed the $\alpha 4\beta 2$ nAChR heterodimer with 9 different murine Ly6 proteins in human embryonic kidney cells (HEKtsa). This approach revealed novel roles of Lynx2 and Ly6h in modulating calcium influx via $\alpha 4\beta 2$ nAChR heterodimer. Furthermore, Ly6e and Ly6g6d also inhibited calcium influx albeit to a lesser extent, and Ly6g6e increased calcium influx by nearly two-fold as compared to receptor alone. Wu and colleagues also demonstrated association of Myc-tagged Lynx2, Ly6h, and Ly6e with green fluorescent protein (GFP)-tagged nAChR $\alpha 4$ subunit by co-immunoprecipitation. Ly6g6e, which promoted calcium influx, was found to associated with HA-tagged nAChR $\alpha 4$ subunit. Interestingly, Lynx2 was found to suppress nAChR activity by preventing protein expression at the cell surface, whereas Ly6g6e potentiated $\alpha 4\beta 2$ activity at the plasma membrane. As such, application of soluble phospholipase C (PLC) to cleave GPI-linked proteins abolished

ectopic Ly6g6e-mediated enhancement but had no effect on the activity of ectopic Lynx2 on calcium influx. While this study revealed previously unidentified associations of certain Ly6 proteins with nAChRs, further study examining the neuronal expression and role of these Ly6 proteins in animal models is required to understand whether these observations are physiologically relevant.

Cell surface Ly6/uPAR proteins have also been demonstrated to bind soluble proteins, resulting in downstream effects such as localizing enzymatic activity. GPIHBP1 is expressed on the luminal face of capillary endothelium located in brown adipose tissue, heart, lung, and liver (Loughner et al. 2016). Through biochemical and animal studies, Beigneux and colleagues have shown that GPIHBP1 captures chylomicrons, or triglyceride-rich lipoproteins, and lipoprotein lipase (LPL) (Beigneux et al. 2007). By enhancing proximity of LPL with chylomicrons, GPIHBP1 promotes hydrolysis of triglycerides which is essential for their removal from the bloodstream. *Gpihbp1*^{-/-} mice have significantly higher plasma cholesterol and triglyceride levels which manifests as ‘milky’ plasma as a result of aberrant LPL-mediated chylomicron processing. *Gpihbp1* deficiency is non-lethal, whereas *Lpl*^{-/-} mice perish shortly after birth, indicating that LPL-mediated lipolysis occurs in the absence of GPIHBP1. Extensive mutagenesis of GPIHBP1 led to the identification of several non-cysteine residues that are important for LPL binding, with 9 of 12 amino acids localizing to the second ‘finger’ of the TFP domain (Beigneux et al. 2011). Missense mutations in GPIHBP1 that affect TFP domain folding and autoantibodies blocking the interaction between GPIHBP1 and LPL have been identified in patient populations (Beigneux et al. 2015; Coca-Prieto et al. 2011; Charriere et al. 2011; Olivecrona et al. 2010; Beigneux et al.

2017). Interference with GPIHBP1 in both instances results in severe hypertriglyceridemia, demonstrating the importance of active GPIHBP1 in a clinical setting.

PLAUR/uPAR, which has 3 TFP domains, binds the urokinase-type plasminogen activator (uPA) which possesses enzymatic activity. Cell surface-bound uPA converts the zymogen plasminogen to active plasmin, a serine protease that targets multiple substrates including fibrin, C3, collagenases (Law, Abu-Ssaydeh, and Whisstock 2013). The crystal structure of PLAUR revealed that uPA engages the central cavity formed by the 3 TFP domains, leaving an external surface open for coupled interactions with other cell surface proteins such as integrins, vitronectin, and G protein-coupled chemotactic receptors (Wei et al. 1996; Llinas et al. 2005; Wei et al. 1994; Fazioli et al. 1997). The versatility of the flexible TFP domains allows PLAUR to modulate a variety of cellular functions, such as cellular adhesion, migration, signal transduction, differentiation, and proliferation (Blasi and Carmeliet 2002).

Other GPI-anchored Ly6 family proteins have also been shown to tether soluble factors to the cell surface to prevent insertion in the plasma membrane. CD59 has been shown to protect homologous cells from complement membrane attack complex by binding complement component 9 (C9) and preventing its insertion into the plasma membrane (Meri et al. 1990; Davies et al. 1989; Chang et al. 1994; Yu et al. 1997). CD59 has also been shown to modulate TCR signaling via the adaptor protein linker for activation of T-cells (LAT), demonstrating broad utility of a single, flexible TFP domain (Korty, Brando, and Shevach 1991; Wang et al. 2018).

In conclusion, Ly6 family proteins exhibit diverse functions by interacting with soluble and cell surface proteins through a flexible TFP domain. The requirement for an interaction partner is further conserved in the secreted Ly6 family members such as Lypd8, which was recently shown to bind to bacterial flagella, and SLURP1 and SLURP2, which associate with and modulate acetylcholine receptor activity (Okumura et al. 2016; Loughner et al. 2016).

The identification of Ly6e/Sca-2/Tsa-1/9804

The initial discovery and characterization of murine and human LY6E orthologs began in 1986 in the hot field of stem cell marker discovery. In a study from the lab of Jan Klein, researchers injected rats with BALB/C strain murine hybridomas originating from bone marrow, fetal liver, and fetal thymocytes (Aihara et al. 1986). Monoclonal antibodies (mAb) for putative T cell precursor markers were obtained by isolating antibody-producing B cell hybridomas from the immunized rats. The mAb E3 81-2 reacted against a small population of cells derived from murine thymus, bone marrow, and fetal liver. Subsequent study of the antigen recognized by E3 81-2, designated as stem cell antigen 2 (Sca-2) by the Klein lab, revealed that Sca-2 expression was limited to immature CD4⁻ CD8⁺ thymocytes in the thymic cortex and a subset of lymph node germinal center B cells (Spangrude et al. 1988). Using a different mAb (MTS 35), the lab of Patrice Hugo also found that Sca-2 (renamed thymic shared antigen 1 or Tsa-1) was restricted to immature thymocytes in the thymic cortex and peripheral B cells (Godfrey et al. 1992). The MTS 35 mAb was also shown to increase the percentage of CD8⁺ single-positive cells when applied to fetal thymic

organ culture, indicating an effect of Tsa-1 on T cell development (Waanders, Godfrey, and Boyd 1989; Randle et al. 1993). The lab of Ken Shortman found that Sca-2 marked multipotent stem cells in the bone marrow that differentiated into B and T lymphocytes, but not myeloid cells, when transferred to irradiated recipient mice (Wu et al. 1991). Overall, these earlier studies demonstrate that murine Ly6e/Sca-2/Tsa-1 is expressed on multipotent stem cells and indicate a potential role in driving T cell differentiation.

Identification and characterization of murine Ly6e and human LY6E

The first description of the cDNA encoding Tsa-1 was published by the lab of Albert Zlotnik in 1993 by expressing a cDNA library and screening for positive staining with the mAb MTS 35 (MacNeil et al. 1993). Northern blot analysis of murine tissues revealed highest expression in thymus, spleen, liver and lung, with lower levels in kidney, brain, muscle, testes, and heart. Tsa-1 was determined to belong to the Ly6 family due to sequence homology with human CD59 and its possession of a hydrophobic carboxyl terminus that is typical of GPI-anchored proteins. Using a similar cDNA library screening approach with the E3 81-2 mAb, the lab of Loretta Coverdale also sequenced the cDNA encoding mouse Sca-2 and determined it to be identical to Tsa-1, with one amino acid different in the signal peptide (Classon and Coverdale 1994).

The human ortholog of Sca-2 was identified by three groups between 1996 to 1998. In the first paper, researchers from Zhu Chen's lab identified retinoic acid-induced gene E (RIG-E) as a novel gene in cells derived from a patient with acute promyelocytic leukemia (APL) (Mao et al. 1996). RIG-E was upregulated in the APL cells upon treatment with all-

trans-retinoic acid (ATRA), a treatment that causes clinical remission for 90% of patients *in vivo*. Northern blot analysis of lysates derived from multiple human tissues and cell lines revealed a broad expression in liver, spleen, uterus, ovary, lung, brain, and thymus, as well as in a T cell line but not in B cell or monocytic cell lines. Homology analysis revealed 60.4% identity to murine *Sca-2* and 26.0% to human *CD59*, which led researchers to conclude that RIG-E belongs to the Ly6 family of proteins. Using fluorescence in situ hybridization (FISH), the human RIG-E gene was mapped to 8q24 (Mao et al. 1996).

The second publication to identify human SCA-2 came from Albert Zlotnik's lab, which used bioinformatic analysis of publicly available databases of expressed sequence tags (EST) to identify the open reading frame (ORF) of the human gene (Capone et al. 1996). Interestingly, the EST sequences encoding SCA-2 originated from cDNA libraries derived from brain, breast, fetal liver/spleen, ovary, and pineal gland. Northern blot analysis of adult tissues revealed the strongest expression of SCA-2 in ovary and liver, and lower levels in all other tissues tested. Monocytes, DCs, B cells, and T cells were also found to express SCA-2.

The third publication to describe human SCA-2 came from Roger Palfree's lab, which identified 9804 from a cDNA library derived from a monocytic cell line (U937) (Shan et al. 1998). Expression of 9804 cDNA in U937, which was subsequently found to be identical to human TSA-1/SCA-2, resulted in T cell costimulation that was independent of B7 (CD80/CD86) expression. Northern blot analysis of human adult tissue extracts revealed highest expression in liver, kidney, ovaries, and peripheral blood lymphocytes (PBL). Moderate expression levels were detected in adult brain, placenta, lung, and colon, while lower levels were found in heart, spleen, thymus, prostate, and small intestine. In fetal

tissues, 9804 was detected in all samples but liver. Upon IFN α treatment, but not IFN γ , 9804 mRNA was upregulated in monocytic cell line U937 and peripheral blood mononuclear cells. Analysis of the 9804 promoter revealed the presence of both ISRE and retinoic acid response element (RARE) binding sites, but no IFN γ activated sites (GAS).

Cumulatively, the earliest studies on LY6E described a widely-expressed protein that may play a role in lymphocyte differentiation from a common multipotent stem cell. Furthermore, *LY6E* expression was also found to be induced by retinoic acid and IFN which implicates LY6E in additional processes aside from cellular differentiation.

LY6E has a complicated naming history

As described above, the original name of LY6E was Sca-2, due to its expression on multipotent stem cells. In the same publication, the lab of Jan Klein also identified Sca-1 as a marker of phenotypically mature CD4⁺CD8⁻ thymocytes (Spangrude et al. 1988). Sca-2 was subsequently renamed by 3 different groups based on its newly discovered functions: Tsa-1 for its role in thymocyte development (Godfrey et al. 1992), 9804 for the cDNA identification code (Shan et al. 1998), and osteoclast inhibitory peptide-1 (OIP-1) or human Sca (hSca) for its involvement in inhibiting osteoclast formation (Choi et al. 1998).

To further add to the confusion, murine Sca-1 was ambiguously renamed Ly6a/e, possibly by the Patrice Hugo lab (Godfrey et al. 1992). A protein named Tsa-2 also exists, but it is unlikely that this protein is identical to Sca-1 as it has a mass nearly double that of Sca-1 as observed by western blot (Berzins et al. 1999). *Ly6a/e* was found to constitute two alleles of the same gene (now called *Ly6a*) that encode proteins that differ by 2 amino acids

and are respectively expressed by two different mouse strains. One allele of *Ly6a* has been called *Ly6a.1*, *Ly6e*, or *Ly6e.1* and is found in BALB/c mice. The second allele of *Ly6a* has been called *Ly6a.2* and is expressed by C57BL/6 mice (van Bragt et al. 2005). Interestingly, in a couple of publications from Alfred Bothwell's lab in which *Ly6a/Sca-1* was called *Ly6e*, *Ly6a* was found to also be induced by IFN in B cells and T cells (Khodadoust, Khan, and Bothwell 1999; Khodadoust et al. 1998). A human ortholog of *Ly6a* does not exist, despite inaccurate claims in the literature (Yu, Liang, and Liu 2017).

The earliest instance of human *TSA-1/SCA-2* being identified as *LY6E* occurred in April 2003 in a study examining genes highly expressed in blood samples from systemic lupus erythematosus (SLE) patients (Han et al. 2003). In July 2003, the chicken ortholog of *TSA-1/SCA-2* was also called *LY6E* in a study identifying it as a putative resistance gene to the chicken virus Marek's disease virus (Liu et al. 2003). In 2008, the International Committee on Standardized Genetic Nomenclature for Mice established new naming nomenclature for *Ly6* family genes which led to the subsequent identification of *Tsa-1/Sca-2* as *Ly6e* (Bult et al. 2008; Spindler et al. 2010).

LY6E is associated with diverse cellular processes

Functional study of *LY6E* spans several fields, ranging from modulation of immune cell signal transduction to regulation of placental development. Like other *Ly6* family members that drive multiple cellular processes such as *CD59* and *PLAUR*, the diverse functions of ubiquitously-expressed *LY6E* depend on interaction with distinct protein partners. Tissue- and developmentally-specific expression of several interactive partners

serves to compartmentalize LY6E function, such as specific expression of the TCR on T cells or syncytin A in the syncytiotrophoblast layer I of the developing placenta.

Murine Ly6e/Tsa-1 modulates TCR signaling to regulate thymocyte development

The lab of Toshiyuki Hamaoka further explored the role of murine Ly6e/Tsa-1 in T cells, as implicated by its expression on thymocyte precursors and putative role in T cell development. Like the labs of Jan Klein and Patrice Hugo, the Hamaoka lab began their study by producing a mAb that reacted with murine Tsa-1 (Kosugi et al. 1994). To generate the mAb, researchers injected hamsters with murine thymocytes and screened for reactivity of the subsequent hamster antibodies with thymocytes, which led to identification of the mAb PRST1. In the earliest study from the Hamaoka lab, Kosugi and colleagues found that PRST1 detected Tsa-1 on the cell surface of immature thymocytes, but not on peripheral naïve T cells which corroborates a previous study by Patrice Hugo's lab (Godfrey et al. 1992). The researchers confirmed that PRST1 detected Tsa-1 by performing cross-blocking experiments with another anti-Tsa-1 antibody, MTS 35, and by sequential immunoprecipitation. Incubation of peripheral T cells or splenic B cells with stimuli such as anti-CD3, lipopolysaccharides (LPS), or concanavalin A induced surface expression of Tsa-1 and increased mRNA levels. PRST1-treatment of a T cell hybridoma constitutively expressing Tsa-1 inhibited anti-CD3-induced IL-2 production but had no effect on these cells without anti-CD3 stimulation. Based on this observation, the researchers concluded that Tsa-1 is unable to act independently as a signaling molecule, but instead interacts with the TCR signaling pathway upon external activation of T cells.

In several follow up studies from the Hamaoka lab, researchers dissected the mechanism by which Tsa-1 modulates TCR signaling. Saitoh and colleagues discovered that Tsa-1-mediated inhibition of IL-2 production by activated T cell hybridomas is independent of GPI anchorage, as fusing the extracellular portion of Tsa-1 to the transmembrane domain of murine major histocompatibility complex class I (MHC I) had no effect (Saitoh et al. 1995). Furthermore, treatment with PRST1 reduced phosphorylation of CD3 ξ of stimulated T cell hybridomas, a key step downstream of TCR activation that occurs prior to IL-2 production. This finding was supported in a later study that demonstrated an association between Tsa-1 and CD3 ξ by immunoprecipitation and confocal microscopy using PRST1 and a novel rat mAb against Tsa-1, GR12 (Kosugi et al. 1998). Interestingly, only the Hamaoka mAb PRST1 blocked IL-2 production, as treatment of stimulated T cell hybridomas with the Hugo lab mAb MTS 35 or the Klein lab mAb E3 81-2 had no effect. Thus, researchers concluded that PRST1 recognized a functional epitope distinct from epitopes recognized by the other two anti-Tsa1 mAb. To assess the physiological role of Tsa-1 on T cells, the authors used freshly harvested T cells from spleen and co-cultured them with accessory cells (AC) from T-cell-depleted (anti-Thy-1 treated) spleen (Saitoh et al. 1995). AC from spleen are mostly comprised of B cells. As mentioned previously, freshly harvested peripheral mature T cells do not express Tsa-1 in the absence of anti-CD3 stimulation, whereas Tsa-1 is constitutively expressed on T cell hybridomas (Kosugi et al. 1994). Addition of PRST1 to the freshly harvested T cells co-cultured with AC surprisingly reduced IL-2 production. The authors concluded that this observation was due to the eventual induction of Tsa-1 expression over the course of the incubation period by anti-CD3, and thus

demonstrated that Tsa-1 engagement by PRST1 was related to TCR signaling in non-hybridoma T cells (Saitoh et al. 1995).

To test whether the observed association of Tsa-1 with the TCR was related to Tsa-1 expression on immature thymocytes, the Hamaoka lab examined the effect of PRST1 on preventing anti-CD3- and anti-TCR-mediated thymocyte apoptosis in newborn mice (Noda et al. 1996). Injection of anti-CD3 ϵ (2C11) or TCR β (H57) intraperitoneally into newborn mice reduced the overall number of cells in the thymus, which mirrors clonal deletion of early double-positive thymocytes by TCR signaling in early development. The additional injection of PRST1 alongside 2C11 rescued deletion of immature double-positive thymocytes, presumably due to PRST1-mediated inhibition of the TCR signal that results in clonal deletion of immature thymocytes. Interestingly, PRST1 was unable to rescue thymocytes from apoptotic cell death driven by glucocorticoids or irradiation, demonstrating that PRST1 specifically blocks TCR-mediated apoptosis.

The early studies on Ly6e in the late 1980's and 1990's ascribed an important role in regulating thymocyte development by association with and modulation of the TCR. A caveat to these studies is that the researchers assumed that antibody treatment activated Ly6e/Tsa-1 through ligation without considering that the large size of these mAbs (~150 kilodaltons or kDa) may instead sterically interfere with the interaction of Ly6e (~11 kDa) with CD3 ξ . Future studies should explore antibody-mediated blockade of Ly6e as an alternate hypothesis to the effects of anti-Tsa-1 on TCR activation. Since *Ly6e* is induced by IFN, additional studies to determine whether Ly6e expression affects the ability of T cells to respond to pathogen infection should also be performed.

LY6E modulates signaling on B cells, osteoclasts, and monocytes

In addition to expression on immature thymocytes, LY6E is also expressed on peripheral B cells. To evaluate the role of LY6E on B cells, the lab of Ethan Shevach also generated an antibody in hamsters that recognized murine Tsa-1, which they named C2F8 (Ding and Shevach 2001). Following up on a finding from the Hamaoka lab that showed that anti-Tsa-1 (PRST1) inhibited IL-2 production from co-culture of anti-CD3 stimulated freshly harvested T cells with AC, the Shevach lab tested whether this was due to Tsa-1 expression on the AC (splenic B cells) rather than the T cells (Saitoh et al. 1995). Instead of IL-2 production, the Shevach lab examined the effect of PRST1 on proliferation of the naïve splenic T cells, which occurs downstream of IL-2 ligation of CD25 (Smith et al. 1980). They separately cultured AC or T cells with C2F8 and observed that only pretreatment of AC, but not the T cells, decreased proliferation of the naïve T cells. A similar decrease in proliferation was observed when C2F8 was added during the co-culture, indicating that the observations by the Hamaoka lab was due to stimulation of AC, not of T cells. C2F8 treatment of AC was found to block induction of CD25 on T cells that is driven by engagement of TCR on T cells with Fc γ RIIB on AC. The authors concluded that Tsa-1 and Fc γ RIIB associate on the cell surface, as pre-incubation of the M12 B cell lymphoma cell line with either C2F8 or MTS 35 blocked subsequent staining with an anti-Fc γ RIIB mAb (2.4G2), whereas preincubation with other hamster mAbs 2C11 (anti-CD3 ϵ) or H1.2F3 (anti-CD69) had no effect. Overall, the findings by the Shevach lab revealed a role for Tsa-1 in

modulating the ability of B cells to promote T cell proliferation via association with B cell Fc γ RIIB.

To identify secreted factors produced by osteoclasts that regulate osteoclast formation and activity, the lab of Sakamuri Reddy expressed a cDNA library derived from purified human osteoclasts in human embryonic kidney cells (293) and screen for capacity to inhibit osteoclast-like multinucleated cell formation in mouse bone marrow cultures (Choi et al. 1998). This screening approach led to the identification of *osteoclast inhibitory peptide 1* (*OIP-1*), as conditioned media from 293 cells expressing this cDNA decreased osteoclast formation. The cDNA was subsequently found to be identical to *LY6E*. Expression of *OIP-1* mRNA was found to be highest in liver, although it was faintly detected in all other tissues probed. Curiously, the OIP-1-mediated inhibition was recapitulated with recombinant OIP-1 (rOIP-1) generated in *Escherichia coli* (*E. coli*) which lacks the GPI anchor, is not glycosylated, and contains the 32 amino acid hydrophobic C-terminus that is cleaved upon GPI anchor attachment in mammalian cells. Furthermore, while Choi and colleagues argued that GPI-anchored OIP-1 is cleaved by phospholipases and released into the supernatant to inhibit osteoclast formation, they were unable to detect secreted OIP-1 in supernatant from *OIP-1*-expressing cells. In a second study, the Reddy lab found that the cleaved 32 amino acid hydrophobic C-terminus of OIP-1 inhibits osteoclast formation by itself. This observation suggests that the ectodomain of OIP-1 is dispensable for inhibition of osteoclast formation and that the hydrophobic C-terminus is released into the supernatant during generation of the mature, GPI-anchored protein.

In a transcriptomic analysis of blood samples from patients with chronic HIV-1 infection, *LY6E* expression was found to correlate with disease progression as measured by low CD4⁺ T cell counts and increased frequencies of inflammatory CD38⁺CD8⁺ T cells (Xu et al. 2014). *LY6E* expression was lower in monocytes from patients receiving antiretroviral drug therapy (ART). Knockdown of *LY6E* in a monocytic cell line by shRNA resulted in increased expression of inflammatory genes, such as *IL1b*, *IL8*, *CD14*, and *Relb*. As CD14 helps TLR4 detect LPS, the researchers explored whether LY6E modulated cellular responses to LPS. Indeed, the immunosuppressive effects of *LY6E* expression appeared to be due to LY6E-mediated repression of *CD14* expression.

Overall, these studies demonstrate that LY6E can modulate signaling on T cells, B cells, osteoclasts, and monocytes in distinct ways.

LY6E is required for embryonic development in mice

In 2002, the lab of Brendan Classon attempted to generate a Ly6e/Tsa-1 knockout mouse by swapping the coding region of *Tsa-1* with a hygromycin phosphotransferase gene cassette (Zammit et al. 2002). While mice heterozygous for the *Tsa-1* null allele were viable, mating the heterozygous mice did not yield homozygous *Tsa-1*^{-/-} offspring. Genotyping of embryos by Southern blot revealed that *Tsa-1*^{-/-} offspring were fully resorbed by embryonic day 16 (E16). The *Tsa-1*^{-/-} embryos had normal thymus on E13.5, but the adrenal gland appeared disorganized which was associated with a respective absence and decrease in adrenaline and noradrenaline relative to wildtype counterparts. By E14.5 to E15.5, ruptured ventricles in the heart was observed and was concluded to be the ultimate cause of death in

the *Tsa-1*^{-/-} embryos. Interestingly, analysis of thymocyte development as measured by frequency appeared normal in the homozygous null mice. Overall, this study revealed that Ly6e/Tsa-1 plays an essential role in embryonic development, putatively through defective adrenal gland development.

The lab of Thierry Heidmann recently identified Ly6e in a cDNA screen as the receptor for syncytin-A (SynA), a mouse protein required for syncytiotrophoblast formation of the placenta (Bacquin et al. 2017). The researchers confirmed that Ly6e is necessary and sufficient for SynA-mediated cell to cell fusion, but that it is not a receptor for the structurally similar SynB. Expression analysis of murine tissues revealed broad *Ly6e* expression in adult tissues as established previously (MacNeil et al. 1993). Strikingly, *Ly6e* expression became highly expressed in placenta between E12.5 and E16.5, which was associated with a significant increase in *SynA*. The *in vitro* findings of the Heidmann lab were more recently complemented by a publication from the lab of David Simmons, which demonstrated that deletion of *Ly6e* resulted in abnormal placental architecture *in vivo* (Langford et al. 2018). A clever genetic approach was used to restore *Ly6e* expression specifically in the trophoblast of the placenta, which resulted in live healthy offspring. The researchers postulated that the cardiac defects observed by Brendan Classon's lab may be downstream of aberrant placental formation in *Ly6e*^{-/-} mice, a connection established in previous studies of peroxisome proliferator-activated receptor gamma (*Pparg*) and mitogen-activated protein kinase 14 (*Mapk14*) knockout mice.

Overall, recent studies have provided strong evidence for an essential role of Ly6e in placental formation, further demonstrating the diverse capabilities of the small Ly6 protein.

LY6E may be involved in the antiviral immune response

A small body of research using genetic, biochemical, and knockdown experimental approaches suggests that LY6E may be important for antiviral immunity. In a large-scale analysis of genetic susceptibility to HIV-1, a SNP occurring near the human Ly6 locus strongly associated with HIV-1 infectivity of lymphoblastoid B cells and primary T cells (Loeuillet et al. 2008). The murine Ly6 locus has also been mapped for susceptibility to mouse adenovirus type 1 (MAV-1) (Spindler et al. 2010). Furthermore, coding region polymorphisms in *Ly6e*, *Ly6a*, and *Ly6g* were identified in mouse strains that were susceptible to MAV-1, but not in resistant inbred strains (Stier and Spindler 2012). Chicken LY6E was identified as a candidate gene for Marek's disease virus (MDV) resistance, as it was found to interact with the MDV protein US10 in a *E. coli* two-hybrid screen using a cDNA library from activated splenic T cells (Liu et al. 2003). In the same study, commercial strain chickens were bred to be heterozygous or homozygous for a previously identified susceptibility locus which included a two-nucleotide substitution in the 3' untranslated region (UTR) of *LY6E*. The chickens were then challenged with MDV at one week of age. Surprisingly, chickens homozygous for the mutations were significantly more likely to succumb to MDV infection, indicating that this locus may affect *LY6E* expression required for resistance to MDV. In a clever screen using siRNA encoded by IAV to knockdown antiviral host genes *in vivo*, viruses that targeted mouse *Ly6e* had increased fitness, suggesting that Ly6e may be important for the antiviral response to IAV (Benitez et al. 2015).

Cumulatively, these studies suggest that LY6E from humans, chickens, and mice may be important for resistance to viral infection.

LY6E promotes viral infection

Several high-throughput screening efforts to respectively identify viral host factors and novel antiviral factors found that LY6E expression enhanced infection of viruses from multiple families. In a genome-wide siRNA screen, Krishnan and colleagues found that knockdown of *LY6E* decreased infection by WNV but not by DENV (Krishnan et al. 2008). Using an ectopic expression approach, Schoggins and colleagues found that lentiviral-mediated expression of *LY6E* in human *STAT1*-deficient fibroblasts enhanced the infectivity of yellow fever virus (YFV), WNV, DENV, IAV, O'nyong nyong virus (ONNV), HIV-1, and Chikungunya virus (CHIKV) (Schoggins et al. 2011; Schoggins et al. 2012; Schoggins et al. 2014).

Two recent mechanistic studies revealed a role for LY6E in enhancing entry of viruses from *Retroviridae* and *Flaviviridae* families. The lab of Shan-Lu Liu found that shRNA-mediated knockdown of *LY6E* impaired HIV-1 replication (Yu, Liang, and Liu 2017).. By using various reporter viruses, they found that knockdown of *LY6E* reduced HIV-1 internalization, Env-mediated membrane fusion, and viral gene expression in immortalized T cell lines. Furthermore, knockdown of *LY6E* also inhibited infection of phorbol 12-myristate 13-acetate (PMA)-treated immortalized monocytes (THP-1), which are typically used as a cell line model of macrophages, as well as untreated THP-1 which are treated as a monocytic cell line

In another recent mechanistic study, the lab of Sara Cherry observed that siRNA-mediated knockdown of *LY6E* impaired WNV infection (Hackett and Cherry 2018). Transfection of a WNV replicon that contained a GFP reporter in lieu of structural genes revealed that LY6E knockdown did not impair replication, which indicated an upstream effect on viral entry. Through further mechanistic study, Hackett and Cherry found that LY6E depletion did not reduce binding but restricted virus internalization. LY6E-mediated enhancement of viral entry was found to extend to like-sized transferrin-coated beads, but not smaller ligands such as transferrin. LY6E was subsequently found to be localized to microtubule-driven tubular structures during viral infection, which may be linked to the activity of end-binding 3 (EB3) which influences the rate of microtubule growth.

Overall, these recent studies indicate that ISG LY6E can promote infection of enveloped RNA viruses representing 4 distinct families. In contrast, previous studies of the LY6 locus and knockdown of *Ly6e* by a siRNA-encoding IAV in mice suggest that LY6E may participate in the antiviral response *in vivo*. Further study to understand how LY6E promotes viral infection may help reveal the contribution of viral enhancement to the antiviral immune response.

CHAPTER TWO

LY6E mediates an evolutionarily conserved enhancement of virus infection by targeting a late entry step

ABSTRACT

Interferons (IFNs) contribute to cell-intrinsic antiviral immunity by inducing hundreds of interferon-stimulated genes (ISGs). In a screen to identify antiviral ISGs, we unexpectedly found that LY6E, a member of the LY6/uPAR family, enhanced viral infection. Here, we show that viral enhancement by ectopically expressed LY6E extends to several cellular backgrounds and affects multiple RNA viruses. LY6E does not impair IFN antiviral activity or signaling, but rather promotes viral entry. Using influenza A virus as a model, we narrow the enhancing effect of LY6E to uncoating after endosomal escape. Diverse mammalian orthologs of LY6E also enhance viral infectivity, indicating evolutionary conservation of function. By structure-function analyses, we identify a single amino acid in a predicted loop region that is essential for viral enhancement. Our study suggests that LY6E belongs to a class of IFN-inducible host factors that enhance viral infectivity without suppressing IFN antiviral activity.

INTRODUCTION

Viral detection by the host cell triggers production of interferons (IFNs), a family of pro-inflammatory cytokines that contribute to the host antiviral response. IFN signaling

activates the transcription of hundreds of IFN-stimulated genes (ISGs), some of which encode known effector proteins that inhibit various stages of the viral life cycle. Although the first antiviral ISGs were discovered several decades ago, effector characterization has so far been limited to a subset of proteins. Recent advances in systematic screening strategies have accelerated discovery of novel antiviral ISGs (Schoggins et al. 2011; Schoggins et al. 2014; Liu et al. 2012; Dittmann et al. 2015). These screens have also revealed that a smaller subset of ISGs enhance viral infectivity through uncharacterized mechanisms.

We recently found that the ISG lymphocyte antigen 6 complex, locus E (LY6E, formerly RIG-E, SCA-2, TSA-1) enhances the infectivity of multiple enveloped RNA viruses (Schoggins et al. 2011; Schoggins et al. 2012; Schoggins et al. 2014). LY6E belongs to the LY6/uPAR superfamily, which consists of multiple proteins containing 8 to 10 cysteines that form a highly-conserved, three-finger folding motif through disulfide bonding (Lee et al. 2013). The LY6/uPAR superfamily is diverse and includes numerous LY6 proteins, complement regulatory protein CD59, and lipoprotein binding protein GPIHBP1 (Loughner et al. 2016; Tsetlin 2015). Like most LY6 family members, LY6E localizes to the cell surface via glycosylphosphatidylinositol (GPI) attachment (Classon and Coverdale 1994). Previous studies implicate LY6E in modulation of cell signaling (Saitoh et al. 1995; Koide et al. 2003; Mao, Hunt, and Cheng 2010), as well as a potential role in host susceptibility to viral infection (Krishnan et al. 2008; Xu et al. 2014; Loeuillet et al. 2008; Liu et al. 2003; Stier and Spindler 2012). LY6E has recently been shown to promote viral entry and replication of HIV-1 (Yu, Liang, and Liu 2017) and an early step of the virus life cycle for West Nile virus,

dengue virus, and Zika virus (Hackett and Cherry 2018). However, it remains unclear how LY6E enhances infectivity of other RNA viruses.

In the current study, we characterize the viral phenotype of LY6E. We show that LY6E enhances infectivity of multiple, enveloped RNA viruses in several cellular backgrounds. In mechanistic studies using influenza A virus as a model virus, we find that LY6E enhances viral uncoating after endosomal escape. Evolutionary analyses coupled with structure-function studies indicate conservation of enhancement by specific protein domains. We conclude that LY6E belongs to a growing class of IFN-inducible factors that broadly enhance viral infectivity in an IFN-independent manner.

RESULTS

LY6E enhances a subset of enveloped RNA viruses

In screens to identify ISGs that modulate viral infection, we previously showed that ectopic expression of human *LY6E* by lentiviral transduction enhanced the infectivity of multiple, genetically diverse viruses. These include members of the *Flaviviridae* (yellow fever virus (YFV), dengue virus (DENV), and West Nile virus (WNV)), *Togaviridae* (Chikungunya virus, O'nyong nyong virus (ONNV)), *Retroviridae* (human immunodeficiency virus, HIV-1) and *Orthomyxoviridae* (influenza A virus (IAV), strain PR8) families (Schoggins et al. 2011; Schoggins et al. 2014; Schoggins et al. 2012). Here, we confirmed that in immortalized human *STAT1*^{-/-} fibroblasts, lentiviral-mediated LY6E expression enhanced the infectivity of the fluorescent reporter virus YFV-17D-Venus after 24 hours, or approximately one replication cycle (Fig. 1a). We used *STAT1*^{-/-} fibroblasts as

these cells are unable to respond to IFN, thus allowing us to study LY6E independent of other IFN-inducible ISGs. To determine whether LY6E has effects beyond the first viral replication cycle, we infected LY6E-expressing cells with a low dose of YFV-17D-Venus and quantified the percentage of infected cells over time by flow cytometry. At every time point, we observed enhanced infection in LY6E cells as compared to control cells expressing either firefly luciferase (fluc) or empty vector control (Fig. 1b, c). The most striking difference in infection was a 300% increase observed at 36 hours post-infection, after the onset of viral spread. At this time point, we observed an increase in the percentage of infected cells expressing low levels of Venus, as reflected by mean fluorescence intensity (MFI) of the fluorescent reporter. Since newly infected cells express lower levels of viral antigens and virally-encoded Venus, our data suggest that these cells were recently infected with virus that was at an early stage of replication. To more precisely determine the effect of ectopic LY6E expression on virus production, we quantified the amount of a non-reporter virus (YFV-17D) secreted into cell supernatants over time by plaque assay (Fig. 1d). We consistently found that compared to empty vector control cells, cells ectopically expressing LY6E produced at least twice as much virus. Together, these time course studies indicate that LY6E enhances infection within the first viral replication cycle, which correlates with more rapid viral spread and overall increased virus production.

We further examined the effect of LY6E expression on viruses representing diverse families. In corroboration with our screen, LY6E enhanced DENV and ONNV infection (Schoggins et al. 2012; Schoggins et al. 2011). LY6E also increased infectivity of a non-reporter A/WSN/33 strain of IAV, the PRVABC59 strain of Zika virus, and a GFP reporter

vesicular stomatitis virus (VSV, Fig. 1e). We further validated our previous screening data suggesting that ectopic LY6E expression does not universally enhance infectivity of enveloped, single-stranded RNA viruses, as Sindbis virus (SINV), equine arteritis virus (EAV), and measles virus (MV) were not affected (Schoggins et al. 2014). Additionally, we observed no enhancement of a replication-defective adenovirus serotype 5 vector (AdV5), which is a non-enveloped, double-stranded DNA virus (Fig. 1f). These results demonstrate that LY6E enhances infection of a subset of enveloped RNA viruses from diverse viral families.

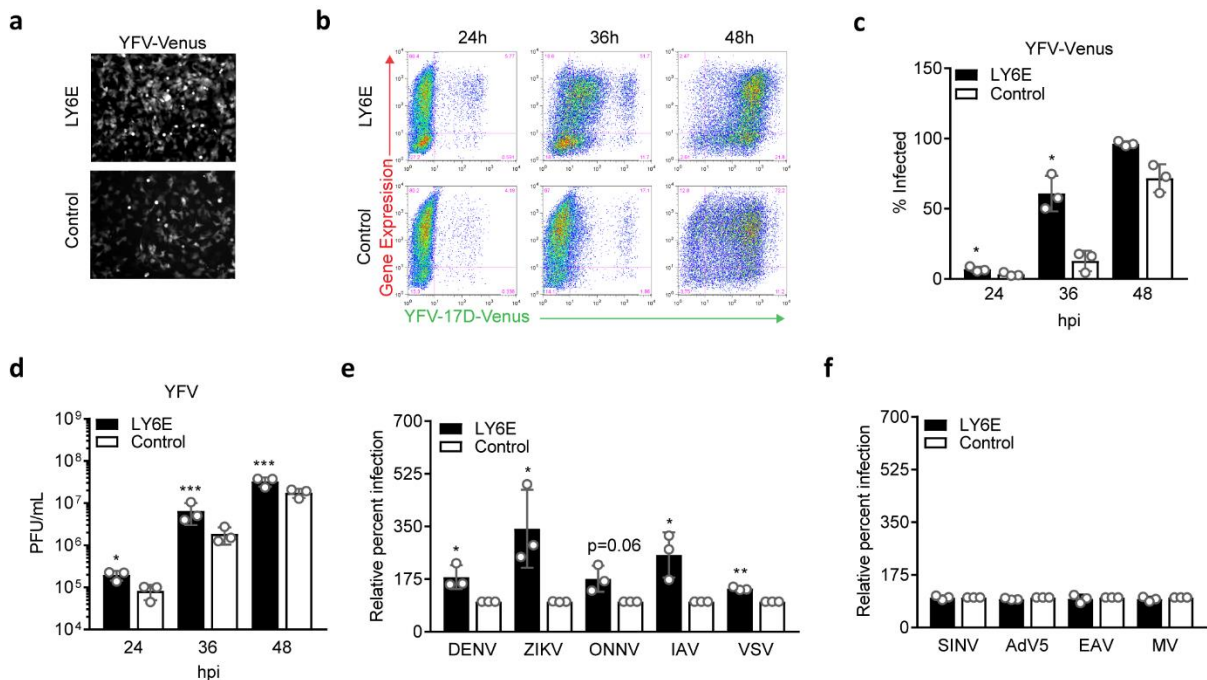


Figure 1. LY6E enhances infection by a subset of enveloped RNA viruses.

a *STAT1*^{-/-} fibroblasts transduced with lentivirus expressing LY6E or a fluc control were infected with 0.7 MOI YFV-17D-Venus and examined at 24 hpi by fluorescence microscopy. Scale bar, 100 μ M. **b** *STAT1*^{-/-} fibroblasts transduced with lentivirus

expressing LY6E or a fluc control were infected with YFV-17D-Venus (0.04 MOI) and harvested for flow cytometry at 24, 36, and 48 hpi. Representative pseudocolor dot plots are shown. **c** Quantification of YFV infection as described in **b**. $n = 3$ biological replicates. **d** *STAT1*^{-/-} fibroblasts transduced with lentivirus expressing LY6E or a fluc control were infected with YFV-17D (0.01 MOI). Supernatants were collected at 24, 36, and 48 hpi and titered on BHK cells by plaque assay. $n = 3$ biological replicates. **e** *STAT1*^{-/-} fibroblasts transduced with lentivirus expressing LY6E or empty vector control were infected with DENV2-GFP (0.005 MOI, 48h, control average 2.4% infection), ZIKV (PRVABC59, 1.2 MOI, 24h, average 13.5% infection), ONNV-GFP (0.2 MOI, 17h, control average 39% infection), IAV (A/WSN/33, 0.01 MOI, 8h, control average 12.3% infection), or VSV (0.2 MOI, 5h, control average 37.8% infection). Cells infected with IAV and ZIKV were permeabilized and respectively stained for NP or E protein. Percent infection was quantified by flow cytometry and is shown normalized to fluc or empty vector control. $n = 3$ biological replicates for each virus. **f** *STAT1*^{-/-} fibroblasts transduced with lentivirus expressing LY6E or an empty vector control were infected with SINV-GFP (S300, 0.2 MOI, 10h, control average 36.9% infection), Adv5-GFP (0.2 MOI, 24h, control average 74% infection), EAV-GFP (0.8 MOI, 19h, control average 22% infection), or MV-GFP (0.7 MOI, 24h, control average 61% infection). Percent infection was quantified by flow cytometry and is shown normalized to fluc or empty vector control. $n = 3$ biological replicates for each virus. * $p < 0.05$, ** $p < 0.01$, *** $p < 0.001$. SD is shown. For **c**, **d**, and **e**, ratio paired t-test was performed to determine statistical significance. Raw data for **d** was log transformed before analysis. Statistical analysis of **e** was performed prior to normalization.

LY6E enhances infectivity of monocytic and fibroblast cells

Because *LY6E* is ubiquitously expressed in multiple human tissues (Shan et al. 1998; Capone et al. 1996), we next sought to test whether ectopic LY6E expression enhanced viral infection in different cellular backgrounds. We observed a robust phenotype in immortalized human fibroblasts (HuFibr) and a moderate enhancement in a human osteosarcoma cell line (U2OS). The strong enhancement phenotype in both wild type and *STAT1*^{-/-} human fibroblasts indicates that the LY6E phenotype is independent of STAT1-mediated signaling. Ectopic LY6E expression in human lung adenocarcinoma cells (A549), human hepatoma cells (Huh7.5), human embryonic kidney cells (HEK293T), or Syrian baby hamster kidney

cells (BHK) did not enhance YFV (Fig. 2a). LY6E overexpression in the monocytic cell line THP-1 also enhanced susceptibility to IAV (Fig. 2b). We examined basal and interferon-induced protein expression of LY6E to determine whether we could discern a pattern underlying cell type dependency. Basal LY6E expression is detectable by Western blot in *STAT1*^{-/-} fibroblasts, HuFibr, U2OS, A549, and HEK293T. Basal expression is not observed in THP-1 or Huh7.5. Treatment with IFN α induced LY6E in THP-1, HuFibr, U2OS, and A549, but had no effect on protein expression in Huh7.5 or HEK293T. As expected, no induction was observed in *STAT1*^{-/-} fibroblasts (Fig. 2c). Overall, our data indicates that LY6E promotes viral infectivity in a cell type-specific manner, with the strongest phenotype in cells of fibroblast and monocytic lineages. This cell-type specificity appears unrelated to endogenous or IFN-inducible levels of LY6E.

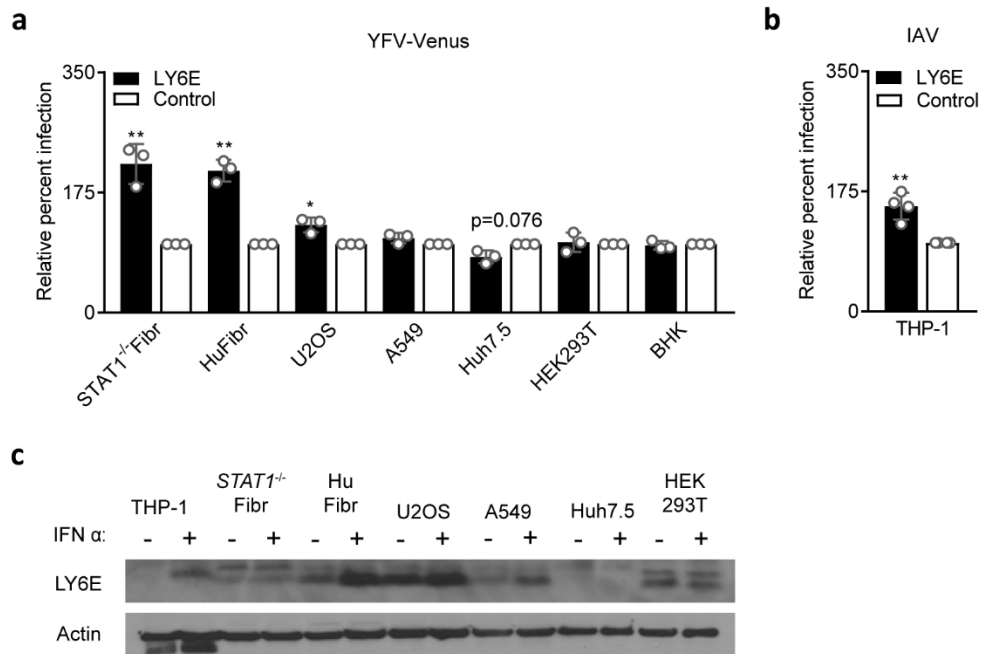


Figure 2. LY6E-mediated enhancement is dependent on cell type.

a LY6E or empty/fluc control constructs were expressed by lentivirus transduction in human *STAT1*^{-/-} fibroblasts, immortalized wildtype human fibroblasts (HuFibr), U2OS, A549, Huh7.5, HEK293T, and BHK-21J cell lines. Cells were infected with YFV-17D-Venus (between 0.3 and 1 MOI, 24h). Percent infection was quantified by flow cytometry and is shown normalized to control. *n* = 3 biological replicates. **b** THP-1 transduced with lentivirus expressing LY6E or fluc control were infected with IAV (A/WSN/33, 0.02 MOI, 8h). Cells were permeabilized and stained for NP. Percent infection was quantified by flow cytometry and is shown normalized to fluc control. *n* = 4 biological replicates. **c** THP-1, *STAT1*^{-/-} fibroblasts, HuFibr, U2OS, A549, Huh7.5 and HEK293T were mock treated or treated with 100 U/mL IFN α for 24 hours. Cells were lysed and probed for basal and IFN-induced LY6E as well as actin. * *p* < 0.05, ** *p* < 0.01. SD is shown. Data was analyzed prior to normalization by ratio paired t-test.

A related LY6/uPAR family member enhances YFV infection

LY6E is the first member of the LY6/uPAR protein family that has been validated in several studies to enhance viral infection. We performed phylogenetic analysis of several LY6/uPAR family member proteins of similar size and localization to LY6E (Fig. 3a, b). While all LY6/uPAR family members share a highly conserved three-finger tertiary structure, only a maximum of 49.64% similarity in primary amino acid sequence is observed between LY6E and its nearest neighbor, prostate stem cell antigen (PSCA). To test whether other LY6/uPAR family members enhance viral infection, we generated lentivirus encoding LY6 family members and transduced *STAT1*^{-/-} fibroblasts with a dose response of viral particles, with input normalized by p24 ELISA. Only PSCA enhanced infection of YFV-17D-Venus, while the expression of family members with less shared identity had no effect (Fig. 3c). Notably, PSCA was classified as a hit in a genome-wide siRNA knockdown screen to identify host factors important for WNV infection (Krishnan et al. 2008). Our results

Evolutionary analyses were conducted in MEGA7 (data generated by Ian Boys). **b** Amino acid sequence identity and similarity of a subset of LY6/uPAR family members relative to human LY6E. The full sequence including the signal peptide and cleaved hydrophobic C-terminus was used for this analysis. The analysis was conducted using Sequence Manipulation Suite (Stothard 2000) **c** *STAT1*^{-/-} fibroblasts transduced with 3 doses of lentivirus (1×10^4 , 5×10^4 , 2.5×10^5 infectious units or IFU) expressing LY6/uPAR family members or fluc control were infected with YFV-17D-Venus (0.5 MOI, 24h, control average 28.3% infection). Percent infection was quantified by flow cytometry and is shown normalized to cells transduced with 1×10^4 IFU fluc lentivirus. $n = 3$ biological replicates. *** $p < 0.0001$. SD is shown. Data was analyzed prior to normalization by ordinary two-way ANOVA with Dunnett's multiple comparisons test, which measured infectivity of LY6 family members relative to fluc control for each respective dose of lentivirus.

Loss of endogenous LY6E reduces viral susceptibility

To investigate the role of endogenous LY6E in viral infectivity, we used CRISPR/Cas9 to genetically ablate protein expression. IFN α treatment induced expression of endogenous LY6E in THP-1 cells, but not in a bulk population of THP-1 transduced with Cas9 and a guide sequence targeting exon 2 of LY6E (Fig. 4a). Loss of LY6E protein expression in the absence of IFN α treatment greatly reduced susceptibility to IAV, indicating that basal protein levels that are undetectable by Western blot can enhance viral infectivity (Fig. 4b).

We chose to further study endogenous protein in U2OS, which basally express high levels of LY6E without IFN treatment. We generated a clonal LY6E knockout (KO) cell line using CRISPR/Cas9 and confirmed by Sanger sequencing that each genomic LY6E allele contained nonsense mutations (Fig. 5a). We observed complete loss of LY6E at the protein level in the KO cell line relative to wild-type (WT) U2OS (Fig. 4c). In the absence of LY6E, infectivity of IAV and YFV was reduced but not completely abrogated (Fig. 4d). To

complement the CRISPR-based LY6E deletion, we carried out a similar line of experiments using siRNA to silence LY6E expression (Fig. 5b-e). Similar results were obtained, confirming that endogenous LY6E is not essential for viral infection, but is required for optimal viral infectivity.

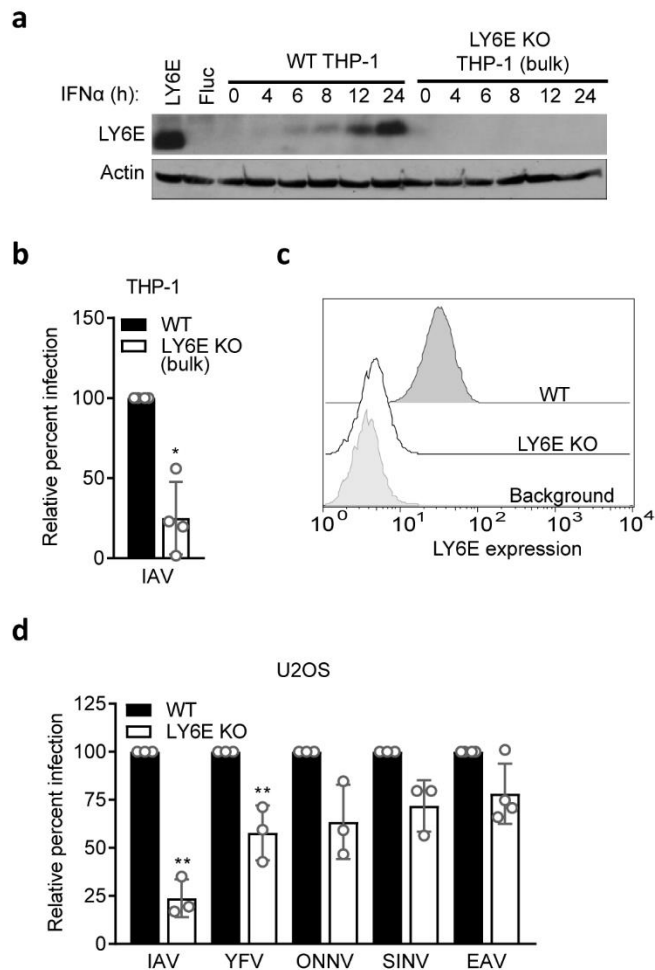


Figure 4. Loss of LY6E reduces but does not abrogate viral infection.

a WT THP-1 cells and a bulk population of THP-1 expressing a LY6E-specific guide sequence and Cas9 (LY6E KO) were treated with 100 U/mL IFN α and harvested at

indicated time points. LY6E and β -actin levels were assessed by Western blot. Lysates prepared from THP-1 ectopically expressing LY6E and fluc control constructs were used as positive and negative controls. Data is from one of three independent experiments. **b** Bulk LY6E KO and WT THP-1 were infected with IAV (A/WSN/33, 0.025 MOI, 8h, WT average 37.7% infection), then permeabilized and stained for NP. Percent infection was quantified by flow cytometry and is shown normalized to infection of WT THP-1. $n = 4$ biological replicates. **c** Cell surface levels of endogenous LY6E in LY6E KO and WT U2OS. Cells were stained with anti-LY6E antibody and analyzed by flow cytometry. Background levels were determined by staining with an isotype control. **d** LY6E KO and WT U2OS were infected with IAV (A/WSN/33, 0.32 MOI, 8h, WT average 27.9% infection), YFV-17D-Venus (0.6 MOI, 24h, WT average 50% infection), ONNV-GFP (0.5 MOI, 17h, control WT 18.9% infection), SINV-GFP (0.2 MOI, 10h, control WT 14.6% infection), and EAV-GFP (0.8 MOI, 19h, average 4.2% infection). Percent infection was quantified by flow cytometry and is shown normalized to infection of WT. $n = 4$ biological replicates for EAV and $n = 3$ biological replicates for IAV, YFV, ONNV, and SINV. * $p < 0.05$, ** $p < 0.01$. SD is shown. Data was analyzed prior to normalization by using student's unpaired t-test with Welch's correction.

a

LY6E KO U2OS cell line generated by targeting exon 2

```

TCGCTGATGTGCTTCTCCTGCTTGAACCCAGAAGAGCAATCTGTA
sgRNA
CTGCCTGAAGCCGACCATCTGCTCCGACCAGGACAACACTACTGC
GTGACTGTG
  
```

cDNA sequencing

```

WT | TCGCTGATGTGCTTCTCCTGCTTGAACCCAGAAGAGCAATCTGTA
   | CTGCCTGAAGCCGACCATCTGCTCCGACCAGGACAACACTACTGC
   | GTGACTGTG
   |
   | Allele 1
   | TCGCTGAT--TGGAAAAGAAA--TTGGGTGAGG--GATGGAA-C-----
   | ACA--CAGGAACCTGAGC--T--TG--TTTT-----
   | ---ACCAGGACAACACTACTGCGTGACTGTG
   | Allele 2
LY6E KO | TCGCTGATGTGCTTCTCCTGCTTGAACCCAGAAGAGCAATCTGTA
        | CTGCCTGAAGCCGACCATCTGCT-----
        | -----CCAGGACAACACTACTGCGTGACTGTG
        | Allele 3
        | TCGCTGATGTGCTTCTCCTGCTTGAACCCAGAAGAGCAATCTGTA
        | CTGCCTGAAGCCGACCATCTGCTCCGCAAGACTTCTTGGGTCC
        | TTTCTAGTACAACACTACTGCGTGACTGTG
  
```

Predicted protein products

```

WT protein aa 20 SLMCFSLNQKSNLYCLKPTICSDQDNYCVTV aa 51
Predicted mutant protein | Allele 1 SLIGKEIG*
                          | Allele 2 SLMCFSLNQKSNLYCLKPTICSRITTA*
                          | Allele 3 SLMCFSLNQKSNLYCLKPTIC SARLLGSFLVQLLRDVC*
  
```

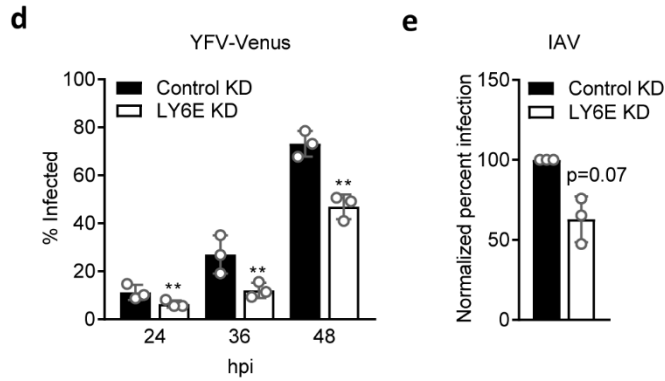
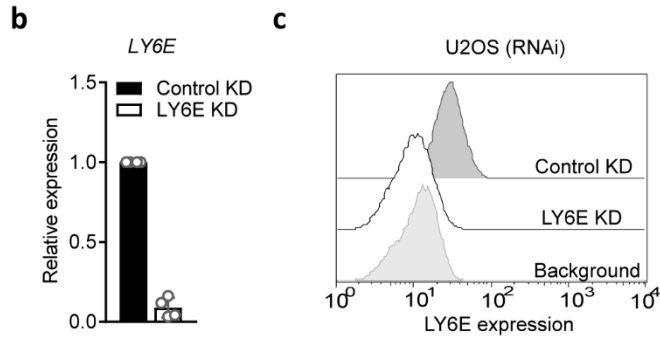


Figure 5. Genotype of LY6E KO cell line and LY6E knockdown studies.

a Sequencing of clonal LY6E KO U2OS cell line. The sequence used to design a guide RNA to target exon 2 is indicated in blue. Red indicates the protospacer adjacent motif (PAM) site that is required for Cas9 nuclease targeting. cDNA sequencing all alleles of LY6E from triploid LY6E KO U2OS is shown. Predicted protein product from each mutated allele is also shown. Italicized letters indicate inserted nucleotides. Hyphens indicate deletions or gaps in the sequence relative to allele 3. **b** *LY6E* expression in U2OS that have been reverse transfected with LY6E-targeting or a non-silencing control (NSC) siRNA. Expression was determined by RT-qPCR using the delta-delta CT method, normalizing to LY6E expression in NSC cells. $n = 3$ biological replicates. **c** Cell surface levels of endogenous LY6E in U2OS reverse transfected with LY6E-targeting or NSC siRNA. Cells were stained with anti-LY6E antibody and analyzed by flow cytometry. Background levels were determined by staining with an isotype control. **d** U2OS reverse transfected with LY6E and NSC siRNA were infected with YFV-17D-Venus (0.7 MOI) and harvested for flow cytometry at 24, 36, and 48 hpi. Percent infection was quantified by flow cytometry. $n = 3$ biological replicates. **e** U2OS reverse transfected with LY6E and NSC siRNA were infected with IAV (A/WSN/33, 0.31 MOI, 8h). Cells were permeabilized and stained for NP. Percent infection was quantified by flow cytometry and is shown normalized to NSC-transfected cells. $n = 3$ biological replicates. ** $p < 0.01$. SD is shown. For **d** and **e**, ratio paired t-test was performed prior to normalization.

LY6E does not regulate interferon-mediated gene expression

To assess whether LY6E could enhance viral infection via transcriptomic modulation, we used RNA-Seq to compare gene expression profiles of *STAT1*^{-/-} fibroblasts expressing an empty vector as a control versus cells expressing LY6E. Aside from ectopic LY6E expression, we observed no difference between the control and LY6E cells, indicating that LY6E does not influence the host transcriptome (Fig. 6a).

IFN induces the expression of negative regulatory genes, such as suppressor of cytokine signaling 1 (*SOCS1*), which can dampen antiviral IFN signaling and increase susceptibility to viral infection (Yoshimura, Naka, and Kubo 2007). To determine whether LY6E modulates the type I IFN response to enhance viral infectivity, we examined the effect

of endogenous LY6E on the antiviral state induced by IFN treatment in LY6E KO and WT U2OS. Loss of endogenous LY6E did not alter the protective dose-dependent effect of IFN pre-treatment on YFV infection. Additionally, calculated IC_{50} values were similar in both cell backgrounds (Fig. 6b). At increasing doses of IFN, viral enhancement by endogenous LY6E was lost, likely due to IFN-mediated induction of antiviral ISGs that masked the enhancement phenotype. Accordingly, IFN-induced expression of antiviral ISGs previously shown to inhibit YFV was unchanged between LY6E KO and control cells, further demonstrating that LY6E-mediated viral enhancement is independent of the type I IFN response (Fig. 6c) (Schoggins et al. 2011). This data is corroborated by IFN-stimulated response element (ISRE) reporter studies (Schoggins et al. 2014). Overall, our data suggest that LY6E acts in a direct manner to enhance viral infectivity, instead of in an indirect manner by influencing the cellular transcriptome or the IFN-mediated antiviral response.

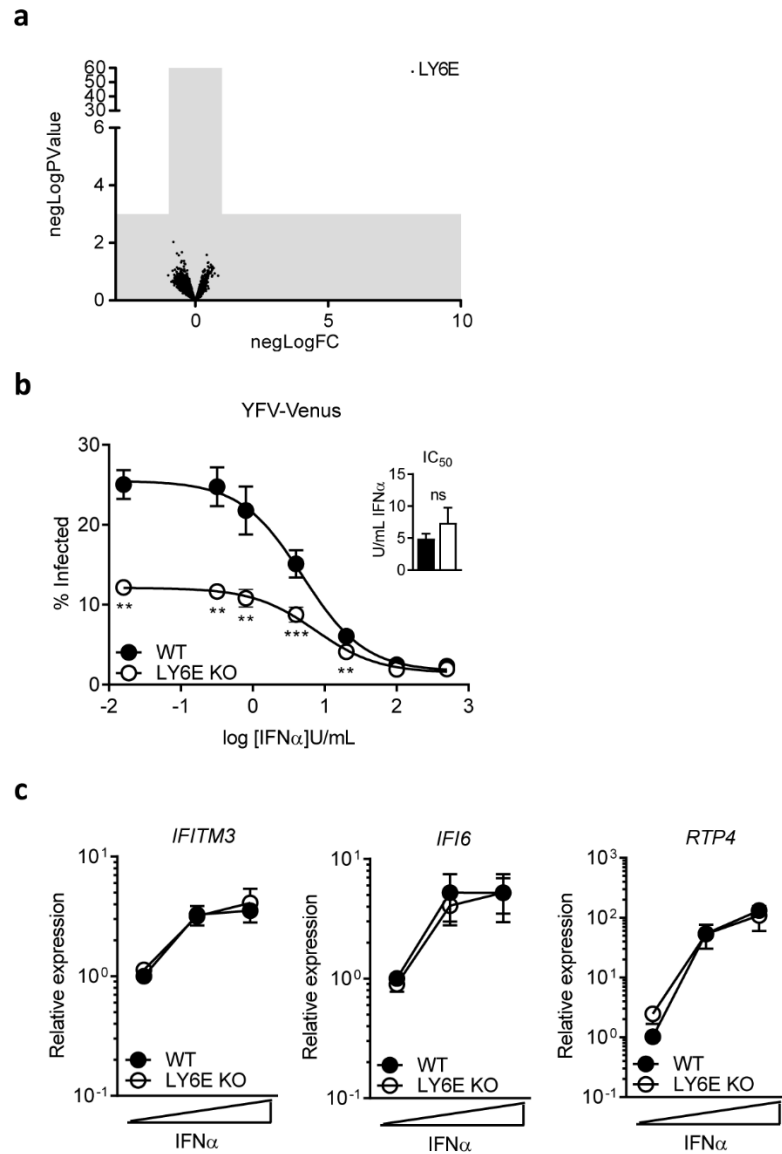


Figure 6. LY6E does not affect the global transcriptome or IFN signaling.

a RNA from $STAT1^{-/-}$ fibroblasts transduced with LY6E or empty vector control was isolated and submitted for RNA-Seq analysis. Log fold change (LogFC) is graphed against negative Log P value (negLogPValue). $n = 3$ biological replicates. **b** LY6E KO and WT U2OS were mock-treated or treated with 0.16 to 500 U/mL $IFN\alpha$ then infected with YFV-17D-Venus (0.43 MOI, 24h, $N=3$). Percent infection was quantified by flow cytometry. IC_{50} was calculated from nonlinear regression analysis using GraphPad Prism 5. LY6E KO $R^2 = 0.9535$. WT $R^2 = 0.9668$. $P=0.2082$. **c** LY6E KO and WT U2OS were treated for 4 hours with 0 to 500 U/mL of $IFN\alpha$ then lysed for RT-qPCR analysis of *IFITM3*, *IFI6*, and *RTP4* transcript induction. Expression was determined using the delta-

delta Ct method, normalizing to expression of the respective genes in untreated WT U2OS. $n = 3$ biological replicates. ** $p < 0.01$, *** $p < 0.001$. SD is shown. Data was analyzed by ratio paired t-test.

LY6E enhances yellow fever virus entry

As a cell surface protein, LY6E may function as a viral attachment factor or receptor. To test this hypothesis, we incubated *STAT1*^{-/-} fibroblasts expressing LY6E or empty vector control with increasing doses of YFV-17D at 4°C to block endocytosis and prevent viral entry. We observed no difference in bound viral RNA between LY6E and control conditions, indicating that LY6E does not affect YFV attachment to the cell surface (Fig. 7a).

To address the effect of LY6E on viral replication, we used a previously published subgenomic YFV-17D replicon assay (Jones, Patkar, and Kuhn 2005). In the replicon, the genes encoding structural proteins have been replaced with a *Renilla* luciferase (rluc) reporter gene. As a result, translation and replication of the subgenome can be inferred by quantifying rluc activity. The absence of structural proteins prevents the production of infectious virions, thereby decoupling viral entry and egress from genome translation and replication. *STAT1*^{-/-} fibroblasts expressing LY6E or fluc control were transfected with replicon RNA, and luciferase activity was quantified at multiple early and late time points, which respectively correspond to viral translation and replication. LY6E expression did not promote YFV replicon translation (2h to 6h) or replication (24h to 72h), whereas IRF1 potently inhibited luciferase activity at all time points (Fig. 7b) (Schoggins and Rice 2011).

To separate virus replication and production from earlier steps in the viral life cycle (attachment and entry), *in vitro*-transcribed viral RNA (YFV-17D) was electroporated

directly into *STAT1*^{-/-} fibroblasts expressing LY6E or empty vector control, bypassing endocytic entry pathways (Taguwa et al. 2015). After 24 hours, we measured replication by quantifying the MFI of YFV envelope protein (Fig. 7c). No difference was observed between *STAT1*^{-/-} fibroblasts expressing LY6E or empty vector control, corroborating our observation with the subgenomic YFV replicon that LY6E does not enhance viral replication. Virus-containing supernatants were also harvested 24 hours after electroporation and titer was determined by plaque assay. In contrast to the plaque assays presented in Fig. 1d in which supernatants were collected from cells that had been infected with intact YFV-17D virions, supernatants collected from *STAT1*^{-/-} fibroblasts expressing LY6E or empty vector control that had been electroporated with YFV-17D RNA had equivalent viral titers (Fig. 7d). Therefore, in the absence of viral uptake, LY6E does not enhance production of YFV.

In Fig. 1a-c, we showed that LY6E enhances YFV-17D-Venus infection by increasing the percentage of infected cells. However, when viral entry is bypassed by direct electroporation of YFV-17D-Venus RNA into *STAT1*^{-/-} fibroblasts expressing LY6E or empty vector control, we observe no difference in the percentage of Venus-positive cells (Fig. 7e). We conclude from these two experiments that the process of viral uptake is required for LY6E-mediated viral enhancement.

To further address the role of LY6E in viral entry, we used bafilomycin A1 (bafA), an inhibitor of endosomal acidification that blocks pH-dependent viral fusion (de Vries et al. 2011). YFV-17D-Venus virions that have already undergone endosomal fusion and escape before bafA treatment is able to replicate and express the Venus reporter. Because the number of internalized viral particles is limited by the capacity for attachment to the cell

surface, we analyzed infection after 48 hours to allow amplification of intracellular Venus expression for detection by flow cytometry. Addition of 5 nM bafA as early as 30 minutes after synchronized infection resulted in a greater percentage of Venus-positive cells in LY6E-expressing *STAT1*^{-/-} fibroblast populations than in control fluc-expressing populations (Fig. 7f). However, Venus MFI was the same in *STAT1*^{-/-} fibroblasts expressing LY6E as it was in cells expressing the fluc control, suggesting that viral uptake at the level of individual cells is similar in both cell backgrounds (Fig. 7g). Cumulatively, these mechanistic studies indicate that LY6E enhances YFV infectivity by affecting an early step in the viral life cycle that is after attachment to the cell surface but before viral translation, replication, and production.

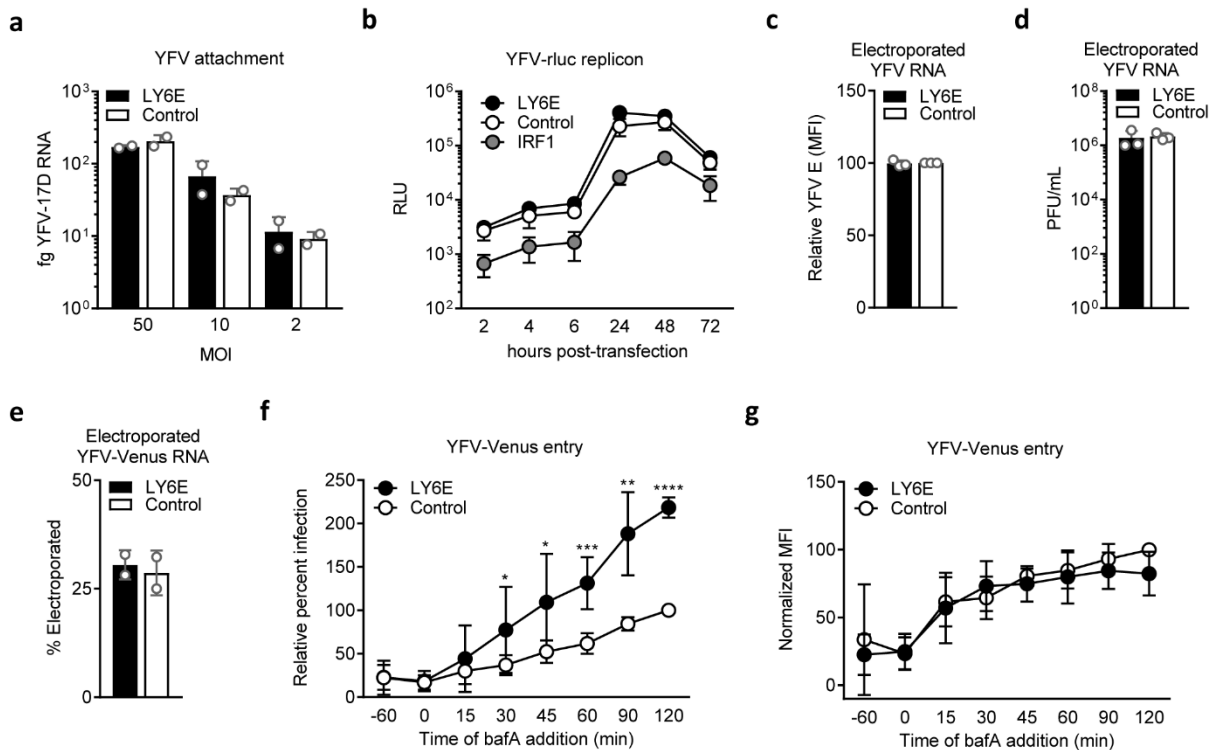


Figure 7. LY6E enhances entry of yellow fever virus.

a *STAT1*^{-/-} fibroblasts transduced with lentivirus expressing LY6E or an empty vector control were incubated with 50, 10, or 2 MOI YFV-17D at 4°C for 1h then harvested for RT-qPCR. *n* = 2 biological replicates. **b** *STAT1*^{-/-} fibroblasts transduced with lentivirus expressing LY6E, IRF1, or a fluc control were transfected with YFV-17D-rluc replicon RNA. Lysates were assayed for *Renilla* luciferase activity at the indicated time points. Relative light units (RLU) are shown. *n* = 3 biological replicates. **c** *STAT1*^{-/-} fibroblasts transduced with lentivirus expressing LY6E or an empty vector control were electroporated with YFV-17D RNA. Cells were permeabilized and stained for YFV E protein 24h after electroporation. Replication was measured by flow cytometry as MFI of E protein. Infection is shown normalized to cells expressing empty vector control. *n* = 3 biological replicates (data generated by Jennifer Eitson). **d** *STAT1*^{-/-} fibroblasts transduced with lentivirus expressing LY6E or an empty vector control were electroporated with YFV-17D RNA. Supernatants were collected 24h after electroporation and titered on BHK cells by plaque assay. *n* = 3 biological replicates (data generated by Jennifer Eitson). **e** *STAT1*^{-/-} fibroblasts transduced with lentivirus expressing LY6E or an empty vector control were electroporated with YFV-17D-Venus RNA. Percent electroporation was measured by flow cytometry as the percentage of cells that were Venus-positive. *n* = 2 biological replicates (data generated by Jennifer Eitson). **f** *STAT1*^{-/-} fibroblasts transduced with lentivirus expressing LY6E or a fluc control were incubated at 4°C for 1h with YFV-17D-Venus (0.7 MOI). Virus was aspirated and cells were washed and shifted to 37°C. BafA was added at indicated time points after the temperature shift. Cells were harvested 48h after the temperature shift, and flow cytometry was used to quantify percent infectivity. Infection is shown normalized to fluc control at 120 minutes. *n* = 4 biological replicates. **g** Quantification of replication for **f**, as measured by MFI of the Venus reporter. * *p* < 0.05, ** *p* < 0.01, *** *p* < 0.001, **** *p* < 0.0001. SD is shown. In **b**, data for LY6E and control were log10 transformed then analyzed by unpaired t-test with Holm-Sidak correction. Ratio paired t-test was used to analyze **f** and **g** before normalization.

LY6E enhances influenza A virus uncoating

To characterize the mechanism by which LY6E promotes infection of a virus unrelated to YFV, we next examined IAV. Using a similar cold-bind assay as for YFV, we observed that IAV attachment was not affected by LY6E expression (Fig. 8a). To evaluate the effect of LY6E on transcription and replication of IAV, we used a previously published minigenome assay (Hoffmann et al. 2011). IAV polymerase activity was unchanged by the

absence of LY6E in our clonal LY6E KO cell line relative to in WT U2OS (Fig. 8b). These data suggest that LY6E may enhance a post-attachment entry step of IAV, prior to the onset of replication.

IAV entry is composed of multiple steps: attachment, internalization, endosomal escape, capsid uncoating, and translocation of viral ribonucleoproteins (vRNP) into the nucleus. To determine if LY6E affects internalization of virus by endocytosis, we tagged IAV with a sulfo-NHS-SS-biotin tag which allows detection of viral particles by using streptavidin conjugated fluorophores (Rinkenberger and Schoggins 2018). Treatment with the cell-impermeable reducing agent tris(2-carboxyethyl)phosphine hydrochloride (TCEP) cleaves the disulfide bridge linker, efficiently removing the biotin tag from IAV attached to the cell surface but not from virus that has already been internalized. Infection of LY6E KO or WT U2OS with biotinylated IAV revealed equivalent levels of viral internalization (Fig. 8c).

After attachment and internalization, trafficking of endocytosed viruses through endosomal compartments results in exposure to low pH. For viruses that belong to the *Rhabdoviridae*, *Togaviridae*, *Flaviviridae*, and *Orthomyxoviridae* families, fusion of the viral envelope with the endosomal membrane is triggered by acidic pH (White and Whittaker 2016). To assess whether LY6E enhances endosomal escape, we used IAV labeled with lipophilic dye octadecyl rhodamine B (R18) at a concentration that results in self-quenching of the fluorescent signal. Upon fusion with the host endosomal membrane, R18 becomes diluted to the point of de-quenching, which results in a measurable fluorescent signal (Rinkenberger and Schoggins 2018). Pre-treatment with bafA, which blocks endosomal

acidification, resulted in attenuated IAV fusion. Endosomal escape was equivalent in LY6E KO and WT U2OS, indicating that LY6E does not enhance endosomal escape of IAV (Fig. 8d).

Fusion of the viral envelope with host endosomal membranes leads to release of encapsidated viral genome into the cytosol. To assess whether LY6E affects a process downstream of endosomal escape, we used an acid bypass assay, whereby low pH triggers viral fusion at the plasma membrane, thus bypassing endosomal entry. Exposure of cells to acidic pH had no effect on LY6E-mediated enhancement of IAV, suggesting that LY6E affects steps downstream of endosomal escape (Fig. 8e). Performing the acid bypass assay in LY6E KO and WT U2OS corroborated the overexpression data, further indicating that LY6E expression enhances IAV entry after endosomal escape (Fig. 8f).

Disassembly of the IAV capsid, or uncoating, can be monitored by staining for the M1 protein, which is a major component of the capsid. Dispersal of M1 in the cytosol increases accessibility to the monoclonal antibody HB64, resulting in a brighter cytoplasmic signal relative to the endosomal stain that is observed prior to uncoating (Banerjee et al. 2013; Martin and Helenius 1991). To assess the effect of LY6E expression on uncoating, we incubated *STAT1*^{-/-} fibroblasts with 25 MOI IAV at 4°C to synchronize infection. After 1 hour, unbound virus was aspirated and cells were shifted to 37°C in the presence of cycloheximide to prevent translation of nascent M1 protein. As a control, we also treated cells with a combination of bafA and cycloheximide to block endosomal escape and thus prevent uncoating. Cells were harvested at 1, 2, and 4 hours post-infection and stained with HB64. The percentage of cells with a bright M1 signal was assessed by flow cytometry.

Ectopic expression of LY6E increased the percentage of M1-positive cells relative to control, indicating that LY6E promotes IAV uncoating (Fig. 8g). When both LY6E and control cells were treated with bafA, fewer cells were identified as M1-positive. This reduction in M1-positive cells is consistent with M1 antigen from acid-exposed, uncoated IAV being more accessible to HB64 than M1 antigen from endosomal IAV.

After endosomal escape and uncoating, the segmented genome of IAV translocates into the nucleus, where it is transcribed and replicated. Each genome segment is associated with nucleoprotein (NP), to form viral ribonucleoproteins (vRNP). By staining for NP and nuclei, we can distinguish cytoplasmic and nuclear vRNPs after addition of bafA (Fig. 8h). We batch-compared ten thousand infected *STAT1*^{-/-} fibroblasts expressing LY6E or empty vector control for NP translocation into the nucleus. A low similarity score indicates cytoplasmic restriction of NP whereas a high similarity score indicates NP has completely translocated into the nucleus. When cells were pre-treated with bafA, *STAT1*^{-/-} fibroblasts expressing LY6E or fluc control had identical similarity scores, confirming that inhibition of endosomal acidification blocks viral escape and nuclear import of vRNP. When bafA was added as early as 10 minutes post-infection, a greater number of LY6E-expressing cells had nuclear vRNP as compared to control cells. By 2 hours, most LY6E-expressing cells showed complete overlay of NP and nuclear signals, indicating that the LY6E enhancing effect results in increased NP import into the nucleus (Fig. 8i, j). Because vRNP translocation is downstream of viral uncoating, we hypothesize that the enhancement observed in the ImageStream assay is likely a result of the uncoating phenotype, though we cannot rule out that LY6E may also directly affect vRNP nuclear import. Further experimentation in which

uncoating is uncoupled from vRNP nuclear translocation would be needed to distinguish these possibilities.

One common process shared by flaviviruses and IAV during viral entry is the use of clathrin-mediated endocytosis (CME) (Smit et al. 2011; Lakadamyali, Rust, and Zhuang 2004). To test if LY6E affects uptake of non-viral particles, we used the classic CME ligand transferrin conjugated to the pH-dependent fluorophore pHrodo (Tfn-pHrodo). LY6E KO and control U2OS had a similar percentage of cells positive for Tfn-pHrodo, indicating that non-viral CME is not influenced by LY6E expression (Fig. 8k). Expression of LY6E also had no effect on caveolar endocytosis of cholera toxin, subunit B (Fig. 8l) or micropinocytosis of dextran (Fig. 8m).

Cumulatively, our data shows that LY6E promotes viral entry by two enveloped RNA viruses from distinct families. While we were able to narrow the effects of LY6E to uncoating using IAV as a model, additional studies are needed to determine whether this mechanism applies to other viral families enhanced by LY6E expression.

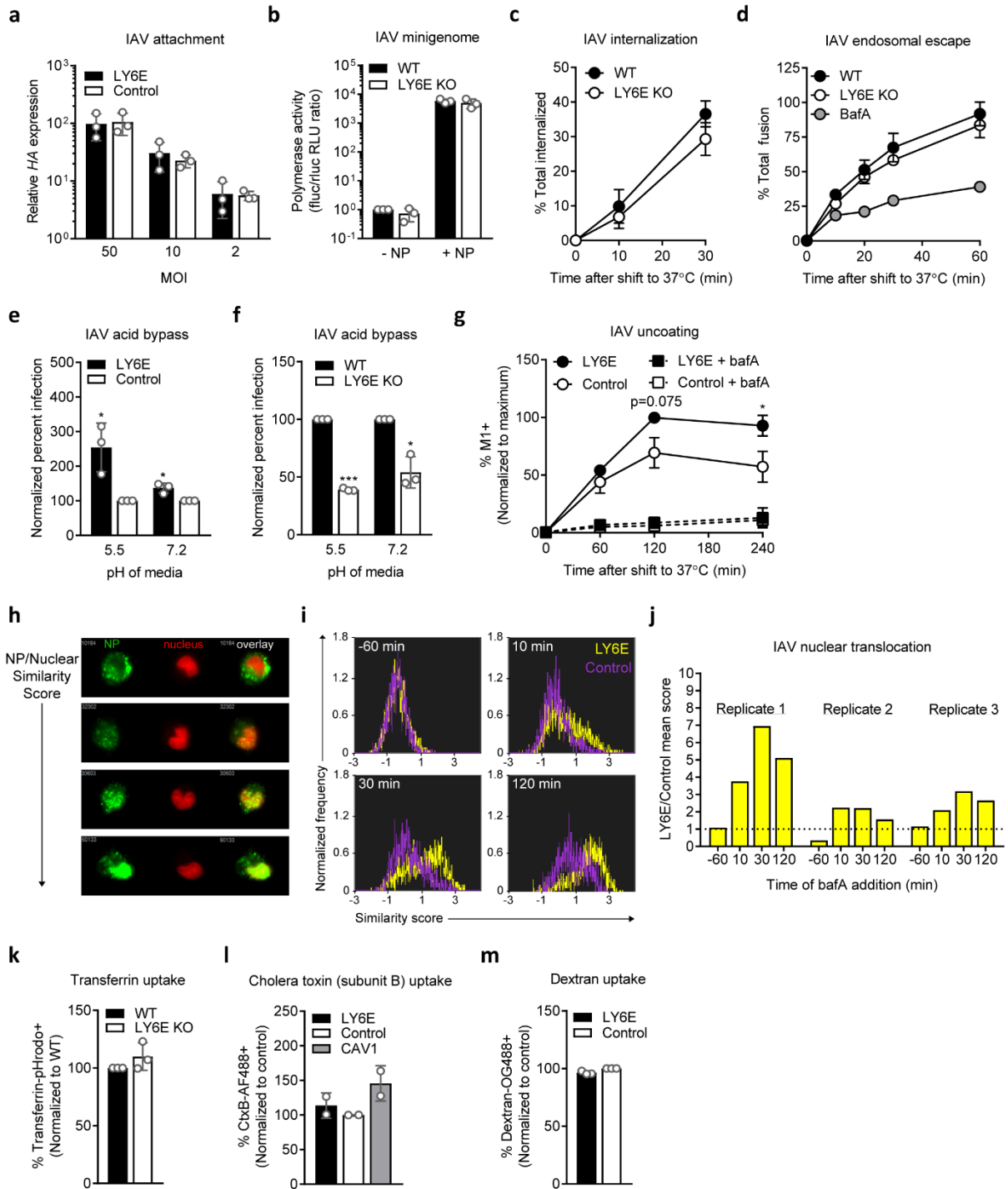


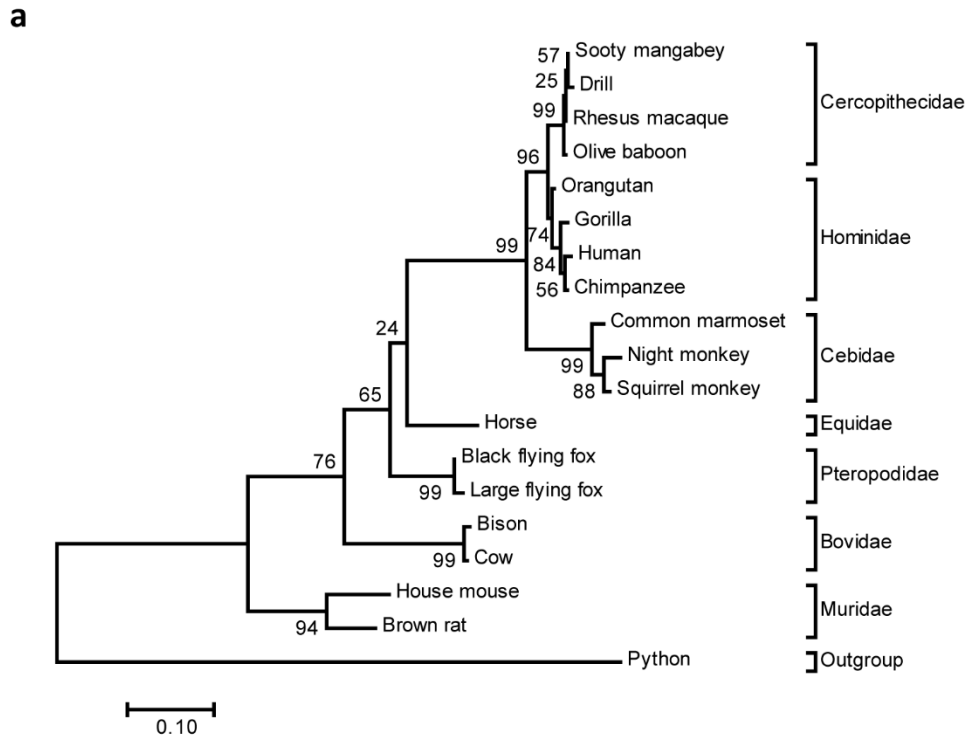
Figure 8. LY6E enhances entry of influenza A virus at the step of uncoating.

a Cold-bind of IAV with *STAT1*^{-/-} fibroblasts. Relative HA expression of each sample to 50 MOI fluc control is shown. *n* = 3 biological replicates. **b** U2OS were transfected with an IAV minigenome plasmid. The fluc/rLuc RLU ratio is shown normalized to the WT, no NP (-NP) condition. *n* = 3 biological replicates (data generated by John Schoggins). **c** Internalization of biotinylated IAV with U2OS. Percentage of IAV internalization was calculated relative to the signal from cells not treated with TCEP. *n* = 2 biological replicates (data generated by Nicholas Rinkenberger). **d** Endosomal escape of R18-labeled IAV with U2OS. Percentage of total fusion was calculated relative to maximal R18 dequenching. *n* = 4 biological replicates (data generated by Nicholas Rinkenberger). **e** Acid bypass of IAV with *STAT1*^{-/-} fibroblasts. Data is shown normalized to infection of control cells. *n* = 3 biological replicates. **f** Acid bypass of IAV with U2OS. Data is shown normalized to infection of WT cells. *n* = 3 biological replicates. **g** Viral uncoating as measured by M1 stain in *STAT1*^{-/-} fibroblasts. Data is shown normalized to maximum percentage of positive cells within each experiment. *n* = 3 biological replicates (data for one biological replicate generated by Ian Boys). **h** Representative images of NP stain from *STAT1*^{-/-} fibroblasts infected with IAV and treated with bafA at different time points by ImageStream. **i** Histograms indicating NP and nuclear signal overlay of IAV-infected cells as in **h** from Replicate 1. **j** Fold difference of inverse log mean NP/nuclear similarity scores from *STAT1*^{-/-} fibroblasts expressing LY6E relative to empty vector control. Scores are averaged from approximately 10⁴ cells per condition. **k** Transferrin uptake in U2OS. Data is shown normalized to WT control. *n* = 3 biological replicates. **l** Cholera toxin subunit B uptake in *STAT1*^{-/-} fibroblasts. Data is shown normalized to fluc control. *n* = 2 biological replicates. **m** Dextran uptake in *STAT1*^{-/-} fibroblasts. Data is shown normalized to fluc control. *n* = 3 biological replicates. * *p* < 0.05, ** *p* < 0.01, *** *p* < 0.001, **** *p* < 0.0001. SD is shown. Prior to data normalization, ratio paired t-test was used to determine statistical significance for **e**, **f**, and **g**.

Viral enhancement by LY6E is conserved across evolution

To gain insight into the significance of broad viral enhancement by an IFN-inducible gene, we tested whether the LY6E phenotype was conserved across evolution. First, we performed phylogenetic analysis on LY6E orthologs from 8 families (Fig. 9a, b). While LY6E is well conserved in primates, we observed a 24% or greater decrease in amino acid identity and 15% or greater decrease in amino acid similarity when comparing human LY6E to non-primate orthologs. We tested for conservation of the LY6E-mediated viral enhancement phenotype by using orthologs representing diverse mammalian families. We

expressed LY6E from Cercopithecidae (*Macaca mulatta* or rhesus macaque), Pteropodidae (*Pteropus alecto* or black flying fox), and Muridae (*Mus musculus* or house mouse) in human *STAT1*^{-/-} fibroblasts and compared enhancement of YFV-17D-Venus to that of human LY6E. All orthologs enhanced infection by YFV-17D-Venus relative to the control when expressed in a heterologous cell type (Fig. 10a). Furthermore, expression of both human LY6E and the *M. musculus* ortholog Ly6e in murine fibroblasts (3T3) enhanced YFV-17D-Venus infectivity relative to the control (Fig. 10b). Expression of the murine ortholog in LY6E KO U2OS partially restored viral infectivity (Fig. 10c). Collectively, our analyses reveal that viral enhancement by LY6E is functionally conserved in diverse mammals.



b

LY6E ortholog	Alignment length	Identical residues	Similar residues	Percent identity	Percent similarity
Chimpanzee	131	131	0	100.00	100.00
Orangutan	131	130	1	99.24	100.00
Gorilla	131	130	1	99.24	100.00
Rhesus macaque	131	127	3	96.95	99.24
Baboon	131	127	3	96.95	99.24
Drill	131	127	3	96.95	99.24
Sooty mangabey	131	127	3	96.95	99.24
Squirrel monkey	131	111	11	84.73	93.13
Common marmoset	131	109	11	83.21	91.60
Night monkey	131	109	11	83.21	91.60
Black flying fox	131	100	9	76.34	83.21
Horse	131	100	10	76.34	83.97
Large flying fox	131	99	9	75.57	82.44
Cow	131	92	10	70.23	77.86
Bison	131	91	10	69.47	77.10
Brown Rat	132	82	15	62.12	73.48
House mouse	132	80	17	60.61	73.48
Python	131	43	20	32.82	48.09

Figure 9. Phylogenetic analysis of LY6E orthologs.

a Molecular phylogenetic analysis of LY6E ortholog nucleotide sequences by maximum likelihood method. Bootstrap values resulting from 1000 replicates are shown next to the branches. The tree is drawn to scale, with branch lengths measured in the number of substitutions per site. Evolutionary analyses were conducted in MEGA7 (data generated by Ian Boys). **b** Amino acid sequence identity and similarity of a subset of LY6E orthologs relative to human LY6E. The full sequence including the signal peptide and cleaved hydrophobic C-terminus was used for this analysis. The analysis was conducted using Sequence Manipulation Suite (Stothard 2000) (data generated by Ian Boys).

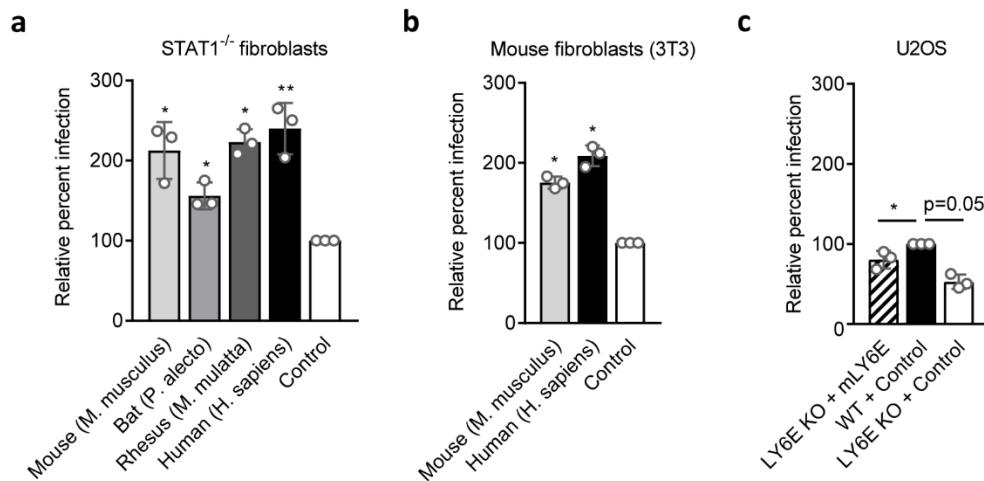


Figure 10. LY6E-mediated viral enhancement is conserved across mammalian species.

a *STAT1*^{-/-} fibroblasts transduced with lentivirus expressing human, rhesus, bat, or mouse LY6E orthologs or an empty vector control were infected with YFV-17D-Venus (0.25 MOI, 24h, control average 13.1% infection). Percent infection was quantified by flow cytometry and is shown normalized to infection of control cells. *n* = 3 biological replicates. **b** Mouse fibroblasts (3T3) were transduced with lentivirus expressing human or mouse LY6E or empty vector control were infected with YFV-17D-Venus (1 MOI, 24h, control average 5.5% infection). Percent infection was quantified by flow cytometry and is shown normalized to infection of control cells. *n* = 3 biological replicates. **c** LY6E KO and WT U2OS transduced with lentivirus expressing mouse Ly6e or empty vector control were infected with YFV-17D-Venus (0.6 MOI, 24h, control average 51.8% infection). Percent infection was quantified by flow cytometry and is shown normalized to infection of WT U2OS transduced with empty vector. *n* = 3 biological replicates. * *p* < 0.05, ** *p* < 0.01. SD is shown. Statistical analyses were performed before data normalization using repeated measures one-way ANOVA, with the Greenhouse-Geisser

correction and Dunnett's multiple comparisons test. Comparisons are relative to control for **a** and **b** and relative to WT + control for **c**.

Leucine 36 is essential for viral enhancement by LY6E

We hypothesized that the conservation of viral enhancement by LY6E orthologs may be due to sequence similarities. Initially we used an unbiased block mutagenesis approach in which stretches of approximately 4 amino acids within the mature LY6E protein were mutated to alanine (Fig. 11a, numbered blocks). The N-terminal signal peptide and post-GPI anchor hydrophobic C-terminus were not mutated for this experiment, as both segments are cleaved to produce the mature LY6E protein. Highly conserved cysteine residues contribute to disulfide bonding that is essential for the three-finger folding motif and were also not mutated. The block mutants were expressed in *STAT1*^{-/-} fibroblasts by lentiviral transduction and tested for loss of LY6E-mediated viral enhancement. Alanine mutagenesis of blocks 1, 4, 5, 7, 8, 12, 13, 19, and 20 reduced YFV-17D-Venus infection to control levels, indicating either disruption of structure or of function (Fig. 11b). A partial reduction of viral enhancement was observed when blocks 10, 11, and 18 were mutated to alanine, suggesting that residues in these regions contribute, but are not essential, for the viral phenotype of LY6E.

For targeted structure-function analyses, we narrowed our mutagenesis to the predicted loop regions based off a structural model derived from the crystal structure of the three-finger protein iridotoxin subunit B from Brown tree snake (*Boiga irregularis*, Fig. 12a). Analogous regions of other LY6/uPAR family members have previously been shown to be functionally important for intermolecular interactions (Kjaergaard et al. 2008; Lyukmanova

et al. 2013). Because LY6E orthologs from mouse, rhesus macaque, and bat enhanced YFV-17D-Venus infectivity to the same effect as the human protein, we hypothesized that conserved residues shared by the four orthologs may be important for the viral phenotype. We identified 9 loop residues of interest within blocks of amino acids that resulted in a loss of phenotype as shown in Fig. 7b, including blocks 4, 9, 10, and 11 (Fig. 11a and Fig. 12a, arrows indicate mutated residues). The mutations were cloned into human LY6E with a HA tag added immediately before the GPI anchored serine at position 101 (S101), and the resulting HA-tagged mutants were expressed in *STAT1*^{-/-} fibroblasts by lentiviral transduction. Input lentivirus was normalized between mutants by p24 ELISA. A partial loss of viral phenotype was observed with I57A. A complete loss of phenotype occurred with L36A, which fully recapitulated the loss of phenotype observed with mutagenesis of block 4 (Fig. 11c). To test whether these point mutations affected cell surface localization and protein expression, we used immunofluorescence and Western blotting to examine expression of the HA epitope. The point mutations had no effect on localization to the cell surface when compared to WT LY6E-HA (Fig. 12b). Several mutations, including L33A, L36A, N59A, and G64A reduced protein expression as detected by Western blot for HA epitope (Fig. 12c). Increasing protein expression of the L36A mutant by transducing with a greater amount of lentivirus did not rescue the viral phenotype relative to wild type LY6E, indicating the loss of phenotype is not due to impaired LY6E expression or stability (Fig. 11d and Fig. 12d). L36 was also required for enhancement of IAV, further demonstrating the importance of this residue (Fig. 11e). Overall, these structure-function analyses reveal L36 as an evolutionarily

magenta residues (RK): basic (except H); green residues (STYHCNGQ): have hydroxyl, sulfhydryl, or amine groups (plus G). Hyphens (-) indicate absence of a residue presents in other sequences. Consensus symbols indicate the following: * (asterisk) indicates a single, fully conserved residue, : (colon) indicates conservation between groups of strongly similar properties, . (period) indicates conservation between groups of weakly similar properties. **b** *STAT1*^{-/-} fibroblasts expressing LY6E block mutants as shown in **a**, WT LY6E, or fluc control were infected with YFV-17D-Venus (0.33 MOI, 24h, control average 33% infection). Infection is shown normalized to fluc control. *n* = 3 biological replicates. **c** *STAT1*^{-/-} fibroblasts expressing HA-tagged LY6E point mutant clones as shown in **a**, LY6E-HA, or fluc control were infected with YFV-17D-Venus (0.25 MOI, 24h, control average 16.4% infection). Infection is shown normalized to fluc control. *n* = 3 biological replicates. **d** *STAT1*^{-/-} fibroblasts were transduced with 5 volumes of lentivirus (two-fold increase per dose) expressing LY6E(L36A)-HA, LY6E-HA, or fluc control. Cells were infected with YFV-17D-Venus (0.25 MOI, 24h, control average 24% infection). Infection is shown normalized to fluc control (not shown) for respective lentivirus doses. *n* = 3 biological replicates. **e** *STAT1*^{-/-} fibroblasts expressing LY6E, LY6E (L36A), or CD59 were infected with IAV (A/WSN/33, 0.25 MOI, 8h, control average 17.4% infection) and stained for NP. Infection is shown normalized to CD59 as a control. *n* = 4 biological replicates. * *p* < 0.05, ** *p* < 0.01, *** *p* < 0.001. SD is shown. **b** and **c** were analyzed before normalization by repeated measures one-way ANOVA with Greenhouse-Geisser correction followed by Dunnett's multiple comparison test relative to WT LY6E. For **d**, ratio paired t-test was used to compare L36A and LY6E at equivalent doses of lentivirus prior to data normalization. Data for **e** was analyzed prior to normalization by repeated measures one-way ANOVA with Holm Sidak's multiple comparison test relative to WT LY6E.

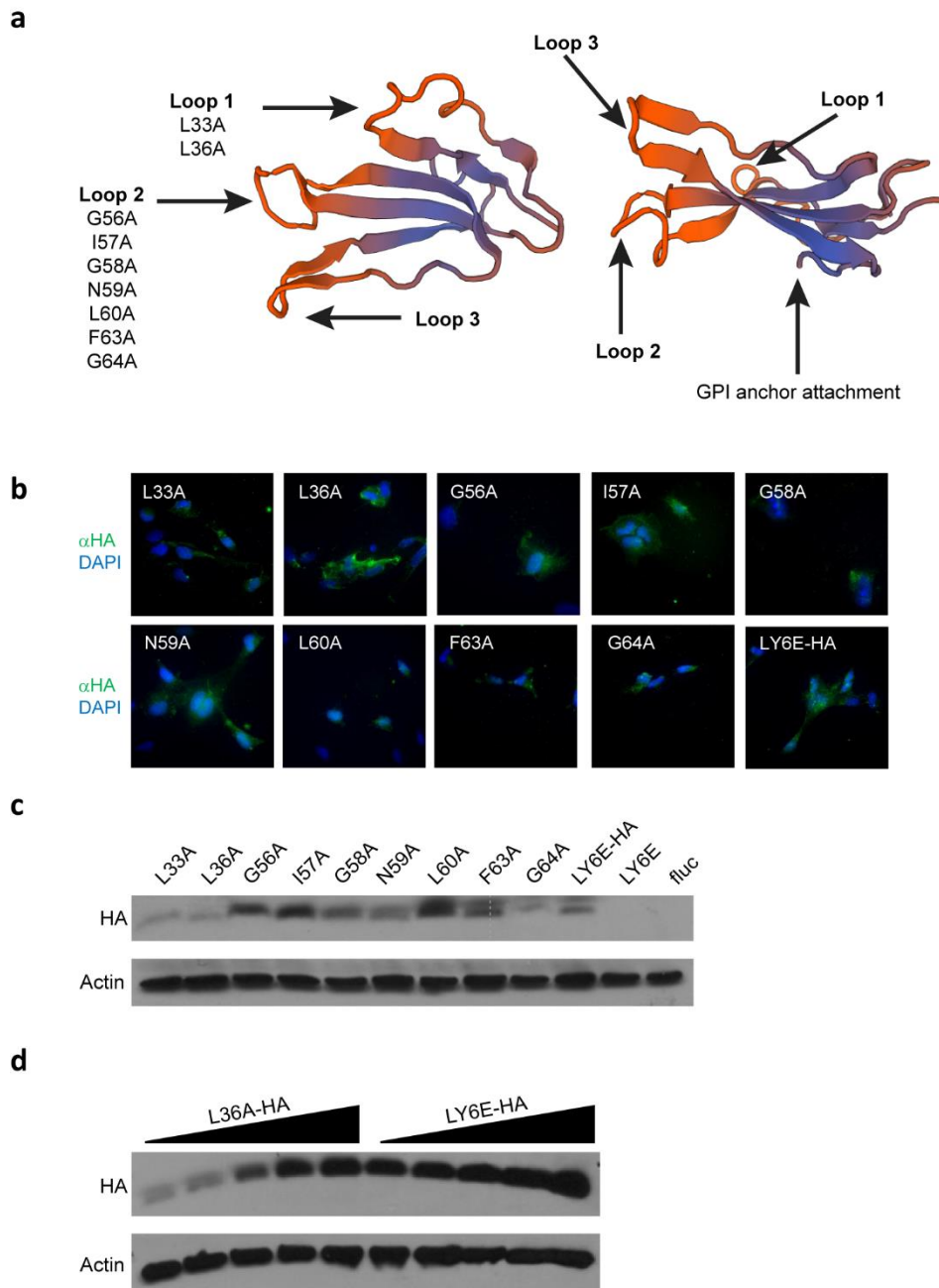


Figure 12. Site-directed mutagenesis of LY6E.

a Predicted structural model of LY6E rendered from a template of the structurally similar three finger protein iridotoxin subunit B (2h7z.1.B, 25.35% shared sequence identity) by using SWISS-MODEL (Biasini et al. 2014). Orange indicates low quality modeling while blue indicates high quality modeling. The model was assigned a QMEAN Z-score of -

2.13 which indicates that the model is comparable to what one would expect from experimental structures of similar size. LY6E point mutations are indicated at their respective loop regions. **b** *STAT1*^{-/-} fibroblasts expressing LY6E-HA or HA-tagged point mutants shown in **a**. The cell surface was probed for HA (green) and DAPI was added to stain nuclei (blue). **c** Whole cell lysates from *STAT1*^{-/-} fibroblasts described in **b** were lysed and probed for HA or actin expression. *n* = 1 of 3 biological replicates. **d** *STAT1*^{-/-} fibroblasts were transduced with 5 volumes of lentivirus (two-fold increase per dose) expressing LY6E (L36A)-HA or LY6E-HA. Cells were lysed and whole cell lysate was probed for HA or actin expression. *n* = 1 of 3 biological replicates.

DISCUSSION

The ISG LY6E has previously been implicated by us and others to modulate viral infection. In the data presented here, we demonstrate that LY6E enhances viral infection in a cell type- and virus-specific manner. Using YFV, we show that LY6E expression promotes viral uptake, thereby increasing the percentage of cells in a heterogenous population that become infected (Fig. 7f). In the context of IAV infection, we show that LY6E promotes uncoating of IAV (Fig. 8g), though this mechanism of enhancement may differ for other viruses (Yu, Liang, and Liu 2017; Hackett and Cherry 2018). We further show that LY6E expression also increases the rate at which IAV enters cells as measured by NP translocation into the nucleus, which may be dependent on enhancement of uncoating (Fig. 8j).

What factors contribute to the specificity of LY6E-mediated viral enhancement? We demonstrate here that LY6E promotes infection by several viral families, but that the phenotype does not extend to all enveloped viruses. This selectivity may be due to differences in both entry strategies and dependence on host machinery. As a small cell surface protein lacking a cytoplasmic tail, we hypothesize that LY6E requires interaction

with other plasma membrane-associated proteins to confer activity. The flexible three-finger motif may allow multiple interacting partners depending on cellular context, as has been previously demonstrated with the T cell receptor in lymphocytes (Kosugi et al. 1998), nicotinic acetylcholine receptor (Wu et al. 2015), or SynA (Bacquin et al. 2017). Dependence on an interacting partner may also explain our observation in Fig. 2a that the viral enhancement phenotype is absent in certain cell backgrounds. Furthermore, while we found LY6E expression to enhance VSV infection in STAT1^{-/-} fibroblasts, another group observed inhibition of VSV when LY6E was expressed in HEK293T kidney cells (Liu et al. 2012). We found that LY6E expression neither enhances nor inhibits YFV infection in HEK293T (Fig. 2a), leading us to hypothesize that the viral phenotype of LY6E is variable depending on cell background and virus. This hypothesis may also help explain the diverse effects attributed to LY6E, such as attenuating T cell receptor signaling (Saitoh et al. 1995), suppressing responsiveness to LPS stimulation (Xu et al. 2014), or supporting proper placental formation (Bacquin et al. 2017; Langford et al. 2018). As an IFN-inducible gene, the diverse functions of LY6E suggest that it may have pleiotropic effects that depend on cellular context.

LY6E may be one member of a growing class of ISGs that increases cellular susceptibility to viral infection, but whether the phenotypes in this class are all a result of viral hijacking remains unclear. Several ISGs that possess strong antiviral activity against diverse viruses can also be co-opted to promote infection by specific pathogens. IFITM3, which potently blocks entry of a broad range of viruses such as IAV, DENV, HIV-1, and Ebola virus (EBOV), can be used by human coronavirus OC43 as an entry factor (Zhao et al. 2014; Bailey et al. 2014). Viperin, which can be induced by several viruses independently of

IFN, blocks viral egress or replication of multiple viruses such as IAV, HIV-1, and DENV, but has also been shown to interact with human cytomegalovirus to enhance its infection (Seo et al. 2011; Helbig and Beard 2014). ISGs with regulatory function but without antiviral activity have also been co-opted to promote infection of specific viruses, such as suppressor of cytokine signaling 3 (SOCS3) which can bind to EBOV protein VP40 to facilitate egress (Okumura et al. 2015). The receptor tyrosine kinase AXL is an example of an ISG that enhances infectivity by multiple viruses (Meertens et al. 2012; Shimojima, Ikeda, and Kawaoka 2007; Morizono et al. 2011; Bhattacharyya et al. 2013), but is also essential for cellular antiviral immunity by contributing to dendritic cell (DC) maturation. *Axl*^{-/-} mice are more susceptible to IAV and WNV infection, indicating that the defect in DC maturation overshadows the effects of viral hijacking (Schmid et al. 2016).

In an alternate model to viral hijacking, LY6E may serve to promote viral uptake in certain cell types to accelerate or amplify innate and possibly downstream adaptive immune responses. This model would be consistent with data indicating that LY6E is ubiquitously expressed in multiple human tissues (Capone et al. 1996), and has been detected in multiple subsets of murine and human immune cells, both basally (Classon and Coverdale 1994; Antica, Wu, and Scollay 1997; Ding and Shevach 2001) and in response to IFN (Shan et al. 1998; Xu et al. 2014). Identification of LY6E as a signature ISG that is upregulated in samples from IAV-infected patients suggests a potential role in host immunity (Andres-Terre et al. 2015). Murine Ly6e was also identified by an *in vivo* RNAi screen as a potential contributor to the murine antiviral response to IAV, making an intriguing case for further study of LY6E in the context of an intact immune system (Benitez et al. 2015). Our

evolutionary analyses indicate functional conservation of the viral enhancement phenotype across distinct LY6E orthologs, which suggests a potentially beneficial role for the host. Whole body ablation of Ly6e has been reported to be embryonic lethal in mice due to defective placental formation (Zammit et al. 2002; Langford et al. 2018); therefore, we propose that mouse models in which Ly6e expression is ablated in specific cell types will be critical for testing complex models that are less tractable in cell culture systems.

METHODOLOGY

Cell lines

STAT1^{-/-} fibroblasts, C8 human fibroblasts (HuFibr) and THP-1 were grown in RPMI (Invitrogen) with 10% FBS/0.1 mM non-essential amino acids (NEAA- Life Technologies). U2OS, A549, 3T3, Huh7.5, HEK293T and MDCK cells were grown in DMEM (Invitrogen) with 10% FBS/0.1 mM NEAA. BHK-21J and Vero cells were respectively maintained in MEM (Invitrogen) supplemented with 10% FBS/0.1 mM NEAA and OptiPRO serum-free medium supplemented with 4 mM glutamine (Gibco). *STAT1*^{-/-} fibroblasts, C8 fibroblasts, BHK-21J, 3T3, U2OS, THP-1, Huh7.5, HEK293T and A549 stable cell lines were maintained with the addition of 4 µg/mL puromycin. U2OS and THP-1 KO cell lines were generated through transduction with lentiCRISPRv2-containing single guide RNAs predicted to target exons of LY6E and selected for 21 days in 2-4 µg/mL puromycin (Chen et al. 2015). For LY6E KO in U2OS, a single-cell clonal population was isolated by FACS (MoFlo, UTSW Flow Cytometry Facility Core) and subsequently validated and expanded. The clonal population was confirmed by isolation of genomic DNA and Sanger sequencing. *STAT1*^{-/-}

and C8 fibroblasts were a kind gift from J.-L. Casanova. MDCK, BHK-21J, Huh7.5 and Vero cells were a kind gift from C. Rice. 3T3 mouse fibroblasts cells were a kind gift from M. Diamond. THP-1, U2OS, A549, and HEK293T were obtained from the ATCC.

Viruses

YFV-17D-Venus and YFV-17D were generated by electroporating *in vitro* transcribed viral RNA into BHK-21J or *STAT1*^{-/-} fibroblasts cells as described previously (Lindenbach and Rice 1997). DENV2-GFP was generated by electroporating *in vitro* transcribed T7-RNA into Huh7.5 cells as described previously (Schoggins et al. 2012). IAV (A/WSN/33) virus was generated by inoculation of sub-confluent MDCK per protocol (Balish, Katz, and Klimov 2013). MV-GFP, SINV-GFP, EAV-GFP, and ONNV-GFP were generated as previously described (Schoggins et al. 2014). ZIKV-PRVABC59 was generated as previously described (Hanners et al. 2016). AdV5-GFP was kindly provided by Robert Gerard and propagated in E1A-complementing 293 cells. VSV-GFP was produced in BHK cells. Concentrated IAV was obtained per protocol with several modifications (Hutchinson and Fodor 2014). In brief, viral supernatant from infected MDCK was centrifuged once at 2000 x g for 30 min at 4°C and then subjected to ultracentrifugation (Sorvall Discovery 100SE, SW28 rotor) for 30 min at 18,000 x g at 4°C to pellet cell debris. Virions from the resulting supernatants were pelleted through a 5 mL 30% sucrose cushion by ultracentrifugation for 90 min at 112,000 x g at 4°C. Viral pellets were resuspended in a small volume of 1X NTC (0.1 M NaCl/0.02 M Tris-HCl, pH 7.4/5 mM CaCl₂) and then diluted into a larger volume of 1X NTC. Virus was finally pelleted by ultracentrifugation at 154,000 x g (SW40 rotor) for 60 min at 4°C.

Supernatant was aspirated and IAV was resuspended in a small amount of 1X NTC and titered in MDCK by plaque assay.

In vitro transcription of viral and replicon RNA

The following viral/replicon RNA were in vitro transcribed with mMessage mMachine SP6 kit (Ambion): YFV-17D-Venus RNA from XhoI-linearized YF17D(5'C25Venus2AUbi) plasmid(Jones et al. 2010), YFV-17D from XhoI-linearized pACNR-17D-Yfx(Bredenbeek et al. 2003), YFV-R.luc2A-RP replicon RNA from XhoI-linearized YFV-R.luc2A-RP(Jones, Patkar, and Kuhn 2005). The following RNAs were in vitro transcribed with mMessage mMachine T7 kit (Ambion): DENV2-GFP RNA from XbaI-linearized pDV2.IC30P.A.eGFP.P2AUbFIX plasmid(Schoggins et al. 2012). RNA was purified from the transcription reaction using RNeasy mini kit (Qiagen) and quantified by Nanodrop.

Pseudoparticle generation

Lentiviral pseudoparticles using the TRIP lentiviral backbone were generated as previously described(Schoggins et al. 2011). Stable cell lines were generated using the SCRPSY lentiviral backbone as described previously (Schoggins et al. 2012). When stated, p24 ELISA (Clontech) was used per manufacturer's instructions to normalize lentiviral input.

Transductions, infections, and plaque assays

One day before transduction 7×10^4 cells were plated into 24 well plates. The next day, cells were transduced with lentiviral pseudoparticles by spinoculation at 800 x g, for 45 min at

37°C in DMEM or RPMI containing 3% FBS/0.1 mM NEAA/20 mM HEPES/4µg/mL polybrene. Six hours after transduction, media was changed to 10% FBS/0.1 mM NEAA/RPMI or DMEM. THP-1 cells were transduced with RPMI containing 3% FBS/0.1 mM NEAA/20 mM HEPES/10 µg/mL polybrene and media was changed immediately after transduction to 10% FBS/0.1 mM NEAA/RPMI. Forty-eight hours post transduction SCRPSY stable cell lines were pooled in a 10 cm dish and allowed to reach confluency prior to addition of puromycin (titrated for each cell line, between 2-8 µg/mL). For transient transductions with TRIP construct lentiviruses, cells were split 1:3 (7-10x10⁴ cells) for infection approximately 48 hours post-transduction and infected the following day.

Infections were carried out in a minimum volume of complete media with 1% FBS for 1 hour (all viruses except IAV, MV, ONNV), and the infection was stopped by aspiration of virus and addition of fresh media. Infection with IAV was carried out in a minimum volume of 0.3% BSA/0.1% FBS/PBS++ for 1 hour, and the infection was stopped by aspiration of virus and addition of 0.3% BSA/0.1% FBS/0.1 mM NEAA/1 µg/mL TPCK/RPMI. Infections with MV were carried out for 2 hours in 1% FBS/media, followed by addition of complete media. Infections with ONNV were carried out for 1 hour in 1% FBS/media followed by addition of complete media. Adherent cells (all but THP-1) were dissociated with 200 µL Accumax (Sigma, diluted 1:4 in PBS for some *STAT1*^{-/-} fibroblast infections) and transferred to a 96-well V-bottom plate. Cells were pelleted at 800 x g for 2 min at 4°C and resuspended in 1% PFA for 10 min at room temperature or 30 min at 4°C. Cells were pelleted and resuspended in 3% FBS/PBS and kept at 4°C until FACS analysis. IAV-infected and ZIKV-infected cells

were permeabilized and respectively stained with a primary antibody reactive to IAV nucleoprotein (1:500-1:1000 anti-NP, MAB8251, Millipore) or with a primary antibody reactive to flavivirus E protein (1:1000 anti-E, D1-4G2-4-15, Millipore) and a goat anti-mouse secondary IgG antibody conjugated to AlexaFluor488 using Cytofix/Cytoperm Kit (BD Bioscience) per protocol. Samples were run in a Stratadigm S1000 flow cytometer with a A600 96-well plate high throughput extension and compensated using CellCapture software (Stratadigm). Data was analyzed with FlowJo software (Treestar). The flow gating strategy for infection with GFP-expressing viruses of cell lines expressing RFP and a gene of interest is included in Supplementary Fig. 8a.

For YFV plaque assays, *STAT1*^{-/-} fibroblasts were infected with YFV-17D for 1 hour. Viral supernatant was then removed and cells were washed twice with serum-free RPMI. 500 μ L complete medium was added to wells and harvested 24, 36, and 48 hours post-infection and stored at -80°C. Collected supernatants were thawed and diluted, then used to infect BHK-21J cells. After 1 hour infection with viral supernatants, 3 mL of overlay medium (0.1% NaHCO₃/4% FBS/10 mM HEPES/1.3% Avicel/1000 U/mL penicillin/1000 μ g/mL streptomycin/1X DMEM) was added to infected cells and allowed to incubate for 4 days at 37°C. After 4 days, 37% PFA was added to overlay medium/viral supernatant to fix cells. The supernatant was then aspirated and wells were stained with crystal violet to visualize plaques.

A similar method was used for titrating concentrated IAV preps. In brief, confluent layers of MDCK were infected with concentrated IAV diluted ten-fold for 1 hour at 37°C. Viral supernatant was aspirated and 3 mL of flu overlay medium (0.1% NaHCO₃/0.3% BSA/1% Avicel/1000 U/mL penicillin/1000 µg/mL streptomycin/2 µg/mL TPCK/1X DMEM) was added to infected cells and allowed to incubate for 2 days at 37°C. Cells were fixed and stained as described above to visualize plaques.

LY6E antibody staining

Cells were harvested with Accumax and fixed in 1% PFA as described above. Cells were then washed once in 3% FBS/PBS before incubating with primary antibody (1:250 anti-LY6E, HPA027186, Sigma, discontinued) for 30 min at 4°C. Cells were washed twice with 3% FBS/PBS before incubation with goat anti-rabbit secondary IgG conjugated to AlexaFluor594 for 30 min at 4°C. Incubation was followed with two washes and resuspension in 3% FBS/PBS pending FACS analysis.

Western blotting

Samples were washed once in 1X PBS before pellets were resuspended in cold RIPA (50 mM Tris, pH 8.0/150 mM NaCl, 0.1% SDS/2 mM EDTA/0.5% sodium deoxycholate/1% NP-40/1X cOmplete Protease Inhibitor Cocktail Tablets [Roche]) and sonicated at 20% power for 2 x 10 sec (Sonics Vibra-Cell Model CV188) Samples were subject to centrifugation at 10,000 x g for 10 min to remove cellular debris. The protein concentration of the remaining supernatants was quantified by bicinchoninic acid assay (Pierce),

normalized to a BSA standard curve, on a LUMIstar OPTIMA Microplate Reader (BMG LABTECH). 1X SDS loading buffer (63 mM Tris-HCl, pH 6.8/0.25% SDS/0.0025% bromophenol blue/10% glycerol/5% β -ME) was added and samples were boiled at 95°C for 5 min and frozen at -80°C. THP-1 lysates (25 μ g) were thawed and loaded into a low molecular weight tricine gel (running gel: 10% acrylamide/13.3% glycerol/0.1% SDS/1.0 M Tris base, pH 8.45/0.05% ammonium persulfate[AMPS]/0.05% tetramethylethylenediamine[TEMED]; stacking gel: 4% acrylamide/0.07% SDS/0.7 M Tris base, pH 8.45/0.08% AMPS/0.08% TEMED) and ran at 75-150 V in running buffer (0.1 M Tris/0.1 M tricine/0.1% SDS, pH 8.25 [inner chamber] and 0.2 M Tris, pH 8.9 [outer chamber]). Protein was transferred to PVDF membrane at 100V for 40 min at 4°C in transfer buffer (25 mM Tris/192 mM glycine/20% methanol). Membranes were blocked in 5% milk/TBST (10 mM Tris, pH 7.5/50 mM NaCl/0.1% Tween-20) for 30 min at room temperature before overnight incubation at 4°C in 1:1000 α LY6E (a kind gift from Jyoti Asundi, Genentech)/1:40,000 $\alpha\beta$ -actin (ab6276, Abcam) diluted in 5% milk/TBST. Membranes were washed 3 x 5 min in TBST then incubated for 30 min at room temperature with 1:2000 goat anti-mouse IgG conjugated to HRP and diluted in 5% milk/TBST. Membranes were again washed 3 x 5 min in TBST before ECL and preparation for film exposure and development. Uncropped blots are included in Supplementary Fig. 6a.

siRNA-mediated gene silencing

LY6E siRNA (Qiagen SI03019415) or Allstars Negative Control siRNA (Qiagen 1027280) at 5 nM were used for knockdown using HiPerfect Transfection Reagent (Qiagen) according

to the manufacturer's reverse transfection protocol for 6 well plates. Cells were collected 48 h after transfection and replated for infection in 24 well plates at a density of 70,000 cells per well for YFV-Venus infection and 150,000 cells per well for IAV infection.

RNA isolation and RT-qPCR

All RNA isolations were performed per protocol using RNeasy Mini Kit (Qiagen) with on column DNase (Qiagen) digest. 40 ng total RNA was analyzed by one-step RT-qPCR using QuantiFast SYBR Green RT-PCR kit (Qiagen) which was run on (Applied Biosciences 7500 Fast Real-Time PCR System) with the following program: 10 m at 50°C, 5 m at 95°C, 35 x (10 s at 95°C, 30 s at 60°C), followed by melting curve analysis. RT-qPCR primers were purchased from Qiagen (*LY6E*: QT00087521, *IFITM3*: QT00049238, *RTP4*: QT00202188, *IFI6*: QT00244503, normalized to *RPS11*: QT00061516).

IFN α IC₅₀ assay

LY6E KO U2OS and WT U2OS were plated in a 48 well plate at 32,000 cells per well. The next day, cells were pre-treated for 4 h with various amounts of human IFN α (PBL Interferon Source 11100-1) at 0.016 U to 500 U/mL diluted in 10% FBS/0.1 mM NEAA/DMEM. After 4 h, media was aspirated and cells were infected with YFV-17D-Venus for 1h at 37°C. Media was then aspirated and replaced with complete media. Infections were harvested 24 hpi for FACS analysis.

mRNA-seq

RNA from uninfected LY6E and control *STAT1*^{-/-} fibroblasts was isolated as described above and submitted to the UTSW McDermott Center Sequencing Core.

Samples were run on the Agilent 2100 Bioanalyzer to determine level of degradation thus ensuring only high-quality RNA is used (RIN Score 8 or higher). The Qubit fluorimeter was used to determine the concentration prior to starting library prep. Four micrograms of total DNase-treated RNA were then prepared with the TruSeq Stranded Total RNA LT Sample Prep Kit from Illumina. Poly-A RNA was purified and fragmented before strand specific cDNA synthesis. cDNA were then a-tailed and indexed adapters were ligated. After adapter ligation, samples were PCR amplified and purified with AmpureXP beads, then validated again on the Agilent 2100 Bioanalyzer. Before being normalized and pooled, samples were quantified by Qubit then run on the Illumina Hiseq 2500 using SBS v3 reagents. Samples were subject to single-end, 50 bp read length whole transcriptome sequencing with 35 x 10⁶ read coverage. The McDermott Center Bioinformatics Core used edgeR for differential expression analysis. Only genes that exceeded a logCPM of 1 were included for further statistical analysis using GraphPad Prism.

YFV cold-bind assay

One day after plating, transduced cells were equilibrated to 4°C for 30 min in complete medium. Media was then aspirated and YFV-17D diluted in cold 1% FBS/RPMI was added and incubated for 1 hour at 4°C. Cells were then washed 2 x with ice cold 1X PBS and harvested for RNA by RNeasy Mini Kit (Qiagen). Viral concentration was quantified by RT-

qPCR with published primers (Dash et al. 2012). A standard curve was generated by spiking in vitro transcribed YFV-17D-Venus RNA into a background of 40 ng uninfected cellular RNA and used to back-calculate fg YFV RNA for each sample based on C_T value.

YFV replicon assay

Transduced cells were plated at 35,000 cells per well in a 48 well plate the day before transfection. Viral replicon RNA was transfected into cells using the TransIT mRNA Transfection Kit (Mirus Bio) with a modified protocol (0.065 μ g viral RNA, 0.25 μ L mRNA Boost Reagent, 0.375 μ L *TransIT*-mRNA reagent, and 25 μ L serum-free Optimem [Gibco]). *Renilla* luciferase activity was quantified per protocol using the *Renilla* Luciferase Assay System (Promega) and LUMIstar OPTIMA Microplate Reader (BMG LABTECH).

YFV electroporation assay

STAT1^{-/-} fibroblast cell lines expressing LY6E or vector control were pelleted, washed twice with ice cold 1X PBS, counted, and diluted to 1.5×10^7 cells/mL in ice cold 1X PBS. Cells (6×10^6) were electroporated (BTX-Harvard Apparatus ECM 830 Square Wave Electroporator) with 5 pulses of 860 V, at 99 μ s, 1.1 sec intervals with 7.5 μ g YFV-17D or YFV-17D-Venus RNA. After 10 min, cells were plated on a 100 cm² tissue culture plate. Media was changed 6 hours post-electroporation to complete media. Supernatant and cells were harvested 24 hours later. Cells were washed, resuspended in PBS, stained for YFV E protein (4G2, Millipore MAB10216) and harvested for FACS analysis as described above. Supernatant was used to infect BHK-21J for plaque assay as described above.

YFV bafilomycin A1 entry time course

Transduced *STAT1*^{-/-} fibroblasts were plated at 70,000 cells per well in a 24 well plate the day before infection. Plates were equilibrated to 4°C on ice prior for 30 min to addition of YFV-17D-Venus diluted in cold 1% FBS/RPMI. Cells were cold-bound for 1 hour at 4°C and then washed twice with cold 1X PBS. Warm complete RPMI was then added and cells were shifted to 37°C. Bafilomycin A1 (Sigma) was added to cells at indicated time points for a final concentration of 5 nM. Infections proceeded for 48 hours before cells were harvested for flow cytometry.

IAV cold-bind assay

One day after plating, transduced cells were equilibrated to 4°C for 30 min in complete medium. Cells were incubated for 1 hour at 4°C with IAV (A/WSN/33) at the indicated MOI in cold 0.3% BSA/0.1% FBS/PBS++. Cells were washed 2 x with ice cold 1X PBS and harvested for RNA by RNeasy Mini Kit (Qiagen). Expression of *HA* was quantified by RT-qPCR with published primers (Rinkenberger and Schoggins 2018). Data shown is relative to the HA expression of cells transduced with fluc and bound with 50 MOI IAV.

IAV minigenome assay

The influenza A virus minigenome plasmids (pCAGGS-WSN-PB1, pCAGGS-WSN-PB2, pCAGGS-WSN-PA, pCAGGS-WSN-NP, pCAGGS-empty, and pPoll-Luc-GFP) have been described previously and were kindly provided by H. Hoffmann and P. Palese (PMID:

21436031) (Hoffmann et al. 2011). LY6E KO and WT U2OS were plated at 25,000 cells per well in a 48-well plate. The next day cells were transfected with the influenza A (A/WSN/33 strain) minigenome constructs pCAGGS expressing PB1, PB2, PA (25 ng each), NP (50 ng), the influenza virus-specific RNA polymerase I driven firefly-GFP dual reporter (pPolI-Luc-GFP) (37.5 ng), and a RNA polymerase II driven *Renilla* luciferase reporter pRLTK (Promega) (25 ng). In control wells, NP was replaced with pCAGGS-empty vector. Twenty-four hours post-transfection, cells were harvested and firefly luciferase and *Renilla* luciferase activity were assayed on a Berthold luminometer with the Dual Luciferase Assay kit (Promega).

IAV internalization assay

Biotin labeling of IAV and the subsequent internalization assay were performed as previously described (Rinkenberger and Schoggins 2018). In brief, concentrated IAV stocks were diluted to 1 mg/mL viral protein and labeled with sulfo-NHS-SS-biotin (Fisher). Labeled virus was purified by ultracentrifugation through a 30% sucrose cushion. Efficiency of labeling was determined using Pierce Biotin Quantitation Kit. LY6E KO and U2OS cells were incubated in suspension with biotinylated IAV (MOI 10) at 4°C to promote attachment. Cells were shifted to 37°C to permit endocytosis. At the indicated timepoints, 15 mM TCEP was added for 15 min at 4°C to cleave the biotin tag, and then cells were fixed with 1% PFA. Cells were permeabilized with 0.5% saponin, stained for 30 min with 1 µg/mL streptavidin conjugated to AlexaFluor488, and fluorescence intensity was quantified by flow cytometry.

IAV endosomal escape assay

R18 labeling of IAV and the subsequent endosomal escape assay were performed as previously described (Rinkenberger and Schoggins 2018). In brief, IAV pelleted through a 30% sucrose cushion was diluted to 100 µg/mL was labeled with 7.2 µM rhodamine B (R18). The labeled virus was filtered through a 0.22 µM filter and purified by ultracentrifugation on a 30-50% sucrose gradient. LY6E and KO U2OS were incubated at 4°C with R18-labeled IAV (MOI 10) to permit attachment. Unbound virus was removed, and cells were shifted to 37°C. At the indicated time points, 4% PFA was added to fix cells. Fluorescence intensity of the dequenched R18 signal was quantified by flow cytometry.

IAV acid bypass assay

The acid bypass assay was performed as previously described by others (Hackett et al. 2015). In brief, U2OS or *STAT1*^{-/-} fibroblasts were chilled on ice in culture media then incubated for 1 hour at 4°C with concentrated IAV (5 MOI) to allow binding. The cells were washed and incubated for 10 min in either 1X PBS at pH 5.5 or 1X PBS at pH 7.2. PBS was aspirated, replaced with warmed 10% FBS/0.1 mM NEAA/RPMI or DMEM, and cells were shifted to 37°C. To block spread, bafilomycin A1 at a final concentration of 5 nM was added to the cells 2 hours after the temperature shift. Cells were harvested 24 hours after the temperature shift, permeabilized, and stained for NP. Percent infection was quantified by flow cytometry.

IAV uncoating assay

STAT1^{-/-} fibroblasts expressing LY6E or an empty control vector were incubated with concentrated IAV (25 MOI) on ice for 1 hour at 4°C to allow binding. The virus was aspirated and warm media (0.3% BSA/0.1% FBS/1 mM cycloheximide/0.1 mM NEAA/RPMI) was added to cells prior to shifting to 37°C. Bafilomycin A1 at a final concentration of 5 nM was also added as a control when indicated. Cells were harvested at the indicated time points, fixed, permeabilized, and stained for M1 (1:25 HB64, a kind gift from Andrew Pekosz, Johns Hopkins University) with an AlexaFluor488 secondary. The percentage of M1-positive cells was quantified by flow cytometry.

IAV NP/nucleus co-localization by ImageStream

Stable *STAT1*^{-/-} fibroblasts were plated at 720,000 cells per well on 6 well plates that had been previously coated overnight with poly-lysine (10 mg/mL). Plates were equilibrated to 4°C on ice for 5 min prior to addition of 25 MOI concentrated IAV in 0.3% BSA/0.1% FBS/PBS++. Cells were incubated on ice with virus for 40 min. After the incubation, virus was aspirated and complete media (10% FBS/0.1 mM NEAA/RPMI) was added back and cells were shifted to 37°C. Bafilomycin A1 was added to a final concentration of 5 nM at indicated time points. After 2 hours at 37°C, cells were trypsinized and stained for NP-AlexaFluor488 as described above. The day of analysis, nuclei were stained with DRAQ5 (Life Technologies) at 20 µM final concentration. A minimum of 10,000 in focus cells were collected per sample using Amnis ImageStreamX (Millipore). Analysis of this data was carried out using IDEAS Software (Millipore). To calculate nuclear localization of NP, the mask function was first used to define nuclei based on DRAQ5 staining. We applied the

similarity feature, which is the log transformed Pearson's Correlation Coefficient, to measure the degree to which DRAQ5 staining and NP-AF488 signal are linearly correlated pixel by pixel within the masked nuclear region. The resulting similarity value is the NP/nuclear localization score.

Transferrin uptake assay

LY6E KO and WT U2OS were plated on a 6 well plate at 200,000 per well. Cells were incubated for 6 hours at 37°C to allow adherence to the plate. Cells were washed twice with PBS⁺⁺⁺⁺ (1 mM CaCl₂/1 mM MgCl₂/0.2% BSA/5 mM glucose/1X PBS pH 7.4) and incubated on ice for 10 min. pHrodoTM Red transferrin Conjugate (Fisher, P35376) was diluted in cold PBS⁺⁺⁺⁺ and incubated with cells for 10 min on ice. Cells were shifted to 37°C for 10 min to allow uptake. Cells were then harvested on ice and the percentage of transferrin-positive cells was determined by flow cytometry.

Cholera toxin uptake assay

STAT1^{-/-} fibroblasts stably expressing LY6E, empty vector, or CAV1 were plated at 150,000 cells per well on a poly-lysine coated 24 well plate. The next day, cells were washed twice with cold PBS. Cholera Toxin Subunit B (Recombinant), Alexa Fluor 488 Conjugate (Fisher, C34775) was diluted to 1 µg/mL in PBS⁺⁺⁺⁺ and incubated with cells on ice for 30 min. Cells were shifted to 37°C to allow internalization for 30 min. After incubation, cells were washed three times with cold acid (0.2 M acetic acid/0.2 M NaCl, pH 2.0) for 1 min per wash. Cells

were then harvested and the percentage of cholera toxin-positive cells was determined by flow cytometry.

Dextran uptake assay

STAT1^{-/-} fibroblasts stably expressing LY6E or fluc were incubated with 0.5 mg/mL 70,000 anionic dextran, Oregon Green 488 (Fisher, D7173) diluted in complete RPMI media for 15 min at 37°C. Cells were harvested on ice and percentage of dextran-positive cells was determined by flow cytometry.

Molecular phylogenetic analysis

LY6/uPAR ortholog sequences were selected based on similarity to LY6E, presence of a predicted GPI anchor, and possession of a single three finger protein motif. The evolutionary history was inferred by using the maximum likelihood method based on the JTT matrix-based model (Jones, Taylor, and Thornton 1992). The tree with the highest log likelihood (-3984.60) is shown. The percentage of trees in which the associated taxa clustered together is shown next to the branches. Initial trees for the heuristic search were obtained automatically by applying Neighbor-Join and BioNJ algorithms to a matrix of pairwise distances estimated using a JTT model, and then selecting the topology with superior log likelihood value. The tree is drawn to scale, with branch lengths measured in the number of substitutions per site. The analysis involved 11 amino acid sequences. There were a total of 212 positions in the final dataset. Evolutionary analyses were conducted in MEGA7 (Kumar, Stecher, and Tamura 2016).

LY6E ortholog molecular phylogenetic analysis

LY6E sequences from nineteen species were aligned using MUSCLE (Edgar 2004) as implemented in MEGA7 (Kumar, Stecher, and Tamura 2016). The alignment was manually curated to ensure preservation of coding sequences. A maximum likelihood phylogenetic tree was constructed by the HKY85 substitution model. The tree with the highest log likelihood (-2703.7050) is shown. Initial trees for the heuristic search were obtained automatically by applying Neighbor-Join and BioNJ algorithms to a matrix of pairwise distances estimated using the Maximum Composite Likelihood (MCL) approach, and then selecting the topology with superior log likelihood value.

The number of amino acid substitutions per site between sequences for the four indicated LY6E orthologs are shown. Analyses were conducted using the Dayhoff matrix-based model (Schwartz and Dayhoff 1979). All positions with less than 95% site coverage were eliminated. That is, fewer than 5% alignment gaps, missing data, and ambiguous bases were allowed at any position. There were a total of 131 positions in the final dataset. Evolutionary analyses were conducted in MEGA7.

Determining amino acid sequence identity and similarity

Protein sequences of select LY6/uPAR family members were obtained from UniProt (The UniProt 2018). LY6E ortholog nucleotide sequences were obtained from GenBank (NCBI) and translated to obtain the protein sequence using MEGA7 (Kumar, Stecher, and Tamura

2016). Both analyses were performed using the Ident and Sim feature of the Sequence Manipulation Suite (Stothard 2000).

Alignment of LY6E orthologs to determine conserved residues for alanine mutagenesis

Protein sequences of select LY6E orthologs were obtained from UniProt(The UniProt 2018). Clustal Omega was used to align the sequences (Sievers et al. 2011).

Structural prediction using SWISS-MODEL

The predicted structural model of LY6E was obtained using SWISS-MODEL (Biasini et al. 2014).

Immunofluorescence

STAT1^{-/-} fibroblasts transduced with lentivirus expressing LY6E point mutants were plated on poly-lysine coated chamber slides at 35,000 cells per well. Cells were fixed, stained with α HA epitope tag (16B12, BioLegend #901501) for 30 minutes, then a AF488-conjugated secondary antibody for 30 minutes. Cells were stained with DAPI for 5 minutes.

Statistical analyses

Statistical analyses were performed using GraphPad Prism version 7.02. Individual statistical tests are specified within the figure legends. All statistical analyses were performed prior to normalization. For data with two groups, two-tailed t-tests were used under the assumption of

normality. Grouped data with more than two groups were analyzed by analysis of variance (ANOVA) under assumption of normality.

Cloning

Overlap-extension PCR (OE PCR) was used to generate block and point mutations, as well as to add HA tags to LY6E and CD59. The published *P. alecto* Ly6e annotation was corrected by removing 99 amino acids prior to the predicted signal peptide, using OE PCR. BP arms were added to *M. musculus* Ly6e for Gateway cloning. All genes were transferred to Gateway-compatible pSCRPSY or pTRIP lentiviral backbones by LR reaction. sgRNA sequences for targeting LY6E were cloned into the lentiCRISPRv2 plasmid as detailed by the GeCKO protocol (Sanjana, Shalem, and Zhang 2014; Shalem et al. 2014). Appendix A contains a detailed list of primers.

CHAPTER THREE

Ly6e in alveolar macrophages contributes to the antiviral response

ABSTRACT

Influenza virus (IAV) is a global health concern due to its contagiousness and ability to cause severe lung disease. Years of intensive research using mouse models has established a requirement for a cellular immune response to successfully combat and clear a respiratory infection by IAV. In recent years, alveolar macrophages (AM) have been shown to be critical for survival of low inoculum IAV infections. As demonstrated recently by lab of Thomas Braciale, loss of AMs leads to increased lung pathology and death, but surprisingly does not affect viral burden (Cardani et al. 2017). Mechanistically, AMs were shown to protect type I alveolar epithelial cells (T1AEC) from viral infection and subsequent T cell-mediated killing. Protection from infection was conferred by an AM-secreted ligand that suppressed arachidonic acid metabolism and was independent of interferon, but putatively required infection of AM. My studies indicate that the ISG Ly6e promotes infection in AMs. Loss of Ly6e expression reduced *ex vivo* infectivity of isolated AMs in culture. Mice lacking Ly6e in AMs were more susceptible to a low dose of IAV infection. I hypothesize that Ly6e-mediated enhancement of IAV infection of AMs may help trigger production of the unidentified secreted factor that protects T1AEC and restricts immunopathology.

INTRODUCTION

Influenza A virus is an enveloped -ssRNA virus with a segmented genome that belongs to the family *Orthomyxoviridae*. In humans, IAV enters the respiratory tract via nasal and oral mucosa. Productive infection of the respiratory epithelium promotes viral spread to resident lung immune cells, such as AM, interstitial macrophages, and two subsets of DCs expressing either CD11b or CD103 (Iwasaki and Pillai 2014). Antigen presented by resident lung DCs to naïve T cells in the draining respiratory lymph nodes instigates IAV-specific adaptive immune responses. Cytolytic CD8⁺ T cells that target virally-infected epithelium help clear the infection at the cost of severe damage to the lung tissue (Hufford et al. 2015).

How alveolar macrophages contribute to the immune response to IAV remained unclear until recently. Chemical ablation of airway macrophages in pigs and ferrets have revealed that AMs are critical for surviving IAV infection (Kim et al. 2013; Kim et al. 2008). Furthermore, genetic and chemical ablation of AM in mice results in susceptibility to a low dose of IAV that is sub-lethal in AM-replete mice (Tumpey et al. 2005; Laidlaw et al. 2013; Purnama et al. 2014; Schneider et al. 2014; Cardani et al. 2017). A recent mechanistic study by the lab of Thomas Braciale revealed that AMs regulated the severity of IAV infection by producing an IFN-independent secreted factor that makes T1AEC resistant to IAV and subsequent targeting by cytolytic virus-specific T cells (Cardani et al. 2017). Depletion of AMs in this study did not affect induction of the adaptive immune response nor did it cause a significant increase in viral burden, indicating that the main cause of lethality is the loss of AM-mediated protection of T1AEC.

Cardani and colleagues also showed that AM-mediated protection of T1AEC may require IAV infection of AM (Cardani et al. 2017). Using a mouse model expressing the diphtheria toxin receptor under control of the CD11c promoter, they found that depletion of AMs by administration of diphtheria toxin on the day before or the day after infection increased susceptibility of T1AECs to IAV. However, depletion of AMs 2 days after infection did not alter infectivity of T1AECs, suggesting that AM-mediated protection occurs prior to this time point. The infection kinetics of AMs isolated from bronchoalveolar lavage fluid showed that infected AMs express IAV genes during this time frame, indicating that regulation of T1AEC susceptibility by AMs is associated with exposure of AMs to IAV. In further support of the hypothesis that protection is driven by infection of AM, incubation with only infected AM, but not naïve AM, was shown to restrict clathrin-mediated endocytic uptake of transferrin by a T1AEC cell line. The level of inhibition conferred by incubation with infected AM was statistically identical to treatment with the drug Acivicin that blocked arachidonic acid metabolism.

I have previously shown that LY6E enhances infection of IAV, specifically by promoting viral uncoating (Mar et al. 2018). To investigate whether viral enhancement by Ly6e *in vivo* has a net protective or deleterious effect, I generated conditional Ly6e knockout mice. Whole body knockout of Ly6e is embryonic lethal, due to defective formation of the fetal-maternal placental interface that results in cardiac failure *in utero* (Langford et al. 2018). Thus, I generated mice with *Ly6e* ablation in the CD11c- and LysM-expressing compartments to target resident DCs and lung macrophages that constitute the first subsets of cells to encounter IAV *in vivo*. AM harvested from these mice were less susceptible to IAV

infection, corroborating my observation *in vitro* that expression of murine *Ly6e* enhances IAV infectivity (Mar et al. 2018). Infection of these mice revealed a moderate increase in susceptibility that was most pronounced at a sub-lethal dosage. My data so far suggests that *Ly6e* in AMs may contribute to protection against sub-lethal IAV infection.

RESULTS

Generation of Ly6e conditional knockout mice

To generate targeted mice, I obtained $Ly6e^{tm1a(EUCOMM)Hmgu}$ mouse embryonic stem (ES) cells from the European Conditional Mouse Mutagenesis Program (EUCOMM). In these ES cells, the wildtype locus of *Ly6e* was replaced by homologous recombination with a targeting cassette that added conditional knockout potential through Cre recombinase (Cre)-mediated targeting of exon 2 (Fig. 13a). The unmodified targeting cassette was designed to generate a null allele through splicing of exon 2 to a *lacZ* trapping element contained within the gene targeting cassette, resulting in a ‘knockout-first’ design (Skarnes et al. 2011). I acquired the services of the UTSW Transgenic Technology Core facility to scale up the ES cells from frozen stocks and to generate chimeric mice. Injection of ES cells into blastocysts does not guarantee germline transmission; thus, I crossed the chimeric mice with WT C57BL6/N mates until I obtained mice heterozygous for the $Ly6e^{tm1a(EUCOMM)Hmgu}$ allele. I crossed the heterozygous mice to $Gt(ROSA)26Sor^{tm1(FLP1)Dym}$ mice that constitutively express the enhanced variant of *Saccharomyces cerevisiae* FLP1 recombinase (FLPe) under control of the ubiquitous *Rosa26* promoter. Exposing the $Ly6e^{tm1a(EUCOMM)Hmgu}$ allele to FLPe led to excision of the FLP recombination target (FRT)-flanked gene targeting cassette, which

resulted in production of mice bearing the conditional allele of *Ly6e* (Fig. 13b). The mature *Ly6e*-encoding mRNA that is expressed by mice homozygous for this allele (*Ly6e^{fl/fl}*) is identical to that which is expressed by mice with the WT *Ly6e* locus.

To generate conditional knockout mice, I crossed the *Ly6e^{fl/fl}* mice to C57BL/6J mice expressing Cre under control of lysozyme 2 gene (*Lysz2* or *LysM*) or integrin alpha X gene (*Itgax* or *CD11c*). *Ly6e^{fl/fl}* mice that are hemizygous for the *LysM*-cre transgene were predicted to express the knockout allele in alveolar macrophages, peripheral macrophages, neutrophils, and about half of blood monocytes. In comparison, *Ly6e^{fl/fl}* mice that were hemizygous for *CD11c*-cre were predicted to express the knockout allele in alveolar macrophages, a subset of peripheral macrophages, splenic DCs, and a small subset of blood monocytes (Abram et al. 2014). To confirm loss of *Ly6e* expression in the targeted cells of interest, I harvested AMs from bronchoalveolar lavage fluid and plated them on tissue culture-treated plastic, which results in a relatively pure population of AM (Chavez-Santoscoy et al. 2012; Jhingran, Kasahara, and Hohl 2016). Analysis of *Ly6e* expression in these cells by RT-qPCR designed to amplify exon 2 revealed that ablation of gene expression was indeed successful in primary AM (Fig. 13c).

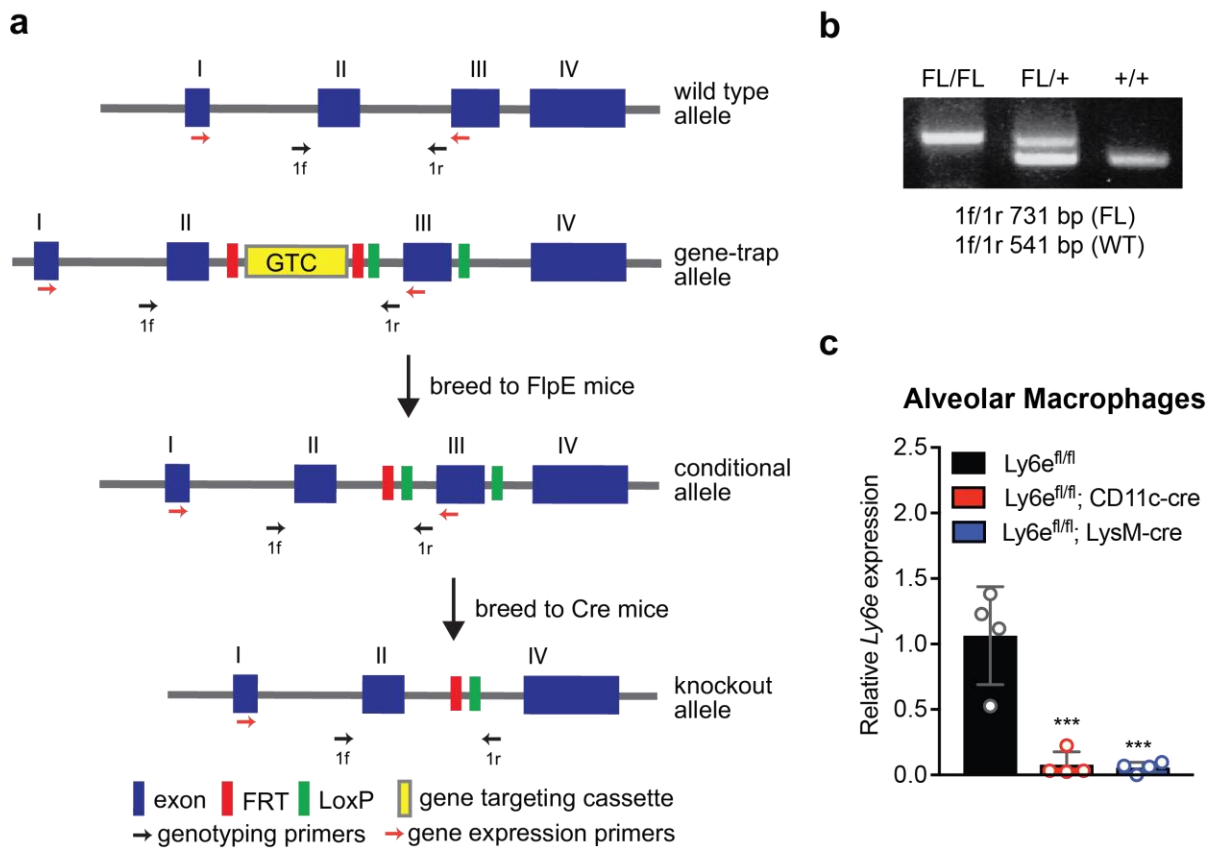


Figure 13. Generation and validation of Ly6e KO mice.

a Cartoon illustration of breeding strategy for generation of Ly6e KO mice. The gene-trap allele represents Ly6e^{tm1a(EUCOMM)Hmgu}. Mice heterozygous for a Ly6e exon 2 gene trap cassette were crossed to FlpE-expressing mice to generate the conditional allele. These mice were then crossed to Cre-expressing mice to produce the knockout allele. **b** PCR products from genomic tail DNA of Ly6e^{fl/fl}, Ly6e^{fl/+}, and Ly6e^{+/+} or WT mice using primers depicted in **a**. **c** Expression of Ly6e in AMs harvested from Ly6e^{fl/fl} and conditional knockout mice expressing CD11c-cre or LysM-cre. Expression was determined by RT-qPCR using the delta-delta CT method, normalizing to Ly6e expression in Ly6e^{fl/fl} AMs. *n* = 4 mice. Error bars represent standard deviation. Statistical significance was determined by t-test. *** *p* < 0.001.

Loss of Ly6e in AMs renders mice more susceptible to sub-lethal IAV infection

In my previous publication, I demonstrated that loss of human LY6E in U2OS cells reduces susceptibility to IAV. I also showed that ectopic expression of murine *Ly6e* in both human and mouse cell lines enhanced viral infection approximately 2-fold, using YFV as a model virus (Mar et al. 2018). Because the viral enhancement phenotype was conserved by ectopic expression of the mouse ortholog of *Ly6e*, I predicted that knockout of *Ly6e* in mouse cells would result in decreased viral infection. To test this hypothesis, I harvested a pure population of AMs from conditional *Ly6e* KO mice that were hemizygous for either *CD11c-cre* or *LysM-cre*. I then infected these cells with a 0.25 MOI of IAV and assessed IAV infectivity by RT-qPCR (Fig. 14a). AMs ablated for *Ly6e* were less susceptible to IAV infection, confirming that the knockout phenotype observed in human cell lines is conserved with endogenous murine *Ly6e* and IAV.

To test whether the loss of *Ly6e* increased or decreased susceptibility to IAV, I infected the conditional KO mice with sub-lethal (10 PFU) and lethal (100 PFU) doses of IAV (Galani et al. 2017). As described above, the *CD11c-cre* and *LysM-cre*-expressing conditional knockout strains have distinct, but partially overlapping, targeting of immune cell compartments. In the context of lung resident cells that are relevant to *in vivo* IAV infection, both strains result in complete ablation in AMs, as demonstrated in Fig. 13c. However, *LysM-cre* additionally targets *Ly6e* in about 80% of blood neutrophils and in about 40% of blood monocytes, both of which infiltrate into the bronchiolar space during IAV infection and can become infected (Manicassamy et al. 2010). *CD11c-cre* targets myeloid DCs, which encompasses both *CD11b+* and *CD103+* lung DCs, as well as 20% of blood monocytes (Abram et al. 2014).

Conditional knockout mice infected with 10 PFU IAV were significantly more susceptible to infection with the sub-lethal dose in comparison to the $Ly6e^{fl/fl}$ control littermates. Surprisingly, the survival phenotype of the $Ly6e^{fl/fl}; CD11c\text{-cre}$ and $Ly6e^{fl/fl}; LysM\text{-cre}$ mice was nearly identical (Fig. 14b). This result indicates that *Ly6e* ablation in a single cell type expressing both CD11c and LysM may increase susceptibility to a sub-lethal dose of IAV. Interestingly, infection of the conditional knockout mice with 100 PFU of IAV revealed that only $Ly6e^{fl/fl}; CD11c\text{-cre}$ mice were more susceptible at this dose (Fig. 14b). This discrepancy may be due to the additional ablation of *Ly6e* in lung resident dendritic cells, which may contribute to survival at lethal doses of IAV.

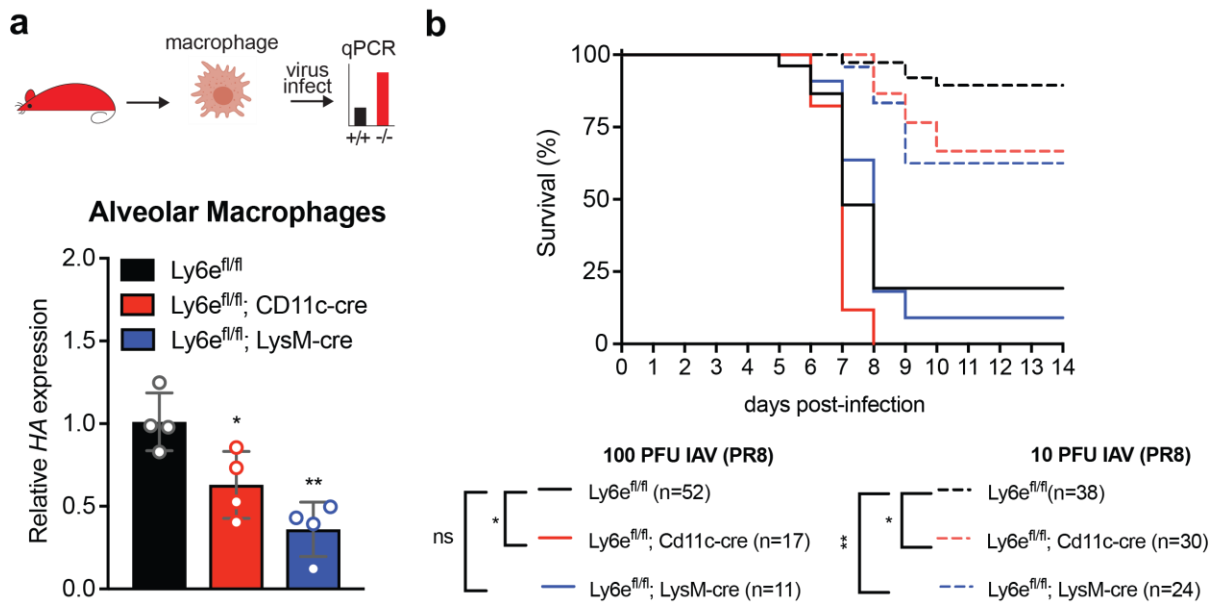


Figure 14. Loss of *Ly6e* in AMs increases susceptibility to IAV infection *in vivo*.

a AMs harvested from $Ly6e^{fl/fl}$ and conditional knockout mice expressing CD11c-cre or LysM-cre and infected with 0.25 MOI IAV (strain WSN, 4h) and replication was

assessed by quantifying viral *HA* gene expression RT-qPCR. *n* = 4 mice. **b** Ly6e^{fl/fl}, Ly6e^{fl/fl}; CD11c-cre, and Ly6e^{fl/fl}; LysM-cre mice were challenged with 10 PFU or 100 PFU IAV (strain PR8) and monitored daily for weight change. Mice that lost greater than 20% of their original weight were humanely euthanized. * *p* < 0.05, ** *p* < 0.01.

DISCUSSION

The generation of Ly6e conditional knockout mice bypasses the complication of embryonic lethality presented by whole body Ly6e knockout (Fig. 13). *Ex vivo* infections of Ly6e knockout AMs demonstrated that endogenous Ly6e enhances IAV infection, which corroborates our previous observations with knockout of human LY6E (Fig. 14a) (Mar et al. 2018). Intriguingly, *in vivo* infections indicate that the loss of *Ly6e* in AMs is detrimental for surviving sub-lethal doses of IAV (Fig. 14b). This result indicates that Ly6e-enhanced infection of AMs may contribute to the overall antiviral immune response *in vivo*.

While the concept of an ISG enhancing viral entry into a cell to contribute to host survival *in vivo* is intriguing, the ISG Axl has been shown to have a similar phenotype. Expression of endogenous Axl *in vitro* results in enhanced entry of diverse viruses by two mechanisms: directly via binding of phosphatidylserine on the viral envelope to AXL agonist growth arrest-specific 6 (GAS6) protein (Morizono et al. 2011; Meertens et al. 2012), and indirectly via induction of the *Socs* family genes which suppress type I IFN production and signaling (Bhattacharyya et al. 2013). While it was predicted that genetic ablation of *Axl* would render mice resistant to IAV infection, *Axl*^{-/-} mice were found to be more susceptible to a sub-lethal dose of IAV, with impaired ability to restrain viral burden (Schmid et al. 2016). Axl was found to contribute to the antiviral response in an indirect manner by inducing *Socs*, which constrains IFN production, thus promoting the maturation of DCs that

present IAV antigen to naïve T cells in the lymph node. Importantly, injection of *Axl*^{-/-} mice with an antibody that blocked IFN signaling (anti-IFNAR) completely restored resistance to sub-lethal IAV infection back to the level of WT mice. This result indicated that *Axl*-mediated downregulation of IFN is essential for proper development of a cellular immune response to IAV.

In contrast, I have shown that human LY6E, and by extension murine Ly6e, has no effect on genomic transcription or IFN signaling. Unlike *Axl*, Ly6e appears to promote viral infection independent of antagonizing the IFN response (Mar et al. 2018). Furthermore, studies to identify genomic loci that confer susceptibility to viral infection have previously indicated that human, chicken, and murine orthologs of LY6E may be important for the antiviral response to several viruses (Liu et al. 2003; Loeuillet et al. 2008; Spindler et al. 2010). Additionally, a study using RNAi *in vivo* also indicated that Ly6e may contribute to immune control of IAV (Benitez et al. 2015).

The data so far implicates a protective role for Ly6e in the overall antiviral response, that is putatively dependent on enhanced viral infection of AMs. Future studies should evaluate whether enhanced viral entry is a result of viral hijacking or if it is important for host defense. Furthermore, the potential role of Ly6e-mediated infection of AMs inducing production of secreted factors that protect T1AEC should also be explored.

METHODOLOGY

Mice

ES cells expressing the $Ly6e^{tm1a(EUCOMM)Hmgu}$ targeting cassette (clone HEPD0821_3_G08) were obtained from EUCOMM (Skarnes et al. 2011). Chimeric mice were generated by the UTSW Transgenic Technology Core facility (Pluck and Klasen 2009). $Ly6e^{fl/fl}$ mice were generated as described in Fig. 13a. A ROSA26::FLPe knock in mouse was obtained from The Jackson Laboratory (Stock #003946) (Farley et al. 2000). CD11c-cre C57BL/6J mice were a kind gift from Lora Hooper. LysM-cre C57BL/6J mice were a kind gift from Tiffany Reese. Genotyping was performed using GoTaq Green Master Mix (Promega M7122). Mice were housed in the UTSW Animal Resource Center in specific-pathogen free facilities and treated according to Institutional Animal Care and Use Committee (IACUC) protocol.

Propagation and titering of viral stocks

IAV (A/WSN/33) virus was generated by inoculation of sub-confluent MDCK (Balish, Katz, and Klimov 2013). Tissue-culture adapted IAV (A/PR/8) was obtained from the ATCC (VR-1469, lot # 61465052) and was also generated by inoculation of sub-confluent MDCK. Titering was performed on MDCK by plaque assay. In brief, MDCK were plated at 1×10^6 cells/well in a 6 well plate exactly 24 hours before inoculation to yield 95% confluency. Supernatant was removed and cells were washed twice in 1X PBS. Cells were incubated in a minimum volume of viral inoculum (800 μ L) containing 10-fold dilutions of IAV in infection media (0.3% BSA/0.1% FBS/PBS⁺⁺) for 1 hour at 37°C with rocking every 15 minutes to evenly distribute virus-containing supernatant. The inoculum was then removed and 3mL of warmed Avicel overlay was added (1% Avicel/0.3% BSA/0.1% NaHCO₃/1X penicillin-streptomycin/2 μ g/mL TPCK/DMEM). Cells were incubated at 37°C for 48 hours

then fixed in 1% PFA for 20 minutes. PFA-containing overlay was aspirated, and cells were stained with crystal violet for 1 hour. Dilutions that yielded greater than 10 plaques but fewer than 100 plaques were used for quantitating titer.

IAV infections in vivo

Mice used in this study were age- and sex-matched in the C57BL/6J background. Mice were stratified according to sex and randomly allocated to different experimental groups. Six to eight-week-old mice were anesthetized by intraperitoneal injection of freshly prepared 12.5 mg/mL avertin (1.25% 2,2,2 tribromoethanol dissolved in 2.5% 2-methyl-2-butanol). Within 10 minutes of anesthetic, ice-cold 10 PFU or 100 PFU PR8 resuspended in 30 to 40 μ L of 1X PBS was intranasally administered. Weight change and overall appearance of health was monitored daily. Mice were sacrificed by CO₂ asphyxiation upon falling below 80% initial starting weight. Mice that did not lose more than 10% of their starting weight were excluded from the dataset, as these mice were deemed insufficiently infected due to technical error.

Alveolar macrophage harvest and ex vivo infection

Nine-week-old female mice were euthanized by CO₂ asphyxiation. Bronchoalveolar lavage fluid was collected by intratracheal flush with 3 mL of chilled 5 mM EDTA/PBS per protocol (Jhingran, Kasahara, and Hohl 2016). Cells were pelleted at 250 xg for 10 min at 4°C and gently resuspended in filter-sterilized AM media (10% FBS/1X penicillin-streptomycin/0.1% 2-mercaptoethanol) for live/dead exclusion counting with trypan blue. Bronchoalveolar cells were then plated on a poly-L-lysine-coated 12 well plate (4 to 8 x 10⁵

cells/well) and incubated at 37°C for 2 hours to allow AMs to adhere. After the incubation, supernatant was carefully removed and rinsed twice with warm PBS⁺⁺ to remove non-adherent cells and debris. Virus inoculum (400 µL) was added (0.25 MOI IAV, A/WSN/33 in 0.3% BSA/0.1% FBS/PBS⁺⁺) and cells were incubated for 1 hour at 37°C. After the incubation, virus was removed, and cells were rinsed twice with warm PBS⁺⁺ to remove unbound virus. Warm AM media was carefully added, and cells were incubated for 3 more hours (4 hours total infection). After the incubation, media was aspirated and cells were lysed in 300 µL cold lysis buffer. Immediately after lysis, the RNAqueous Micro Total RNA Isolation protocol was followed (ThermoFisher, AM1931). RNA was eluted in 20 µL elution solution and 5 µL was allotted for each reaction.

RT-qPCR to analyze Ly6e and IAV gene expression

RNA was analyzed by one-step RT-qPCR using QuantiFast SYBR Green RT-PCR kit (Qiagen) which was run on Applied Biosciences 7500 Fast Real-Time PCR System with the following program: 10 m at 50°C, 5 m at 95°C, 35 x (10 s at 95°C, 30 s at 60°C), followed by melting curve analysis. The following primers were used: *RPL32* (housekeeping): forward 5' AAGCGAAACTGGCGGAAAC 3'; reverse 5' TAACCGATGTTGGGCATCAG 3'; *Ly6e* (exon 2): forward 5' ATCTTCGGGGCCTCTTCAC 3'; reverse 5' ATGAGAAGCACATCAGGGAAT 3'; *IAV (A/WSN/33) HA*: forward 5' TAACCTGCTCGAAGACAGAC 3'; reverse 5' AGAGCCATCCGGTGATGTTA 3'. Expression was determined by RT-qPCR using the delta-delta CT method, normalizing to expression in Ly6e^{fl/fl} AMs.

CHAPTER FOUR

LY6E inhibits infection by the *Coronaviridae* family

ABSTRACT

Viral infection results in the upregulation of hundreds of ISGs that can inhibit various stages of the viral replication cycle. Zoonotic coronaviruses (CoVs) can pose a significant global health threat as exemplified by the emergence of highly pathogenic variants such as Severe Acute Respiratory Syndrome Coronavirus (SARS-CoV) and Middle East Respiratory Syndrome Coronavirus (MERS-CoV), both of which crossed the species barrier from animals to humans. During a research sabbatical in the lab of Charles Rice, the postdoctoral fellow Stephanie Pfaender screened ISGs for the ability to restrict human CoV (HCoV) infection. Surprisingly, she identified LY6E as a potent antiviral CoV restriction factor. In collaboration, I found that ectopic overexpression of LY6E restricted infection of a distinct HCoV. Correspondingly, LY6E knockout cells were more susceptible to HCoV infection. The inhibitory effects of LY6E are evolutionarily conserved, as orthologs from human, rhesus, bat, and mouse resulted in inhibition of HCoV. Bone marrow-derived macrophages (BMDM) and AM lacking Ly6e were more susceptible to HCoV and mouse hepatitis virus (MHV) infection. Future studies will focus on uncovering the contributions of Ly6e in CD11c-, LysM-, and Vav1-expressing immune compartments to restrict MHV infection *in vivo*.

INTRODUCTION

The *Coronaviridae* family is composed of enveloped +ssRNA viruses. CoV are further subdivided into four genera: alpha, beta, gamma, and delta (Corman et al. 2018). In humans, only six CoV have been described: HCoV-229E and HCoV-OC43 which were described in the 1960's, SARS-CoV in 2002, HCoV-NL63, HCoV-HKU1, and MERS-CoV (Owczarek et al. 2018). In humans, HCoV cause respiratory tract infections that typically manifest as mild disease but can develop into life-threatening pneumonia. All HCoV are thought to have zoonotic origins, as exemplified by the recent outbreaks caused by SARS-CoV and MERS-CoV, which jumped the species barrier (Corman et al. 2018).

To identify novel ISGs that restrict HCoV infection, Stephanie Pfaender, a postdoctoral fellow from the lab of Volker Thiel, used an ectopic overexpression approach with a previously published lentiviral library (Schoggins et al. 2011; Dittmann et al. 2015). In collaboration with Eleftherios Michailidis, a postdoctoral fellow from the lab of Charlie Rice, Stephanie screened for ISGs that inhibited infection of a GFP reporter HCoV-229E. She identified LY6E as the most inhibitory ISG in the library. Following up on the screen, she demonstrated that LY6E overexpression in Huh7.5 potently inhibited infection by HCoV-229E, confirming that LY6E has diverse effects on multiple viruses (Fig 15a-b).

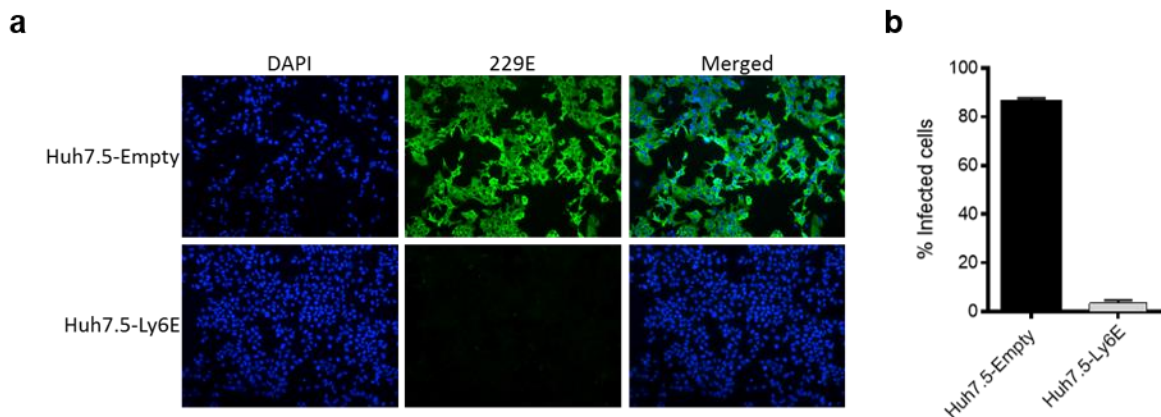


Figure 15. LY6E is antiviral against HCoV-229E (data from Stephanie Pfaender).

a Huh7.5 expressing empty control vector or LY6E by lentiviral transduction were challenged with HCoV-229E. Infected cells were stained for N protein-AlexaFluor488 and DAPI. **b** Quantification of HCoV-229E infection in Huh7.5 expressing empty control vector or LY6E.

RESULTS

LY6E inhibits infection by a human coronavirus

Ectopic overexpression of human LY6E in *STAT1*^{-/-} fibroblasts, Huh7.5, and A549 cells potently inhibited infection of HCoV-OC43 at multiple doses (Fig. 16a-c). In contrast, I previously observed enhancement of YFV infection by ectopic LY6E expression in *STAT1*^{-/-} fibroblasts, but not Huh7.5 or A549 cells (Fig. 2a, c) (Mar et al. 2018). I had hypothesized that the cell type-specific enhancement phenotype was due to variable expression of a putative interaction partner that works with LY6E to promote infection. While the ability of LY6E to inhibit HCoV-OC43 in Huh7.5 and A549 cells in addition to *STAT1*^{-/-} fibroblasts indicates that, according to my hypothesis, LY6E-mediated inhibition engages a separate pathway than LY6E-mediated enhancement, it is also possible that IAV and CoV engage the same pathway in distinct ways. Interestingly, A549 cells express a similar level of basal

LY6E as *STAT1*^{-/-} fibroblasts and yet A549 expressing the vector control infected poorly relative to *STAT1*^{-/-} fibroblasts expressing the vector control. Additionally, Huh7.5 did not have detectable levels of LY6E and infected poorly relative to *STAT1*^{-/-} fibroblasts (Fig. 2c and Fig. 16a-c). Intrinsic resistance to HCoV-OC43 in these cell types suggests the existence of either basal antiviral host factors or differential expression of receptors that promote HCoV-OC43 attachment and entry. Overall, my data corroborates Stephanie's data, and extends the antiviral effects of LY6E to an additional human coronavirus in multiple cellular backgrounds.

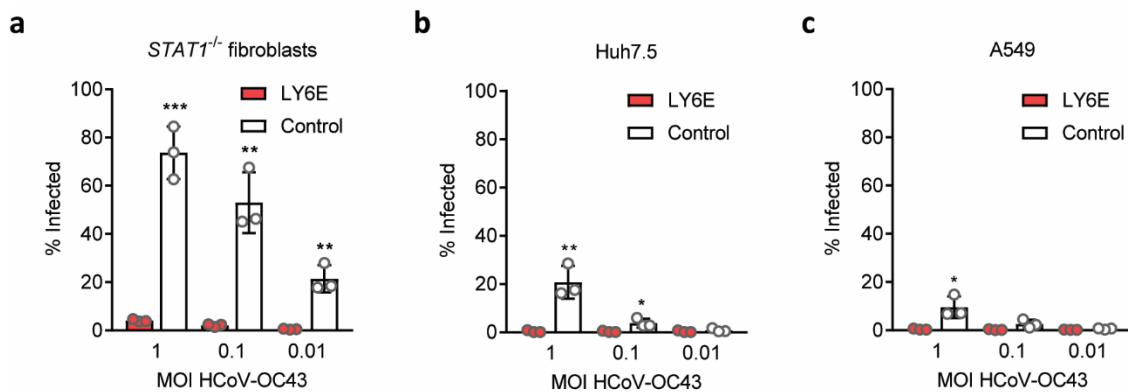


Figure 16. Ectopic overexpression of LY6E inhibits HCoV-OC43.

a LY6E or empty control constructs were expressed by lentivirus transduction in human *STAT1*^{-/-} fibroblasts, **b** Huh7.5, **c** or A549. Cells were infected with HCoV-OC43 (between 0.01 and 1 MOI, 24h). After harvest, cells were permeabilized and stained for N. Percent infection was quantified by flow cytometry. *n* = 3 biological replicates. * *p* < 0.05, ** *p* < 0.01, *** *p* < 0.001. SD is shown. Data was analyzed by student's T test.

Loss of endogenous LY6E increases susceptibility to HCoV-OC43

Because I had observed that ectopic LY6E expression inhibited HCoV-OC43 in A549 (Fig. 16c), I next wanted to test whether ablation of endogenous LY6E in A549 increased

susceptibility. Indeed, a bulk population of A549 expressing a LY6E-specific guide sequence and Cas9 were more susceptible to HCoV-OC43 than WT A549 (Fig. 17a).

Previously, I had established a clonal LY6E KO cell line in the U2OS background (Fig. 4c, 5a) that was less susceptible to infection by YFV and IAV (Fig. 4d). I had used U2OS due to the high basal expression of LY6E (Fig. 2c) (Mar et al. 2018). LY6E KO U2OS were highly susceptible to HCoV-OC43 infection relative to their WT counterparts (Fig. 17b). To confirm that the increased infectivity of LY6E KO U2OS was due to specific loss of LY6E, I generated a CRISPR-resistant LY6E (CR-LY6E) that was mutated to be resistant to the sgRNA encoded by lentiCRISPRv2-LY6E #4 which had been used to make the LY6E KO cells (Mar et al. 2018). Expression of CR-LY6E, but not LY6E or vector control, almost fully restored the inhibitory effects of endogenous LY6E (Fig. 17c). The incomplete rescue may be due to less efficient expression of the modified codons used to generate CR-LY6E.

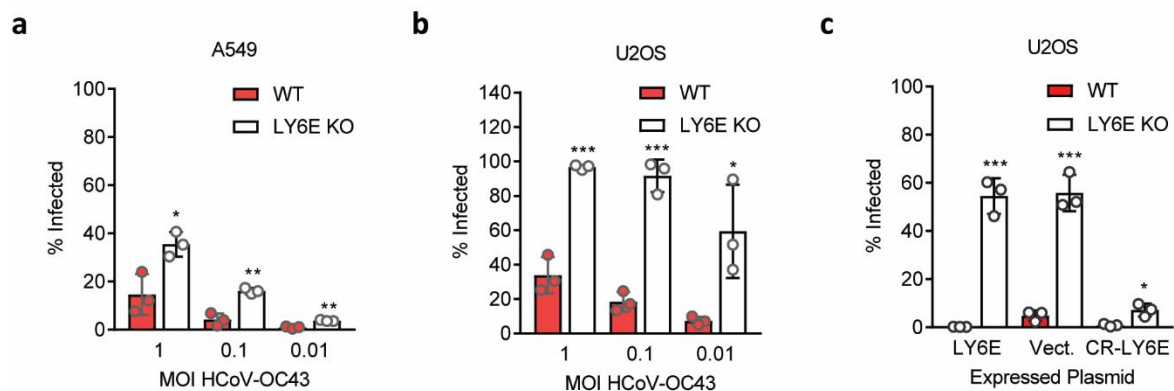


Figure 17. Knockout of endogenous LY6E increases HCoV-OC43 infectivity.

a WT A549 and a bulk population of A549 expressing a LY6E-specific guide sequence and Cas9 (LY6E KO) were infected with HCoV-OC43 (between 0.01 and 1 MOI, 24h). $n = 3$ biological replicates. **b** LY6E KO and WT U2OS were infected with HCoV-OC43 (between 0.01 and 1 MOI, 24h). $n = 3$ biological replicates. **c** LY6E KO and WT U2OS expressing LY6E, vector control (Vect.), or a CRISPR-resistant LY6E by lentiviral transduction. Cells

were infected with HCoV-OC43 (0.1 MOI, 24h). $n = 3$ biological replicates. For **a**, **b**, and **c**, cells were permeabilized after 24h infection and stained for N. Percent infection was quantified by flow cytometry. * $p < 0.05$, ** $p < 0.01$, *** $p < 0.001$. SD is shown. Data was analyzed by student's T test.

LY6E-mediated inhibition of coronaviruses is evolutionarily conserved.

Previously I had found that viral enhancement of YFV mediated by LY6E expression was evolutionarily conserved, as expression of LY6E orthologs from *Macaca mulatta* (rhesus macaque), *Mus musculus* (house mouse), and the *Pteropus alecto* (black flying fox, a megabat) also enhanced YFV (Fig. 10a) (Mar et al. 2018). To test whether inhibition of CoV is also conserved across evolution, I expressed the LY6E orthologs in human *STAT1*^{-/-} fibroblasts and challenged with HCoV-OC43. Perhaps unsurprisingly, all LY6E orthologs restricted coronavirus infection, albeit to variable degrees (Fig. 18a). However, more biological replicates need to be performed in order to perform statistical analyses.

Loss of LY6E in murine macrophages increases coronavirus susceptibility

To test whether Ly6e in an immune cell is important for inhibiting HCoV-OC43 infection, I generated BMDM from Ly6e^{fl/fl} and Ly6e^{fl/fl}; LysM-cre mice. Loss of Ly6e in the LysM-cre-expressing cells significantly increased susceptibility to HCoV-OC43 (Fig. 18b). I also generated AMs from Ly6e^{fl/fl} and Ly6e^{fl/fl}; CD11c-cre mice. Since the readout for HCoV-OC43 infection is antibody staining, I opted to pool cells harvested from four mice per genotype to ensure that my cell numbers were enough. Loss of *Ly6e* in AMs drastically enhanced susceptibility to HCoV-OC43 (Fig. 18c). The stark phenotype in AM may be due

to the relative purity of this *ex vivo* population, and higher basal expression of *Ly6e* relative to *in vitro* cultured BMDM.

MHV is a betacoronavirus and natural mouse pathogen. Different strains of MHV are grouped based on the ability to infect multiple tissues (polytropic) or only the intestinal tract (enterotropic). Stephanie provided a preparation of a GFP reporter MHV, strain A59 (MHV-GFP), that had been previously generated in the Thiel lab (Zust et al. 2007). The A59 strain is polytropic, with the ability to disseminate to and replicate in the liver, spleen, lung, and brain from intranasal administration (Cervantes-Barragan et al. 2009). To test whether *Ly6e* restricts MHV, I generated BMDM from *Ly6e* conditional knockout mice that also expressed a modified Cre (iCre) under the *Vav1* promoter, which potently expresses Cre recombinase in all immune compartments (Abram et al. 2014). *Ly6e* KO BMDM from *Ly6e^{fl/fl}; Vav1-iCre* mice were more susceptible to MHV-GFP infection than BMDM from *Ly6e^{fl/fl}* mice at all doses tested (Fig.18d). Cumulatively, the strong coronavirus phenotype in *ex vivo* and *in vitro* cultured *Ly6e* KO mouse macrophages is promising for future studies of *Ly6e* and MHV *in vivo*.

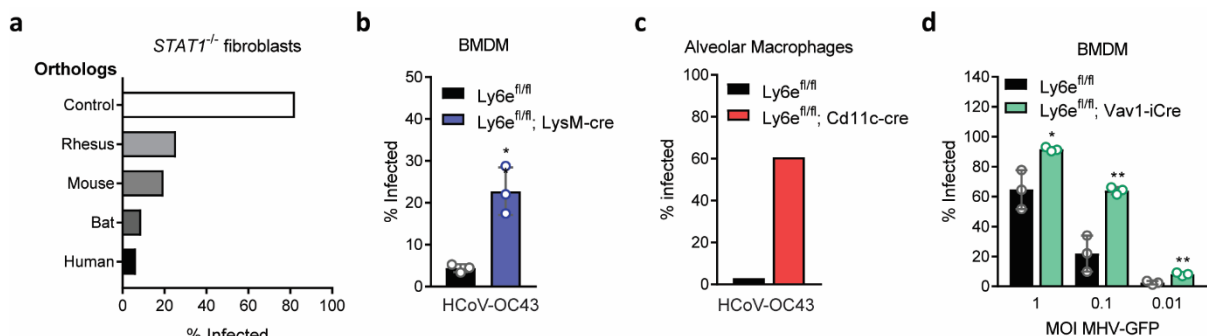


Figure 18. Murine *Ly6e* is antiviral against *Coronaviridae* viruses.

a Empty vector control, rhesus LY6E, mouse Ly6e, bat LY6E, or human LY6E constructs were expressed by lentivirus transduction in human *STAT1*^{-/-} fibroblasts. Cells were infected with HCoV-OC43 (1 MOI, 24h). *n* = 1 biological replicate. **b** BMDM differentiated from myeloid progenitors harvested from Ly6e^{fl/fl} or Ly6e^{fl/fl};LysM-cre mice were infected with HCoV-OC43 (0.1 MOI, 24h). *n* = 3 biological replicates. **c** AMs harvested from 4 Ly6e^{fl/fl} or 4 Ly6e^{fl/fl}; CD11c-cre mice were pooled into a single sample per genotype. Cells were infected with HCoV-OC43 (0.1 MOI, 2h). *n* = 1 biological replicate. For **a**, **b**, and **c**, cells were permeabilized after infection and stained for N. Percent infection was quantified by flow cytometry. **d** BMDM differentiated from myeloid progenitors harvested from Ly6e^{fl/fl} or Ly6e^{fl/fl};Vav1-iCre mice were infected with MHV-GFP (between 0.01 and 1 MOI, 8h). *n* = 3 biological replicates. Percent infection was quantified by flow cytometry. * *p* < 0.05, ** *p* < 0.01. SD is shown. Data was analyzed by student's T test.

DISCUSSION

The discovery that LY6E exhibits specific antiviral activity against viruses from the *Coronaviridae* family was surprising, but not completely unexpected for a protein that is highly induced by IFN (Shan et al. 1998; Mar et al. 2018). I have added to Stephanie's finding, by showing that both overexpressed and endogenous LY6E inhibit HCoV-OC43 in multiple cellular backgrounds. Furthermore, I have also shown that endogenous murine Ly6e restricts infection by both HCoV-OC43 and MHV. In data that I have not shown, Stephanie has also found that LY6E inhibits infection by blocking entry of HCoV. The antiviral effects of LY6E also restrict infection by SARS-CoV and MERS-CoV, for a total of 4 of the 6 known human CoV. Furthermore, LY6E also reduces entry of viral pseudoparticles expressing glycoproteins from EBOV and Marburg virus. Surprisingly, Eleftherios Michailidis of the Charlie Rice's lab has also shown that LY6E inhibits infection by HCV, a finding that contrasts previously published work and requires further investigation (Schoggins et al. 2011). Combined, our efforts have demonstrated that further study of LY6E as an antiviral host restriction factor is merited. Our collaboration will hopefully uncover the

molecular mechanism and physiological relevance of Ly6e in the context of *in vivo* CoV infection.

How is it possible for LY6E to enhance the entry of a subset of enveloped RNA viruses, while potentially inhibiting infection by a different subset of viruses? The Ly6 proteins have a flexible TFP domain that allow for interactions with multiple partners (Loughner et al. 2016). Indeed, orthologs of LY6E have been shown to associate with TCR, nAChR, a viral protein, FcγRIIB, and SynA (Kosugi et al. 1998; Wu et al. 2015; Liu et al. 2003; Ding and Shevach 2001; Bacquin et al. 2017). My observation that LY6E-mediated enhancement occurs in specific cellular backgrounds, whereas inhibition by LY6E overexpression is comparatively universal, may also indicate a distinct signaling mechanism.

In terms of physiological relevance, I have two hypotheses. One hypothesis is that the true function of LY6E is to inhibit entry of CoV and a subset of other viruses, and viral enhancement of a distinct subset of viruses is a result of viral hijacking. However, several pieces of data contradict this hypothesis. Examples of viral hijacking of ISGs have so far been shown to require physical interaction. For example, EBOV matrix protein VP40 binds SOCS3 to increase viral egress (Okumura et al. 2015). Human cytomegalovirus (HCMV) has been shown to induce expression of viperin, and relocalize its activity through direct interaction with the viral protein viral mitochondrial inhibitor of apoptosis (vMIA) (Seo et al. 2011). AXL interacts with its ligand GAS6 to indirectly bind phosphatidylserine on viral envelopes to promote internalization (Meertens et al. 2012). HCoV-OC43 hijacking of the IFITM proteins needs to be further studied to determine whether direct interaction is required (Zhao et al. 2014; Zhao et al. 2018). I have shown that LY6E does not promote attachment of

YFV or IAV, which indicates that a direct virus-protein interaction does not exist (Mar et al. 2018). My observation in Chapter 3, that loss of Ly6e in AMs increases susceptibility to IAV infection, also contradicts this hypothesis (Fig. 14b). Finally, genomic studies that have identified polymorphisms in the Ly6 locus and LY6E that associate with susceptibility to viral infection also contrast with the hijacking hypothesis (Loeuillet et al. 2008; Stier and Spindler 2012; Liu et al. 2003).

An alternative hypothesis is that viral inhibition and viral enhancement are two facets of the same protein that both exist to control infection by a broad and diverse group of enveloped RNA viruses through different mechanisms. As mentioned previously, LY6E orthologs have already been shown to interact with distinct proteins to carry out unrelated cellular processes, so it is not unreasonable that LY6E may have bivalent relations in the context of viral infection. My *in vivo* study of Ly6e also indicates that viral enhancement at the cellular level may be important for a cell-mediated immune response as mice lacking Ly6e in AMs are more susceptible to IAV (Fig. 14b). I have also shown that IFN-induced LY6E does not promote infection, which I hypothesized was due to co-induction of antiviral ISGs (Fig. 6b) (Mar et al. 2018). Therefore, it is perhaps possible that basal LY6E promotes cell-mediated immune responses against a subset of RNA viruses, while IFN-induced LY6E may be more pertinent for restricting infection by a different subset of RNA viruses.

METHODOLOGY

Cells

STAT1^{-/-} fibroblasts, Huh7.5, A549, were maintained as previously described (Mar et al. 2018). HCT-8 cells were cultured in 10% horse serum/1X sodium pyruvate/20 mM HEPES/RPMI. L929 cells were cultured in 10% FBS/1X NEAA/DMEM at confluency to generate L929-conditioned media, an established source of M-CSF (Weischenfeldt and Porse 2008).

Virus

Human coronavirus OC43 (ATCC strain VR-1558) was propagated in HCT-8 cells by Ian Boys as specified by the ATCC. Viral titers were determined by antibody staining for N protein (Millipore MAB9012) and flow cytometry. MHV-GFP was generated by Stephanie Pfaender.

Transductions and infections

Lentiviral transductions were performed as previously described (Mar et al. 2018). HCoV-OC43 infections were carried out in 1% FBS/DMEM at a minimal volume for 1 hour. Virus was then aspirated and 10% FBS/DMEM or 10% FBS/RPMI (for *STAT1*^{-/-} fibroblasts only) was added. Cells were incubated at 33°C and harvested after 24 h for antibody staining for N protein and AlexaFluor 488-conjugated secondary antibody. Percent infection was quantified by flow cytometry.

Mice

Ly6e conditional knockout mice were generated and maintained as described in Chapter 3. To generate the Ly6e^{fl/fl}; Vav1-iCre strain, Vav1-iCre transgenic mice were obtained from Jackson Laboratories (Strain #: 008610).

Production and infection of bone marrow-derived macrophages

BMDM were generated as described previously from 7 to 8 week old gender- and litter-matched mice (Agac et al. 2018). In brief, bone marrow cells were isolated from femurs and tibias of euthanized mice. Red blood cells (RBC) were lysed by using 1X RBC lysis buffer (Tonbo Biosciences, TNB-4300-L100). The remaining cells were cultured in 30% L929-conditioned media. The next day, the non-adherent myeloid progenitor cells were harvested, counted, and plated at 4×10^6 cells per petri dish in the same conditioned media. After four days of culturing, BMDM are lifted from petri dish using 2 mM EDTA/PBS and counted for experimental use.

For HCoV-OC43 experiments, BMDM were plated at 5×10^6 cells per well in a tissue culture-treated 24 well plate and infected the next day in 1% FBS/DMEM. The infected cells were then incubated at 33°C for 24 h before harvest for antibody staining with anti-N protein and AlexaFluor 488-conjugated secondary antibody.

For MHV-GFP experiments, BMDM were plated at 2.5×10^5 cells per well in an untreated 24 well plate and infected the next day in 1% FBS/DMEM. The infected cells were then incubated at 37°C for 8 h before harvest in 2 mM EDTA/PBS.

Isolation and infection of alveolar macrophages

AMs were isolated and purified as described in Chapter 3. For HCoV-OC43 infection cells were counted and pooled before plating. Cells were incubated at 33°C for 1 hour to allow AMs to adhere. Cells were then infected with HCoV-OC43 as described above and incubated at 33°C for 24 h before harvest for antibody staining with anti-N protein and AlexaFluor 488-conjugated secondary antibody.

CHAPTER FIVE

Conclusions and Recommendations

CONCLUSIONS

Through my studies, I have identified two opposing effects of LY6E on viral infection: enhancement of IAV uncoating *in vitro*, and a requirement for surviving sub-lethal IAV infection *in vivo*. My *in vitro* study narrowed the effects of LY6E-mediated enhancement to the step of entry for both YFV and IAV. My discovery that viral enhancement is evolutionarily conserved is indicative that the physiological contribution of this phenotype may be beneficial to the host. By generating a Ly6e knockout mouse model, I also discovered a putative protective role for Ly6e in lung resident AMs during IAV infection. Overall, my findings suggest a novel paradigm for an ISG: enhanced viral uptake by AMs contributes to organismal-level protection.

In collaboration with Stephanie Pfaender, I have also demonstrated that Ly6e is a potent antiviral restriction factor of CoV. Further study of CoV infection in Ly6e knockout mice may establish a major role for Ly6e in controlling infection by *Coronaviridae* family viruses. Understanding the activity of Ly6e in lung resident immune cells may contribute to the development of therapeutic treatment for zoonotic CoV outbreaks.

The ISG LY6E mediates evolutionarily conserved enhancement of viral entry

My first project in the lab was to characterize the ISG LY6E, which had been previously demonstrated to enhance infectivity by a subset of unrelated, enveloped RNA

viruses (Schoggins et al. 2011; Schoggins et al. 2012; Schoggins et al. 2014). I first demonstrated that LY6E expression does not affect attachment, translation, replication, or production of YFV and IAV (Fig. 7,8). Focusing on IAV, which has well-established molecular tools, I then found that LY6E expression promotes uncoating, and subsequently enhances vRNP translocation into the nucleus, which is a critical upstream step prior to viral replication. Interestingly, LY6E did not promote uptake of non-viral ligands that are internalized via endocytosis. Subsequently, I found that viral enhancement was conserved by testing LY6E orthologs from divergent species, and used this knowledge to screen for and identify an essential residue required for the viral enhancement phenotype (Mar et al. 2018).

While I was working on my project, several other groups published studies showing that LY6E enhanced entry of HIV-1 and the *Flaviviridae* members WNV, DENV, and ZIKV (Hackett and Cherry 2018; Yu, Liang, and Liu 2017). In the study from Sara Cherry's lab, LY6E was found to selectively enhance uptake of large cargo of similar size to viruses, such as transferrin-coated beads (Hackett and Cherry 2018). Cell surface LY6E was found to associate with microtubule-associated tubular protrusions formed in response to viral infection or transferrin-coated beads that had a similar size as viruses. RNAi-mediated knockdown of the microtubule-associated EB3 reduced tubularization of LY6E, implicating a potential interaction between these proteins. Cumulatively, research from three independent groups uncovered a role for LY6E in promoting entry of diverse enveloped RNA viruses.

Ly6e expression in AMs is important for surviving sub-lethal IAV infection

To address the physiological relevance of LY6E-mediated enhancement of viral entry, I generated Ly6e conditional knockout mice as whole body knockout has been established to be embryonic lethal by several groups (Langford et al. 2018; Zammit et al. 2002). Upon availability of Ly6e^{fl/fl} mice, I used commercially available cre recombinase driver mice to generate crosses with LysM-cre, CD11c-cre, and Vav1-iCre strains, all of which result in hemizygous cre expression in various immune cell compartments (Abram et al. 2014). In addition, I also generated Ly6e^{fl/fl} mice hemizygous for Ubc-CreERT2, which allows for inducible, widespread cre expression upon tamoxifen administration. Unfortunately, this strain has now been established to have spontaneous cre activation in the absence of drug treatment (Kristianto et al. 2017). At the time of writing this document, conclusive experimental IAV infection data was not available using the Ly6e^{fl/fl}; Vav1-iCre or Ly6e^{fl/fl}; Ubc-CreERT2 mouse strains. However, all Ly6e conditional knockout mouse models that I generated were viable and fertile, making these strains valuable tools for future study of Ly6e.

Initially, I sought to confirm that Ly6e knockout would affect susceptibility to IAV using *in vitro* and *ex vivo* infection models. My original attempts at using *in vitro* BMDM and bone marrow derived DC (BMDC) preparations with bone marrow respectively from LysM-cre and CD11c-cre mice were inconclusive, potentially due to low basal Ly6e expression or population heterogeneity (Helft et al. 2015). In my next approach, I isolated AMs from bronchoalveolar lavage fluid, modifying a technique that I was previously taught in the lab of Tobias Hohl (Jhingran, Kasahara, and Hohl 2016; Chavez-Santoscoy et al. 2012). These primary macrophages were homogenous, as assessed by surface marker

staining and analysis of *Ly6e* knockout by RT-qPCR (Fig. 13c). Infection of the *Ly6e* knockout AMs from both *CD11c-cre* and *LysM-cre* mice resulted in decreased IAV gene expression, which indicated that loss of murine *Ly6e* recapitulated my observations with human LY6E knockout (Fig. 14a).

Surprisingly, I found that both *Ly6e^{fl/fl}; LysM-cre* and *Ly6e^{fl/fl}; CD11c-cre* mice were identically more susceptible than their *Ly6e^{fl/fl}* littermates to sub-lethal IAV infection (10 PFU). However, only *Ly6e^{fl/fl}; CD11c-cre* mice were more susceptible to a lethal IAV dose (100 PFU) (Fig. 14b). I hypothesized that the difference between the *LysM-cre* and *CD11c-cre* mice may be the additional ablation of *Ly6e* in lung resident DCs, which are known to present viral antigen to naïve T cells to activate an IAV-specific adaptive response (Waithman et al. 2013). In a study comparing the effect of genetic ablation of macrophages (*Csf2^{-/-}*) to *CD8 α ⁺* and *CD103⁺* DCs (*Batf3^{-/-}*) on infection with IAV, macrophages were found to be essential for survival while loss of DCs presented as a trend towards slower, but complete recovery relative to WT mice (Schneider et al. 2014). The identical survival phenotypes of the *LysM-cre* and *CD11c-cre* mice is thus suggestive of a role in a redundant cell type targeted by both promoters, specifically AMs.

The literature supporting a critical role for AMs in surviving IAV infection is overwhelmingly homogenous in its conclusions (Tumpey et al. 2005; Schneider et al. 2014; Purnama et al. 2014; Kim et al. 2008; Kim et al. 2013; Cardani et al. 2017). As discussed extensively in Chapter 3, eloquent work from Thomas Braciale's lab uncovered the mechanism underlying the indispensable role of AMs in IAV infection: AMs release an unidentified, IFN-independent, and infection-dependent secreted factor that protects T1AEC

from IAV infection by blocking clathrin-mediated endocytosis (Cardani et al. 2017). As a result, T1AEC are resistant to killing by virus-specific cytolytic CD8⁺ T cells, and thus adverse immunopathology that contributes to impaired respiratory function and death is avoided.

It is conceivable that Ly6e expression may be important for complete resistance to IAV infection by promoting infectivity of AMs and subsequently protecting against immunopathology. Further study to unravel the role of Ly6e *in vivo* may put the *in vitro* enhancement phenotype into context of the overall antiviral response. However, the relatively minor effects of Ly6e loss on IAV survival makes studying this phenotype difficult. Thus, careful and skilled efforts are required to dissect the role of Ly6e-mediated enhancement *in vivo*.

LY6E restricts infection by *Coronaviridae* family viruses

During preparation of my manuscript on LY6E-mediated enhancement of viral infection *in vitro*, I was informed by Charlie Rice that a visiting post-doctoral fellow in his lab had discovered that LY6E is highly antiviral to a subset of RNA viruses, including from the *Coronaviridae* family. That was how I began my unexpected but entirely pleasant international collaboration with Stephanie Pfaender of Volker Thiel's lab and Eleftherios Michailidis of Charlie Rice's lab. By applying tools that I had developed for my study of LY6E-mediated viral enhancement, I have added to Stephanie's work by showing that both ectopically expressed and endogenous LY6E inhibits HCoV-OC43 (Fig. 16, 17). My contribution to the collaboration has naturally expanded toward using my conditional

knockout mouse models, and in preliminary *ex vivo* and *in vitro* studies using cells from these mice, I have shown that Ly6e in macrophages is important for restricting HCoV-OC43 and natural mouse pathogen MHV (Fig. 18). My work on this project is in relatively early stages but will be integral for demonstrating the *in vivo* role of Ly6e as an antiviral restriction factor in the context of the cellular immune response.

RECOMMENDATIONS

Unraveling the molecular mechanism for viral enhancement and inhibition

Ly6 proteins are known modulators of diverse cellular processes through flexible TFP motifs (Loughner et al. 2016). LY6E has previously been described to interact with tissue-specific proteins, such as TCR, SynA, and Fc γ RIIB, which are unlikely to contribute to the viral enhancement phenotype in a human fibroblast cell line (Kosugi et al. 1998; Bacquin et al. 2017; Ding and Shevach 2001). Thus, a broad approach to identify interaction partners is likely the best. Tandem affinity purification (TAP) using epitope-tagged LY6E followed by mass spectrometry to identify interacting proteins would be ideal. However, certain epitope tags may interfere with the activity of LY6E, as a C-terminal Myc tag prior to the GPI anchored S101 residue resulted in loss of detection by western blotting. N-terminal tagging with the negatively charged 3x FLAG after the signal peptide interfered with the viral enhancement phenotype in a proximity-based manner, as increasing the length of the glycine linker from three to seven residues rescued the phenotype. Amino terminus tagging with the StrepII epitope also resulted in a loss of viral enhancement. So far, only carboxyl terminal tagging with HA or 6x His prior to the GPI-anchored serine residue yielded a properly

expressed LY6E that enhanced viral infection. Further optimization to identify usable epitope tags is merited before attempting to identify interactive partners by TAP. In addition to using LY6E with the L36A point mutation as a control, comparing LY6E's co-immunoprecipitated partners from different cell lines, such as *STAT1*^{-/-} fibroblasts in which viral enhancement is observed and A549 in which enhancement is absent, may be an important tool for identifying relevant partner proteins. Furthermore, performing co-immunoprecipitation in the absence or presence of IAV or HCoV infection may reveal an interaction that is only present during viral infection.

While a two-fold enhancement phenotype may be insufficient to discern a potential 'hit' through a genome-wide CRISPR screening approach, the potent inhibition of HCoV by LY6E may be useful. In this approach, LY6E-expressing cells would be pre-treated with IFN and transduced with a genome-wide CRISPR library. The LY6E cells would then be challenged with a GFP reporter HCoV and subject to FACS to isolate cells that had been transduced with a sgRNA that rescued infectivity in the context of LY6E overexpression. The sgRNA sequence would then be amplified and identified by sequencing.

One major complication of using this approach is whether LY6E engages the same protein partner to enhance infection as it does to inhibit infection. Given the apparent overlapping effect on viral entry, it may be possible that the same pathway is targeted but is utilized distinctly by the two subsets of inhibited and enhanced viruses. It is also probable that two distinct pathways are engaged by LY6E, as suggested by my observation in Chapter 4 that cell background matters for viral enhancement but does not impact viral restriction. Thus, great care needs to be taken to not generalize observations from one viral phenotype to

the other. A simple experiment to test whether the enhancement and inhibitory phenotypes balance or compete should be carried out first, such as determining whether co-infection of LY6E-expressing cells interferes with either phenotype.

Untangling the importance of LY6E to the antiviral IFN response

I previously found that the LY6E-mediated viral enhancement phenotype diminishes with increased dosage of IFN treatment prior to infection with YFV (Fig. 6b). Despite increased LY6E induction by IFN, the phenotype was likely drowned out by the overwhelming antiviral effects of ISGs that are known to inhibit YFV, such as IFI6, RTP4, and IFITM3 which I also showed were concomitantly induced (Fig. 6c) (Mar et al. 2018). From this result, I concluded that basal LY6E, not IFN-induced, is important for viral enhancement. At the time, this was a difficult observation to put in perspective- why is LY6E induced by IFN if it is unable to exert its pro-viral phenotype in the presence of other ISGs? However, after learning that LY6E also possesses antiviral activity, I was able to justify the existence of IFN-induced LY6E as required for controlling CoV infection. A previous study from the Ludewig lab revealed that type I IFN signaling on macrophages is indispensable for surviving MHV infection, which hints at a potential protective role of IFN-induced Ly6e in an *in vivo* CoV infection mode (Cervantes-Barragan et al. 2009). Further study of Ly6e in macrophages is warranted, as well as elucidating the role of Ly6e in the context of the IFN response using the same approach as I used in Fig. 6b.

APPENDIX A
Primers used for cloning plasmids used in Chapter 2

Primer name	Usage	Sequence
YFV-17D 5' NTR	qRT-PCR primer for YFV cold-bind assay	aatcagttgctaggcaataaacac
YFV-17D capsid gene junction	qRT-PCR primer for YFV cold-bind assay	tccctgagctttacgaccaga
IAV A/WSN/33 HA forward	qRT-PCR primer for IAV cold-bind assay	taacctgctcgaagacagac
IAV A/WSN/33 HA reverse	qRT-PCR primer for IAV cold-bind assay	agagccatccggtgatgta
Bat Ly6e repair forward	Repair <i>P. alecto</i> Ly6e cDNA	agacctgaattcgggtaccatgaaggctttctgcctgtgc
Bat Ly6e repair reverse	Repair <i>P. alecto</i> Ly6e cDNA	atataactcgagctaggggccagctctgagg
Mouse Ly6e BP arms forward	Add BP arms to mouse Ly6e cDNA	ggggacaagttgtacaaaaagcaggcttcaccatgtctgccactccaacatgagagtcttctgc
Mouse Ly6e BP arms reverse	Add BP arms to mouse Ly6e cDNA	ggggaccactttgtacaagaaagctgggttcaggggctcagctgcagcagagccaacaagc
Human LY6E sgRNA #4 forward	Oligo to target LY6E exon 2	caccggccgaccatctgctccgacc
Human LY6E sgRNA #4 reverse	Oligo to target LY6E exon 2	aaacggtcggagcagatggtcggcc
Human LY6E surveyor nuclease forward	Amplify CRISPR-targeted region to confirm editing	ttctcgggaactgagtaacatcaggaatgg
Human LY6E surveyor nuclease reverse	Amplify CRISPR-targeted region to confirm editing	tgggggacatctgtattatttgaggcacc
LY6E exon 2 genomic DNA forward	Amplify and sequence LY6E exon 2 after CRISPR	ggcctggccacactgtctcac

LY6E exon 2 genomic DNA reverse	Amplify and sequence LY6E exon 2 after CRISPR	ccaagggcacagatcaggcacg
pENTR backbone NspI forward	Backbone forward primer for OE PCR	ctggccttttctggccttttctcacatgttcttctgcgttatcccc
pENTR backbone PvuI reverse	Backbone reverse primer for OE PCR	tcaaccaaaccgttattcattcgtgattgcgcctgagcgagacgaaatacgcgatcctg
LY6E-HA tag forward	Add HA tag to LY6E before GPI anchor by OE PCR	actagcgtaatctggaacatcgtatgggtagaaattgcacagaaagctctggcagca
LY6E-HA tag reverse	Add HA tag to LY6E before GPI anchor by OE PCR	ttctaccatacagatgttcagattacgctagtgcggccgatggcgggct
CD59-HA tag forward	Add HA tag to CD59 before GPI anchor by OE PCR	acgatgtccagattacgctaattggtgggacatccttatcagag
CD59-HA tag reverse	Add HA tag to CD59 before GPI anchor by OE PCR	ctctgataaggatgtcccaccattagcgtaatctggaacatcgt
Block ASM forward 1	Mutate AA 21-24 to alanine	ttgctcttctggtcaagcaggaggcgcacgcagccgagctggctcgtccaca
Block ASM reverse 1	Mutate AA 21-24 to alanine	tgtggagcgagccagctcggctgcgtgcgcctcctgcttgaaccagaagagcaa
Block ASM forward 2	Mutate AA 25-28 to alanine (not cysteine)	aggcagtacagattgctcttctgggcccgcgcaggcgaagcacatcagcgagctggct
Block ASM reverse 2	Mutate AA 25-28 to alanine (not cysteine)	agccagctcgtgatgtgcttcgcctgcgcggcccagaagagcaatctgtactgcct
Block ASM forward 3	Mutate AA 29-32 to alanine	ggcttcaggcagtacagattgctcgcgcggcccgcgcaggagaagcacatcagcgca
Block ASM reverse 3	Mutate AA 29-32 to alanine	tcgctgatgtgcttctcctgcgcggcccgcgcaggcaatctgtactgcctgaagcc
Block ASM forward 4	Mutate AA 33-36 to alanine (not cysteine)	tcggagcagatggtcggcttcgcgcaggccgcattgctcttctggtcaagcagga

Block ASM reverse 4	Mutate AA 33-36 to alanine (not cysteine)	tcctgcttgaaccagaagagcaatgaggcctgagcgaagccgaccatctgctccga
Block ASM forward 5	Mutate AA 37-40 to alanine	gtagttgtcctggtcggagcagggcgccgccaggcagtacagattgcttct
Block ASM reverse 5	Mutate AA 37-40 to alanine	agaagagcaatctgtactgctggcgggcgccgctgctccgaccaggacaactac
Block ASM forward 6	Mutate AA 41-44 to alanine (not cysteine)	gacacagtcacgcagtagttgtccggcgggcgagatggtcggcttcaggcagta
Block ASM reverse 6	Mutate AA 41-44 to alanine (not cysteine)	tactgctgaagccgaccatctgcccggcggaactactgctgactgtgtc
Block ASM forward 7	Mutate AA 45-48 to alanine (not cysteine)	ggcactagcagacacagtcacgcagggcgggcctggtcggagcagatggtcg
Block ASM reverse 7	Mutate AA 45-48 to alanine (not cysteine)	cgaccatctgctccgaccaggccggcctgctgactgtgtctgctagtgcc
Block ASM forward 8	Mutate AA 49-52 to alanine	attcccaatgccggcactagcagccgcagccgcagtagttgtcctggtcgga
Block ASM reverse 8	Mutate AA 49-52 to alanine	tccgaccaggacaactactgcgcggtgaggctgctagtgccggcattgggaat
Block ASM forward 9	Mutate AA 53-56 to alanine	gccaaatgtcacgagattcccaatggcggcagcagcagacacagtcacgcagtagttgtc
Block ASM reverse 9	Mutate AA 53-56 to alanine	gacaactactgctgactgtgtctgctgctgccgcatgggaatctcgtgacattggc
Block ASM forward 10	Mutate AA 57-60 to alanine	caggctgtggccaaatgtcacggcagccgcagcggcgactagcagacaca
Block ASM reverse 10	Mutate AA 57-60 to alanine	tgtgtctgctagtccggcgctgaggctgccgtgacattggccacagcctg
Block ASM forward 11	Mutate AA 61-64 to alanine	acaggtcttctcaggctgtggcagctgccgcgagattcccaatgccggcacta
Block ASM reverse 11	Mutate AA 61-64 to alanine	tagtgccggcattgggaatctcggcgagctgccacagcctgagcaagacctgt
Block ASM forward 12	Mutate AA 65-68 to alanine	aggccggggaacaggtcttggccggcgggcgccaaatgtcacgagattcccaat
Block ASM reverse 12	Mutate AA 65-68 to alanine	attgggaatctcgtgacattggcgccggcgcccaagacctgttccccggcct
Block ASM forward 13	Mutate AA 69-72 to alanine (not cysteine)	ggatggggcagggcggggcacaggccgctcaggctgtggccaaatgtc

Block ASM reverse 13	Mutate AA 69-72 to alanine (not cysteine)	gacatttgccacagcctgagcgcggcctgtgccccggcctgccccatcc
Block ASM forward 14	Mutate AA 73-76 to alanine (not cysteine)	ccaacattgacgccttctgggatggcgcaggccgcggaacaggcttctgctcaggct
Block ASM reverse 14	Mutate AA 73-76 to alanine (not cysteine)	agcctgagcaagacctgttccgcggcctgcgccatcccagaaggcgtcaatgttg
Block ASM forward 15	Mutate AA 77-80 to alanine	atggaagccacaccaacattgacggctgctgcggcggggcaggccggggaa
Block ASM reverse 15	Mutate AA 77-80 to alanine	ttccccggcctgccccgccgcagcagccgtcaatgttggtgtggcttccat
Block ASM forward 16	Mutate AA 81-84 to alanine	ctgatgccccatggaagccacagcagcagcggcgccttctgggatggggcag
Block ASM reverse 16	Mutate AA 81-84 to alanine	ctgccccatcccagaaggcggcgtgctgctgtggcttccatgggcatcag
Block ASM forward 17	Mutate AA 85-88 to alanine	tctggcagcagctgatgcccgcggcagccgcaccaacattgacgccttctgggat
Block ASM reverse 17	Mutate AA 85-88 to alanine	atcccagaaggcgtcaatgttggtgcggctgccgcgggcatcagctgctgccaga
Block ASM forward 18	Mutate 89-92 to alanine (not cysteine)	gaaattgcacagaaagctctggcagcaggcggcggccatggaagccacaccaacattga
Block ASM reverse 18	Mutate 89-92 to alanine (not cysteine)	tcaatgttggtgtggcttccatggccgccgctgctgccagagcttctgtgcaatttc
Block ASM forward 19	Mutate 93-96 to alanine (not cysteine)	atggccgactgaaattgcacagagcggccgcgcagcagctgatgccccatggaa g
Block ASM reverse 19	Mutate 93-96 to alanine (not cysteine)	cttccatgggcatcagctgctgcggccgctctgtgcaatttcagtgccggccgat
Block ASM forward 20	Mutate 97-100 to alanine (not cysteine)	agcccccatcgccgcagcggcattgcacgcaaagctctggcagcagctgatg
Block ASM reverse 20	Mutate 97-100 to alanine (not cysteine)	catcagctgctgccagagcttgcgtgcaatgccgctgcggccgatggcgggct
Point ASM forward 1	Mutate L33 to alanine (L33A)	ggagcagatggtcggctcaggcagctacgcattgctcttctggtcaagc
Point ASM reverse 1	Mutate L33 to alanine (L33A)	gcttgaaccagaagagcaatgcgtactgctgaagccgaccatctgctcc

Point ASM forward 2	Mutate L36 to alanine (L36A)	gagcagatggtcggcttcgcgcagtacagattgctcttctgg
Point ASM reverse 2	Mutate L36 to alanine (L36A)	ccagaagagcaatctgtactgcgcgaagccgaccatctgctc
Point ASM forward 3	Mutate G56 to alanine (G56A)	tcacgagattcccaatggcggcactagcagacacagtcacgcagt
Point ASM reverse 3	Mutate G56 to alanine (G56A)	actgcgtgactgtgtctgctagtgccgccattgggaatctcgtga
Point ASM forward 4	Mutate I57 to alanine (I57A)	gccaaatgtcacgagattccccgcgccggcactagcagac
Point ASM reverse 4	Mutate I57 to alanine (I57A)	gtctgctagtgccggcgcggggaatctcgtgacatttggc
Point ASM forward 5	Mutate G58 to alanine (G58A)	gccaaatgtcacgagattcgaatgccggcactagcagacacagtc
Point ASM reverse 5	Mutate G58 to alanine (G58A)	gactgtgtctgctagtgccggcattgcgaatctcgtgacatttggc
Point ASM forward 6	Mutate N59 to alanine (N59A)	gccaaatgtcacgagcgcaccaatgccggcactagcagac
Point ASM reverse 6	Mutate N59 to alanine (N59A)	gtctgctagtgccggcattggggcgctcgtgacatttggc
Point ASM forward 7	Mutate L60 to alanine (L60A)	ctgtggccaaatgtcaccgattcccaatgccggcactagcagac
Point ASM reverse 7	Mutate L60 to alanine (L60A)	gtctgctagtgccggcattgggaatgcggtgacatttggccacag
Point ASM forward 8	Mutate F63 to alanine (F63A)	ctcaggctgtggcccgtgtcacgagattcccaatgcc
Point ASM reverse 8	Mutate F63 to alanine (F63A)	ggcattgggaatctcgtgacagcgggccacagcctgag
Point ASM forward 9	Mutate G64 to alanine (G64A)	ggaacaggcttctgctcaggctgtgcgcaaatgtcacgagattccc
Point ASM reverse 9	Mutate G64 to alanine (G64A)	gggaatctcgtgacatttgcgcacagcctgagcaagacctgtcc

BIBLIOGRAPHY

- Abram, C. L., G. L. Roberge, Y. Hu, and C. A. Lowell. 2014. 'Comparative analysis of the efficiency and specificity of myeloid-Cre deleting strains using ROSA-EYFP reporter mice', *J Immunol Methods*, 408: 89-100.
- Agac, D., L. D. Estrada, R. Maples, L. V. Hooper, and J. D. Farrar. 2018. 'The beta2-adrenergic receptor controls inflammation by driving rapid IL-10 secretion', *Brain Behav Immun*, 74: 176-85.
- Aihara, Y., H. J. Buhring, M. Aihara, and J. Klein. 1986. 'An attempt to produce "pre-T" cell hybridomas and to identify their antigens', *Eur J Immunol*, 16: 1391-9.
- Allen, E. K., A. G. Randolph, T. Bhangale, P. Dogra, M. Ohlson, C. M. Oshansky, A. E. Zamora, J. P. Shannon, D. Finkelstein, A. Dressen, J. DeVincenzo, M. Caniza, B. Youngblood, C. M. Rosenberger, and P. G. Thomas. 2017. 'SNP-mediated disruption of CTCF binding at the IFITM3 promoter is associated with risk of severe influenza in humans', *Nat Med*, 23: 975-83.
- Allen, I. C., C. B. Moore, M. Schneider, Y. Lei, B. K. Davis, M. A. Scull, D. Gris, K. E. Roney, A. G. Zimmermann, J. B. Bowzard, P. Ranjan, K. M. Monroe, R. J. Pickles, S. Sambhara, and J. P. Ting. 2011. 'NLRX1 protein attenuates inflammatory responses to infection by interfering with the RIG-I-MAVS and TRAF6-NF-kappaB signaling pathways', *Immunity*, 34: 854-65.
- Andres-Terre, M., H. M. McGuire, Y. Pouliot, E. Bongen, T. E. Sweeney, C. M. Tato, and P. Khatri. 2015. 'Integrated, Multi-cohort Analysis Identifies Conserved Transcriptional Signatures across Multiple Respiratory Viruses', *Immunity*, 43: 1199-211.
- Antica, M., L. Wu, and R. Scollay. 1997. 'Stem cell antigen 2 expression in adult and developing mice', *Immunol Lett*, 55: 47-51.
- Aza-Blanc, P., C. L. Cooper, K. Wagner, S. Batalov, Q. L. Deveraux, and M. P. Cooke. 2003. 'Identification of modulators of TRAIL-induced apoptosis via RNAi-based phenotypic screening', *Mol Cell*, 12: 627-37.
- Bacquin, A., C. Bireau, M. Tanguy, C. Romanet, C. Vernochet, A. Dupressoir, and T. Heidmann. 2017. 'A Cell Fusion-Based Screening Method Identifies Glycosylphosphatidylinositol-Anchored Protein Ly6e as the Receptor for Mouse Endogenous Retroviral Envelope Syncytin-A', *J Virol*, 91.
- Bailey, C. C., G. Zhong, I. C. Huang, and M. Farzan. 2014. 'IFITM-Family Proteins: The Cell's First Line of Antiviral Defense', *Annu Rev Virol*, 1: 261-83.
- Balish, A. L., J. M. Katz, and A. I. Klimov. 2013. 'Influenza: propagation, quantification, and storage', *Curr Protoc Microbiol*, Chapter 15: Unit 15G 1.
- Banerjee, I., Y. Yamauchi, A. Helenius, and P. Horvath. 2013. 'High-content analysis of sequential events during the early phase of influenza A virus infection', *PLoS One*, 8: e68450.
- Barrows, N. J., C. Le Sommer, M. A. Garcia-Blanco, and J. L. Pearson. 2010. 'Factors affecting reproducibility between genome-scale siRNA-based screens', *J Biomol Screen*, 15: 735-47.

- Beigneux, A. P., B. S. Davies, P. Gin, M. M. Weinstein, E. Farber, X. Qiao, F. Peale, S. Bunting, R. L. Walzem, J. S. Wong, W. S. Blaner, Z. M. Ding, K. Melford, N. Wongsiriroj, X. Shu, F. de Sauvage, R. O. Ryan, L. G. Fong, A. Bensadoun, and S. G. Young. 2007. 'Glycosylphosphatidylinositol-anchored high-density lipoprotein-binding protein 1 plays a critical role in the lipolytic processing of chylomicrons', *Cell Metab*, 5: 279-91.
- Beigneux, A. P., B. S. Davies, S. Tat, J. Chen, P. Gin, C. V. Voss, M. M. Weinstein, A. Bensadoun, C. R. Pullinger, L. G. Fong, and S. G. Young. 2011. 'Assessing the role of the glycosylphosphatidylinositol-anchored high density lipoprotein-binding protein 1 (GPIHBP1) three-finger domain in binding lipoprotein lipase', *J Biol Chem*, 286: 19735-43.
- Beigneux, A. P., L. G. Fong, A. Bensadoun, B. S. Davies, M. Oberer, H. Gardsvoll, M. Ploug, and S. G. Young. 2015. 'GPIHBP1 missense mutations often cause multimerization of GPIHBP1 and thereby prevent lipoprotein lipase binding', *Circ Res*, 116: 624-32.
- Beigneux, A. P., K. Miyashita, M. Ploug, D. J. Blom, M. Ai, M. F. Linton, W. Khovidhunkit, R. Dufour, A. Garg, M. A. McMahon, C. R. Pullinger, N. P. Sandoval, X. Hu, C. M. Allan, M. Larsson, T. Machida, M. Murakami, K. Reue, P. Tontonoz, I. J. Goldberg, P. Moulin, S. Charriere, L. G. Fong, K. Nakajima, and S. G. Young. 2017. 'Autoantibodies against GPIHBP1 as a Cause of Hypertriglyceridemia', *N Engl J Med*, 376: 1647-58.
- Benitez, A. A., M. Panis, J. Xue, A. Varble, J. V. Shim, A. L. Frick, C. B. Lopez, D. Sachs, and B. R. tenOever. 2015. 'In Vivo RNAi Screening Identifies MDA5 as a Significant Contributor to the Cellular Defense against Influenza A Virus', *Cell Rep*, 11: 1714-26.
- Berns, K., E. M. Hijmans, J. Mullenders, T. R. Brummelkamp, A. Velds, M. Heimerikx, R. M. Kerkhoven, M. Madiredjo, W. Nijkamp, B. Weigelt, R. Agami, W. Ge, G. Cavet, P. S. Linsley, R. L. Beijersbergen, and R. Bernards. 2004. 'A large-scale RNAi screen in human cells identifies new components of the p53 pathway', *Nature*, 428: 431-7.
- Berzins, S. P., G. M. Davey, E. S. Randle-Barrett, M. A. Malin, B. J. Classon, S. Fraser, and R. L. Boyd. 1999. 'Thymic shared antigen-2: a novel cell surface marker associated with T cell differentiation and activation', *J Immunol*, 162: 5119-26.
- Bhattacharyya, S., A. Zagorska, E. D. Lew, B. Shrestha, C. V. Rothlin, J. Naughton, M. S. Diamond, G. Lemke, and J. A. Young. 2013. 'Enveloped viruses disable innate immune responses in dendritic cells by direct activation of TAM receptors', *Cell Host Microbe*, 14: 136-47.
- Biasini, M., S. Bienert, A. Waterhouse, K. Arnold, G. Studer, T. Schmidt, F. Kiefer, T. Gallo Cassarino, M. Bertoni, L. Bordoli, and T. Schwede. 2014. 'SWISS-MODEL: modelling protein tertiary and quaternary structure using evolutionary information', *Nucleic Acids Res*, 42: W252-8.
- Blasi, F., and P. Carmeliet. 2002. 'uPAR: a versatile signalling orchestrator', *Nat Rev Mol Cell Biol*, 3: 932-43.

- Brass, A. L., I. C. Huang, Y. Benita, S. P. John, M. N. Krishnan, E. M. Feeley, B. J. Ryan, J. L. Weyer, L. van der Weyden, E. Fikrig, D. J. Adams, R. J. Xavier, M. Farzan, and S. J. Elledge. 2009. 'The IFITM proteins mediate cellular resistance to influenza A H1N1 virus, West Nile virus, and dengue virus', *Cell*, 139: 1243-54.
- Bredenbeek, P. J., E. A. Kooi, B. Lindenbach, N. Huijkman, C. M. Rice, and W. J. Spaan. 2003. 'A stable full-length yellow fever virus cDNA clone and the role of conserved RNA elements in flavivirus replication', *J Gen Virol*, 84: 1261-8.
- Bult, C. J., J. T. Eppig, J. A. Kadin, J. E. Richardson, J. A. Blake, and Group Mouse Genome Database. 2008. 'The Mouse Genome Database (MGD): mouse biology and model systems', *Nucleic Acids Res*, 36: D724-8.
- Bushman, F. D., N. Malani, J. Fernandes, I. D'Orso, G. Cagney, T. L. Diamond, H. Zhou, D. J. Hazuda, A. S. Espeseth, R. Konig, S. Bandyopadhyay, T. Ideker, S. P. Goff, N. J. Krogan, A. D. Frankel, J. A. Young, and S. K. Chanda. 2009. 'Host cell factors in HIV replication: meta-analysis of genome-wide studies', *PLoS Pathog*, 5: e1000437.
- Cai, X., J. Chen, H. Xu, S. Liu, Q. X. Jiang, R. Halfmann, and Z. J. Chen. 2014. 'Prion-like polymerization underlies signal transduction in antiviral immune defense and inflammasome activation', *Cell*, 156: 1207-22.
- Capone, M. C., D. M. Gorman, E. P. Ching, and A. Zlotnik. 1996. 'Identification through bioinformatics of cDNAs encoding human thymic shared Ag-1/stem cell Ag-2. A new member of the human Ly-6 family', *J Immunol*, 157: 969-73.
- Cardani, A., A. Boulton, T. S. Kim, and T. J. Braciale. 2017. 'Alveolar Macrophages Prevent Lethal Influenza Pneumonia By Inhibiting Infection Of Type-1 Alveolar Epithelial Cells', *PLoS Pathog*, 13: e1006140.
- Casrouge, A., S. Y. Zhang, C. Eidenschenk, E. Jouanguy, A. Puel, K. Yang, A. Alcais, C. Picard, N. Mahfoufi, N. Nicolas, L. Lorenzo, S. Plancoulaine, B. Senechal, F. Geissmann, K. Tabeta, K. Hoebe, X. Du, R. L. Miller, B. Heron, C. Mignot, T. B. de Villemeur, P. Lebon, O. Dulac, F. Rozenberg, B. Beutler, M. Tardieu, L. Abel, and J. L. Casanova. 2006. 'Herpes simplex virus encephalitis in human UNC-93B deficiency', *Science*, 314: 308-12.
- Cervantes-Barragan, L., U. Kalinke, R. Zust, M. Konig, B. Reizis, C. Lopez-Macias, V. Thiel, and B. Ludewig. 2009. 'Type I IFN-mediated protection of macrophages and dendritic cells secures control of murine coronavirus infection', *J Immunol*, 182: 1099-106.
- Chang, C. P., T. Husler, J. Zhao, T. Wiedmer, and P. J. Sims. 1994. 'Identity of a peptide domain of human C9 that is bound by the cell-surface complement inhibitor, CD59', *J Biol Chem*, 269: 26424-30.
- Charriere, S., N. Peretti, S. Bernard, M. Di Filippo, A. Sassolas, M. Merlin, M. Delay, C. Debard, E. Lefai, A. Lachaux, P. Moulin, and C. Marcais. 2011. 'GPIHBP1 C89F neomutation and hydrophobic C-terminal domain G175R mutation in two pedigrees with severe hyperchylomicronemia', *J Clin Endocrinol Metab*, 96: E1675-9.

- Chaurasiya, K. R., M. J. McCauley, W. Wang, D. F. Qualley, T. Wu, S. Kitamura, H. Geertsema, D. S. Chan, A. Hertz, Y. Iwatani, J. G. Levin, K. Musier-Forsyth, I. Rouzina, and M. C. Williams. 2014. 'Oligomerization transforms human APOBEC3G from an efficient enzyme to a slowly dissociating nucleic acid-binding protein', *Nat Chem*, 6: 28-33.
- Chavez-Santoscoy, A. V., L. M. Huntimer, A. E. Ramer-Tait, M. Wannemuehler, and B. Narasimhan. 2012. 'Harvesting murine alveolar macrophages and evaluating cellular activation induced by polyanhydride nanoparticles', *J Vis Exp*: e3883.
- Chemudupati, M., A. D. Kenney, S. Bonifati, A. Zani, T. M. McMichael, L. Wu, and J. S. Yount. 2018. 'From APOBEC to ZAP: Diverse mechanisms used by cellular restriction factors to inhibit virus infections', *Biochim Biophys Acta Mol Cell Res*.
- Chen, S., N. E. Sanjana, K. Zheng, O. Shalem, K. Lee, X. Shi, D. A. Scott, J. Song, J. Q. Pan, R. Weissleder, H. Lee, F. Zhang, and P. A. Sharp. 2015. 'Genome-wide CRISPR Screen in a Mouse Model of Tumor Growth and Metastasis', *Cell*, 160: 1246-60.
- Choi, S. J., R. D. Devlin, C. Menea, H. Chung, G. D. Roodman, and S. V. Reddy. 1998. 'Cloning and identification of human Sca as a novel inhibitor of osteoclast formation and bone resorption', *J Clin Invest*, 102: 1360-8.
- Chow, K. T., M. Gale, Jr., and Y. M. Loo. 2018. 'RIG-I and Other RNA Sensors in Antiviral Immunity', *Annu Rev Immunol*, 36: 667-94.
- Chung, H., J. J. A. Calis, X. Wu, T. Sun, Y. Yu, S. L. Sarbanes, V. L. Dao Thi, A. R. Shilvock, H. H. Hoffmann, B. R. Rosenberg, and C. M. Rice. 2018. 'Human ADAR1 Prevents Endogenous RNA from Triggering Translational Shutdown', *Cell*, 172: 811-24 e14.
- Ciancanelli, M. J., S. X. Huang, P. Luthra, H. Garner, Y. Itan, S. Volpi, F. G. Lafaille, C. Trouillet, M. Schmolke, R. A. Albrecht, E. Israelsson, H. K. Lim, M. Casadio, T. Hermesh, L. Lorenzo, L. W. Leung, V. Pedergnana, B. Boisson, S. Okada, C. Picard, B. Ringuier, F. Troussier, D. Chaussabel, L. Abel, I. Pellier, L. D. Notarangelo, A. Garcia-Sastre, C. F. Basler, F. Geissmann, S. Y. Zhang, H. W. Snoeck, and J. L. Casanova. 2015. 'Infectious disease. Life-threatening influenza and impaired interferon amplification in human IRF7 deficiency', *Science*, 348: 448-53.
- Classon, B. J., and L. Coverdale. 1994. 'Mouse stem cell antigen Sca-2 is a member of the Ly-6 family of cell surface proteins', *Proc Natl Acad Sci U S A*, 91: 5296-300.
- Coca-Prieto, I., O. Kroupa, P. Gonzalez-Santos, J. Magne, G. Olivecrona, E. Ehrenborg, and P. Valdivielso. 2011. 'Childhood-onset chylomicronaemia with reduced plasma lipoprotein lipase activity and mass: identification of a novel GPIHBP1 mutation', *J Intern Med*, 270: 224-8.
- Corman, V. M., D. Muth, D. Niemeyer, and C. Drosten. 2018. 'Hosts and Sources of Endemic Human Coronaviruses', *Adv Virus Res*, 100: 163-88.
- Dash, P. K., A. Boutonnier, E. Prina, S. Sharma, and P. Reiter. 2012. 'Development of a SYBR green I based RT-PCR assay for yellow fever virus: application in assessment of YFV infection in *Aedes aegypti*', *Virol J*, 9: 27.

- Davies, A., D. L. Simmons, G. Hale, R. A. Harrison, H. Tighe, P. J. Lachmann, and H. Waldmann. 1989. 'CD59, an LY-6-like protein expressed in human lymphoid cells, regulates the action of the complement membrane attack complex on homologous cells', *J Exp Med*, 170: 637-54.
- de Vries, E., D. M. Tscherne, M. J. Wienholts, V. Cobos-Jimenez, F. Scholte, A. Garcia-Sastre, P. J. Rottier, and C. A. de Haan. 2011. 'Dissection of the influenza A virus endocytic routes reveals macropinocytosis as an alternative entry pathway', *PLoS Pathog*, 7: e1001329.
- Ding, L., and E. M. Shevach. 2001. 'Inhibition of the function of the FcγRIIB by a monoclonal antibody to thymic shared antigen-1, a Ly-6 family antigen', *Immunology*, 104: 28-36.
- Dittmann, M., H. H. Hoffmann, M. A. Scull, R. H. Gilmore, K. L. Bell, M. Ciancanelli, S. J. Wilson, S. Crotta, Y. Yu, B. Flatley, J. W. Xiao, J. L. Casanova, A. Wack, P. D. Bieniasz, and C. M. Rice. 2015. 'A serpin shapes the extracellular environment to prevent influenza A virus maturation', *Cell*, 160: 631-43.
- Donelan, N. R., C. F. Basler, and A. Garcia-Sastre. 2003. 'A recombinant influenza A virus expressing an RNA-binding-defective NS1 protein induces high levels of beta interferon and is attenuated in mice', *J Virol*, 77: 13257-66.
- Duncan, C. J., S. M. Mohamad, D. F. Young, A. J. Skelton, T. R. Leahy, D. C. Munday, K. M. Butler, S. Morfopoulou, J. R. Brown, M. Hubank, J. Connell, P. J. Gavin, C. McMahon, E. Dempsey, N. E. Lynch, T. S. Jacques, M. Valappil, A. J. Cant, J. Breuer, K. R. Engelhardt, R. E. Randall, and S. Hambleton. 2015. 'Human IFNAR2 deficiency: Lessons for antiviral immunity', *Sci Transl Med*, 7: 307ra154.
- Dupuis, S., E. Jouanguy, S. Al-Hajjar, C. Fieschi, I. Z. Al-Mohsen, S. Al-Jumaah, K. Yang, A. Chappier, C. Eidenschenk, P. Eid, A. Al Ghoniaim, H. Tufenkeji, H. Frayha, S. Al-Gazlan, H. Al-Rayes, R. D. Schreiber, I. Gresser, and J. L. Casanova. 2003. 'Impaired response to interferon-alpha/beta and lethal viral disease in human STAT1 deficiency', *Nat Genet*, 33: 388-91.
- Edgar, R. C. 2004. 'MUSCLE: multiple sequence alignment with high accuracy and high throughput', *Nucleic Acids Res*, 32: 1792-7.
- Everitt, A. R., S. Clare, T. Pertel, S. P. John, R. S. Wash, S. E. Smith, C. R. Chin, E. M. Feeley, J. S. Sims, D. J. Adams, H. M. Wise, L. Kane, D. Goulding, P. Digard, V. Anttila, J. K. Baillie, T. S. Walsh, D. A. Hume, A. Palotie, Y. Xue, V. Colonna, C. Tyler-Smith, J. Dunning, S. B. Gordon, Isis Investigators Gen, Mosaic Investigators, R. L. Smyth, P. J. Openshaw, G. Dougan, A. L. Brass, and P. Kellam. 2012. 'IFITM3 restricts the morbidity and mortality associated with influenza', *Nature*, 484: 519-23.
- Farley, F. W., P. Soriano, L. S. Steffen, and S. M. Dymecki. 2000. 'Widespread recombinase expression using FLP_{eR} (flipper) mice', *Genesis*, 28: 106-10.
- Fazioli, F., M. Resnati, N. Sidenius, Y. Higashimoto, E. Appella, and F. Blasi. 1997. 'A urokinase-sensitive region of the human urokinase receptor is responsible for its chemotactic activity', *EMBO J*, 16: 7279-86.

- Ferguson, M. A. J., G. W. Hart, and T. Kinoshita. 2015. 'Glycosylphosphatidylinositol Anchors.' in rd, A. Varki, R. D. Cummings, J. D. Esko, P. Stanley, G. W. Hart, M. Aebi, A. G. Darvill, T. Kinoshita, N. H. Packer, J. H. Prestegard, R. L. Schnaar and P. H. Seeberger (eds.), *Essentials of Glycobiology* (Cold Spring Harbor (NY)).
- Fire, A., S. Xu, M. K. Montgomery, S. A. Kostas, S. E. Driver, and C. C. Mello. 1998. 'Potent and specific genetic interference by double-stranded RNA in *Caenorhabditis elegans*', *Nature*, 391: 806-11.
- Franzolin, E., G. Pontarin, C. Rampazzo, C. Miazzi, P. Ferraro, E. Palumbo, P. Reichard, and V. Bianchi. 2013. 'The deoxynucleotide triphosphohydrolase SAMHD1 is a major regulator of DNA precursor pools in mammalian cells', *Proc Natl Acad Sci U S A*, 110: 14272-7.
- Fusco, D. N., C. Brisac, S. P. John, Y. W. Huang, C. R. Chin, T. Xie, H. Zhao, N. Jilg, L. Zhang, S. Chevaliez, D. Wambua, W. Lin, L. Peng, R. T. Chung, and A. L. Brass. 2013. 'A genetic screen identifies interferon-alpha effector genes required to suppress hepatitis C virus replication', *Gastroenterology*, 144: 1438-49, 49 e1-9.
- Galani, I. E., V. Triantafyllia, E. E. Eleminiadou, O. Koltsida, A. Stavropoulos, M. Manioudaki, D. Thanos, S. E. Doyle, S. V. Kotenko, K. Thanopoulou, and E. Andreakos. 2017. 'Interferon-lambda Mediates Non-redundant Front-Line Antiviral Protection against Influenza Virus Infection without Compromising Host Fitness', *Immunity*, 46: 875-90 e6.
- Galat, A., G. Gross, P. Drevet, A. Sato, and A. Menez. 2008. 'Conserved structural determinants in three-fingered protein domains', *FEBS J*, 275: 3207-25.
- Godfrey, D. I., M. Masciantonio, C. L. Tucek, M. A. Malin, R. L. Boyd, and P. Hugo. 1992. 'Thymic shared antigen-1. A novel thymocyte marker discriminating immature from mature thymocyte subsets', *J Immunol*, 148: 2006-11.
- Goldstone, D. C., V. Ennis-Adeniran, J. J. Hedden, H. C. Groom, G. I. Rice, E. Christodoulou, P. A. Walker, G. Kelly, L. F. Haire, M. W. Yap, L. P. de Carvalho, J. P. Stoye, Y. J. Crow, I. A. Taylor, and M. Webb. 2011. 'HIV-1 restriction factor SAMHD1 is a deoxynucleoside triphosphate triphosphohydrolase', *Nature*, 480: 379-82.
- Hackett, B. A., and S. Cherry. 2018. 'Flavivirus internalization is regulated by a size-dependent endocytic pathway', *Proc Natl Acad Sci U S A*, 115: 4246-51.
- Hackett, B. A., A. Yasunaga, D. Panda, M. A. Tartell, K. C. Hopkins, S. E. Hensley, and S. Cherry. 2015. 'RNASEK is required for internalization of diverse acid-dependent viruses', *Proc Natl Acad Sci U S A*, 112: 7797-802.
- Han, G. M., S. L. Chen, N. Shen, S. Ye, C. D. Bao, and Y. Y. Gu. 2003. 'Analysis of gene expression profiles in human systemic lupus erythematosus using oligonucleotide microarray', *Genes Immun*, 4: 177-86.
- Han, J., J. T. Perez, C. Chen, Y. Li, A. Benitez, M. Kandasamy, Y. Lee, J. Andrade, B. tenOever, and B. Manicassamy. 2018. 'Genome-wide CRISPR/Cas9 Screen Identifies Host Factors Essential for Influenza Virus Replication', *Cell Rep*, 23: 596-607.

- Hanners, N. W., J. L. Eitson, N. Usui, R. B. Richardson, E. M. Wexler, G. Konopka, and J. W. Schoggins. 2016. 'Western Zika Virus in Human Fetal Neural Progenitors Persists Long Term with Partial Cytopathic and Limited Immunogenic Effects', *Cell Rep*.
- Heaton, B. E., E. M. Kennedy, R. E. Dumm, A. T. Harding, M. T. Sacco, D. Sachs, and N. S. Heaton. 2017. 'A CRISPR Activation Screen Identifies a Pan-avian Influenza Virus Inhibitory Host Factor', *Cell Rep*, 20: 1503-12.
- Helbig, K. J., and M. R. Beard. 2014. 'The role of viperin in the innate antiviral response', *J Mol Biol*, 426: 1210-9.
- Helft, J., J. Bottcher, P. Chakravarty, S. Zelenay, J. Huotari, B. U. Schraml, D. Goubau, and C. Reis e Sousa. 2015. 'GM-CSF Mouse Bone Marrow Cultures Comprise a Heterogeneous Population of CD11c(+)MHCII(+) Macrophages and Dendritic Cells', *Immunity*, 42: 1197-211.
- Hoffmann, H. H., A. Kunz, V. A. Simon, P. Palese, and M. L. Shaw. 2011. 'Broad-spectrum antiviral that interferes with de novo pyrimidine biosynthesis', *Proc Natl Acad Sci U S A*, 108: 5777-82.
- Hong, M., S. I. Yoon, and I. A. Wilson. 2012. 'Structure and functional characterization of the RNA-binding element of the NLRX1 innate immune modulator', *Immunity*, 36: 337-47.
- Hou, F., L. Sun, H. Zheng, B. Skaug, Q. X. Jiang, and Z. J. Chen. 2011. 'MAVS forms functional prion-like aggregates to activate and propagate antiviral innate immune response', *Cell*, 146: 448-61.
- Hrecka, K., C. Hao, M. Gierszewska, S. K. Swanson, M. Kesik-Brodacka, S. Srivastava, L. Florens, M. P. Washburn, and J. Skowronski. 2011. 'Vpx relieves inhibition of HIV-1 infection of macrophages mediated by the SAMHD1 protein', *Nature*, 474: 658-61.
- Hufford, M. M., T. S. Kim, J. Sun, and T. J. Braciale. 2015. 'The effector T cell response to influenza infection', *Curr Top Microbiol Immunol*, 386: 423-55.
- Hutchinson, Edward, and Ervin Fodor. 2014. 'Purification of influenza virions by haemadsorption and ultracentrifugation'.
- Ibanez-Tallon, I., J. M. Miwa, H. L. Wang, N. C. Adams, G. W. Crabtree, S. M. Sine, and N. Heintz. 2002. 'Novel modulation of neuronal nicotinic acetylcholine receptors by association with the endogenous prototoxin lynx1', *Neuron*, 33: 893-903.
- Ibanez-Tallon, I., H. Wen, J. M. Miwa, J. Xing, A. B. Tekinay, F. Ono, P. Brehm, and N. Heintz. 2004. 'Tethering naturally occurring peptide toxins for cell-autonomous modulation of ion channels and receptors in vivo', *Neuron*, 43: 305-11.
- Iwasaki, A., and P. S. Pillai. 2014. 'Innate immunity to influenza virus infection', *Nat Rev Immunol*, 14: 315-28.
- Iwatani, Y., D. S. Chan, F. Wang, K. S. Maynard, W. Sugiura, A. M. Gronenborn, I. Rouzina, M. C. Williams, K. Musier-Forsyth, and J. G. Levin. 2007. 'Deaminase-independent inhibition of HIV-1 reverse transcription by APOBEC3G', *Nucleic Acids Res*, 35: 7096-108.

- Jhingran, A., S. Kasahara, and T. M. Hohl. 2016. 'Flow Cytometry of Lung and Bronchoalveolar Lavage Fluid Cells from Mice Challenged with Fluorescent Aspergillus Reporter (FLARE) Conidia', *Bio Protoc*, 6.
- Jiang, M., S. Zhang, Z. Yang, H. Lin, J. Zhu, L. Liu, W. Wang, S. Liu, W. Liu, Y. Ma, L. Zhang, and X. Cao. 2018. 'Self-Recognition of an Inducible Host lncRNA by RIG-I Feedback Restricts Innate Immune Response', *Cell*, 173: 906-19 e13.
- Jones, C. T., M. T. Catanese, L. M. Law, S. R. Khetani, A. J. Syder, A. Ploss, T. S. Oh, J. W. Schoggins, M. R. MacDonald, S. N. Bhatia, and C. M. Rice. 2010. 'Real-time imaging of hepatitis C virus infection using a fluorescent cell-based reporter system', *Nat Biotechnol*, 28: 167-71.
- Jones, C. T., C. G. Patkar, and R. J. Kuhn. 2005. 'Construction and applications of yellow fever virus replicons', *Virology*, 331: 247-59.
- Jones, D. T., W. R. Taylor, and J. M. Thornton. 1992. 'The rapid generation of mutation data matrices from protein sequences', *Comput Appl Biosci*, 8: 275-82.
- Kane, M., T. M. Zang, S. J. Rihn, F. Zhang, T. Kueck, M. Alim, J. Schoggins, C. M. Rice, S. J. Wilson, and P. D. Bieniasz. 2016. 'Identification of Interferon-Stimulated Genes with Antiretroviral Activity', *Cell Host Microbe*, 20: 392-405.
- Karlas, A., N. Machuy, Y. Shin, K. P. Pleissner, A. Artarini, D. Heuer, D. Becker, H. Khalil, L. A. Ogilvie, S. Hess, A. P. Maurer, E. Muller, T. Wolff, T. Rudel, and T. F. Meyer. 2010. 'Genome-wide RNAi screen identifies human host factors crucial for influenza virus replication', *Nature*, 463: 818-22.
- Khodadoust, M. M., K. D. Khan, and A. L. Bothwell. 1999. 'Complex regulation of Ly-6E gene transcription in T cells by IFNs', *J Immunol*, 163: 811-9.
- Khodadoust, M. M., K. D. Khan, E. H. Park, and A. L. Bothwell. 1998. 'Distinct regulatory mechanisms for interferon-alpha/beta (IFN-alpha/beta)- and IFN-gamma-mediated induction of Ly-6E gene in B cells', *Blood*, 92: 2399-409.
- Kim, H. M., Y. M. Kang, K. B. Ku, E. H. Park, J. Yum, J. C. Kim, S. Y. Jin, J. S. Lee, H. S. Kim, and S. H. Seo. 2013. 'The severe pathogenicity of alveolar macrophage-depleted ferrets infected with 2009 pandemic H1N1 influenza virus', *Virology*, 444: 394-403.
- Kim, H. M., Y. W. Lee, K. J. Lee, H. S. Kim, S. W. Cho, N. van Rooijen, Y. Guan, and S. H. Seo. 2008. 'Alveolar macrophages are indispensable for controlling influenza viruses in lungs of pigs', *J Virol*, 82: 4265-74.
- Kjaergaard, M., L. V. Hansen, B. Jacobsen, H. Gardsvoll, and M. Ploug. 2008. 'Structure and ligand interactions of the urokinase receptor (uPAR)', *Front Biosci*, 13: 5441-61.
- Kobayashi, M., A. Takaori-Kondo, Y. Miyauchi, K. Iwai, and T. Uchiyama. 2005. 'Ubiquitination of APOBEC3G by an HIV-1 Vif-Cullin5-Elongin B-Elongin C complex is essential for Vif function', *J Biol Chem*, 280: 18573-8.
- Koh, K., W. J. Joiner, M. N. Wu, Z. Yue, C. J. Smith, and A. Sehgal. 2008. 'Identification of SLEEPLESS, a sleep-promoting factor', *Science*, 321: 372-6.
- Koide, M., H. Maeda, J. L. Roccisana, N. Kawanabe, and S. V. Reddy. 2003. 'CytokineRegulation and the signaling mechanism of osteoclast inhibitory

- peptide-1 (OIP-1/hSca) to inhibit osteoclast formation', *J Bone Miner Res*, 18: 458-65.
- Konermann, S., M. D. Brigham, A. E. Trevino, J. Joung, O. O. Abudayyeh, C. Barcena, P. D. Hsu, N. Habib, J. S. Gootenberg, H. Nishimasu, O. Nureki, and F. Zhang. 2015. 'Genome-scale transcriptional activation by an engineered CRISPR-Cas9 complex', *Nature*, 517: 583-8.
- Konig, R., S. Stertz, Y. Zhou, A. Inoue, H. H. Hoffmann, S. Bhattacharyya, J. G. Alamares, D. M. Tscherne, M. B. Ortigoza, Y. Liang, Q. Gao, S. E. Andrews, S. Bandyopadhyay, P. De Jesus, B. P. Tu, L. Pache, C. Shih, A. Orth, G. Bonamy, L. Miraglia, T. Ideker, A. Garcia-Sastre, J. A. Young, P. Palese, M. L. Shaw, and S. K. Chanda. 2010. 'Human host factors required for influenza virus replication', *Nature*, 463: 813-7.
- Korty, P. E., C. Brando, and E. M. Shevach. 1991. 'CD59 functions as a signal-transducing molecule for human T cell activation', *J Immunol*, 146: 4092-8.
- Kosugi, A., S. Saitoh, S. Narumiya, K. Miyake, and T. Hamaoka. 1994. 'Activation-induced expression of thymic shared antigen-1 on T lymphocytes and its inhibitory role for TCR-mediated IL-2 production', *Int Immunol*, 6: 1967-76.
- Kosugi, A., S. Saitoh, S. Noda, K. Miyake, Y. Yamashita, M. Kimoto, M. Ogata, and T. Hamaoka. 1998. 'Physical and functional association between thymic shared antigen-1/stem cell antigen-2 and the T cell receptor complex', *J Biol Chem*, 273: 12301-6.
- Krishnan, M. N., A. Ng, B. Sukumaran, F. D. Gilfoy, P. D. Uchil, H. Sultana, A. L. Brass, R. Adametz, M. Tsui, F. Qian, R. R. Montgomery, S. Lev, P. W. Mason, R. A. Koski, S. J. Elledge, R. J. Xavier, H. Agaisse, and E. Fikrig. 2008. 'RNA interference screen for human genes associated with West Nile virus infection', *Nature*, 455: 242-5.
- Kristianto, J., M. G. Johnson, R. K. Zastrow, A. B. Radcliff, and R. D. Blank. 2017. 'Spontaneous recombinase activity of Cre-ERT2 in vivo', *Transgenic Res*, 26: 411-17.
- Kumar, S., G. Stecher, and K. Tamura. 2016. 'MEGA7: Molecular Evolutionary Genetics Analysis Version 7.0 for Bigger Datasets', *Mol Biol Evol*, 33: 1870-4.
- Laguet, N., B. Sobhian, N. Casartelli, M. Ringeard, C. Chable-Bessia, E. Segeal, A. Yatim, S. Emiliani, O. Schwartz, and M. Benkirane. 2011. 'SAMHD1 is the dendritic- and myeloid-cell-specific HIV-1 restriction factor counteracted by Vpx', *Nature*, 474: 654-7.
- Laidlaw, B. J., V. Decman, M. A. Ali, M. C. Abt, A. I. Wolf, L. A. Monticelli, K. Mozdzanowska, J. M. Angelosanto, D. Artis, J. Erikson, and E. J. Wherry. 2013. 'Cooperativity between CD8+ T cells, non-neutralizing antibodies, and alveolar macrophages is important for heterosubtypic influenza virus immunity', *PLoS Pathog*, 9: e1003207.
- Lakadamyali, M., M. J. Rust, and X. Zhuang. 2004. 'Endocytosis of influenza viruses', *Microbes Infect*, 6: 929-36.

- Lanford, R. E., E. S. Hildebrandt-Eriksen, A. Petri, R. Persson, M. Lindow, M. E. Munk, S. Kauppinen, and H. Orum. 2010. 'Therapeutic silencing of microRNA-122 in primates with chronic hepatitis C virus infection', *Science*, 327: 198-201.
- Langford, M. B., J. E. Outhwaite, M. Hughes, D. R. C. Natale, and D. G. Simmons. 2018. 'Deletion of the Syncytin A receptor Ly6e impairs syncytiotrophoblast fusion and placental morphogenesis causing embryonic lethality in mice', *Sci Rep*, 8: 3961.
- Law, R. H., D. Abu-Ssaydeh, and J. C. Whisstock. 2013. 'New insights into the structure and function of the plasminogen/plasmin system', *Curr Opin Struct Biol*, 23: 836-41.
- Lecossier, D., F. Bouchonnet, F. Clavel, and A. J. Hance. 2003. 'Hypermutation of HIV-1 DNA in the absence of the Vif protein', *Science*, 300: 1112.
- Lee, P. Y., J. X. Wang, E. Parisini, C. C. Dascher, and P. A. Nigrovic. 2013. 'Ly6 family proteins in neutrophil biology', *J Leukoc Biol*, 94: 585-94.
- Lepiller, Q., E. Soulier, Q. Li, M. Lambotin, J. Barths, D. Fuchs, F. Stoll-Keller, T. J. Liang, and H. Barth. 2015. 'Antiviral and Immunoregulatory Effects of Indoleamine-2,3-Dioxygenase in Hepatitis C Virus Infection', *J Innate Immun*, 7: 530-44.
- Li, J., S. C. Ding, H. Cho, B. C. Chung, M. Gale, Jr., S. K. Chanda, and M. S. Diamond. 2013. 'A short hairpin RNA screen of interferon-stimulated genes identifies a novel negative regulator of the cellular antiviral response', *MBio*, 4: e00385-13.
- Li, J., L. Hu, Y. Liu, L. Huang, Y. Mu, X. Cai, and C. Weng. 2015. 'DDX19A Senses Viral RNA and Mediates NLRP3-Dependent Inflammasome Activation', *J Immunol*, 195: 5732-49.
- Liddicoat, B. J., R. Piskol, A. M. Chalk, G. Ramaswami, M. Higuchi, J. C. Hartner, J. B. Li, P. H. Seeburg, and C. R. Walkley. 2015. 'RNA editing by ADAR1 prevents MDA5 sensing of endogenous dsRNA as nonself', *Science*, 349: 1115-20.
- Lindenbach, B. D., and C. M. Rice. 1997. 'trans-Complementation of yellow fever virus NS1 reveals a role in early RNA replication', *J Virol*, 71: 9608-17.
- Liu, H. C., M. Niikura, J. E. Fulton, and H. H. Cheng. 2003. 'Identification of chicken lymphocyte antigen 6 complex, locus E (LY6E, alias SCA2) as a putative Marek's disease resistance gene via a virus-host protein interaction screen', *Cytogenet Genome Res*, 102: 304-8.
- Liu, S., J. Chen, X. Cai, J. Wu, X. Chen, Y. T. Wu, L. Sun, and Z. J. Chen. 2013. 'MAVS recruits multiple ubiquitin E3 ligases to activate antiviral signaling cascades', *Elife*, 2: e00785.
- Liu, S. Y., D. J. Sanchez, R. Aliyari, S. Lu, and G. Cheng. 2012. 'Systematic identification of type I and type II interferon-induced antiviral factors', *Proc Natl Acad Sci U S A*, 109: 4239-44.
- Llinas, P., M. H. Le Du, H. Gardsvoll, K. Dano, M. Ploug, B. Gilquin, E. A. Stura, and A. Menez. 2005. 'Crystal structure of the human urokinase plasminogen activator receptor bound to an antagonist peptide', *EMBO J*, 24: 1655-63.

- Loeuillet, C., S. Deutsch, A. Ciuffi, D. Robyr, P. Taffe, M. Munoz, J. S. Beckmann, S. E. Antonarakis, and A. Telenti. 2008. 'In vitro whole-genome analysis identifies a susceptibility locus for HIV-1', *PLoS Biol*, 6: e32.
- Loughner, C. L., E. A. Bruford, M. S. McAndrews, E. E. Delp, S. Swamynathan, and S. K. Swamynathan. 2016. 'Organization, evolution and functions of the human and mouse Ly6/uPAR family genes', *Hum Genomics*, 10: 10.
- Lyukmanova, E. N., M. A. Shulepko, S. L. Buldakova, I. E. Kasheverov, Z. O. Shenkarev, R. V. Reshetnikov, S. Y. Filkin, D. S. Kudryavtsev, L. O. Ojomoko, E. V. Kryukova, D. A. Dolgikh, M. P. Kirpichnikov, P. D. Bregestovski, and V. I. Tsetlin. 2013. 'Water-soluble LYNX1 residues important for interaction with muscle-type and/or neuronal nicotinic receptors', *J Biol Chem*, 288: 15888-99.
- Ma, H., Y. Dang, Y. Wu, G. Jia, E. Anaya, J. Zhang, S. Abraham, J. G. Choi, G. Shi, L. Qi, N. Manjunath, and H. Wu. 2015. 'A CRISPR-Based Screen Identifies Genes Essential for West-Nile-Virus-Induced Cell Death', *Cell Rep*, 12: 673-83.
- Ma, H., P. Han, W. Ye, H. Chen, X. Zheng, L. Cheng, L. Zhang, L. Yu, X. Wu, Z. Xu, Y. Lei, and F. Zhang. 2017. 'The Long Noncoding RNA NEAT1 Exerts Antihantaviral Effects by Acting as Positive Feedback for RIG-I Signaling', *J Virol*, 91.
- MacNeil, I., J. Kennedy, D. I. Godfrey, N. A. Jenkins, M. Masciantonio, C. Mineo, D. J. Gilbert, N. G. Copeland, R. L. Boyd, and A. Zlotnik. 1993. 'Isolation of a cDNA encoding thymic shared antigen-1. A new member of the Ly6 family with a possible role in T cell development', *J Immunol*, 151: 6913-23.
- Maglott, D., J. Ostell, K. D. Pruitt, and T. Tatusova. 2011. 'Entrez Gene: gene-centered information at NCBI', *Nucleic Acids Res*, 39: D52-7.
- Manicassamy, B., S. Manicassamy, A. Belicha-Villanueva, G. Pisanelli, B. Pulendran, and A. Garcia-Sastre. 2010. 'Analysis of in vivo dynamics of influenza virus infection in mice using a GFP reporter virus', *Proc Natl Acad Sci U S A*, 107: 11531-6.
- Mao, M., M. Yu, J. H. Tong, J. Ye, J. Zhu, Q. H. Huang, G. Fu, L. Yu, S. Y. Zhao, S. Waxman, M. Lanotte, Z. Y. Wang, J. Z. Tan, S. J. Chan, and Z. Chen. 1996. 'RIG-E, a human homolog of the murine Ly-6 family, is induced by retinoic acid during the differentiation of acute promyelocytic leukemia cell', *Proc Natl Acad Sci U S A*, 93: 5910-4.
- Mao, R., J. Zhang, D. Jiang, D. Cai, J. M. Levy, A. Cuconati, T. M. Block, J. T. Guo, and H. Guo. 2011. 'Indoleamine 2,3-dioxygenase mediates the antiviral effect of gamma interferon against hepatitis B virus in human hepatocyte-derived cells', *J Virol*, 85: 1048-57.
- Mao, W., H. D. Hunt, and H. H. Cheng. 2010. 'Cloning and functional characterization of chicken stem cell antigen 2', *Dev Comp Immunol*, 34: 360-8.
- Mar, Katrina B., Nicholas R. Rinkenberger, Ian N. Boys, Jennifer L. Eitson, Matthew B. McDougal, R. Blake Richardson, and John W. Schoggins. 2018. 'LY6E mediates an evolutionarily conserved enhancement of virus infection by targeting a late entry step', *Nature Communications*, 9: 3603.

- Marceau, C. D., A. S. Puschnik, K. Majzoub, Y. S. Ooi, S. M. Brewer, G. Fuchs, K. Swaminathan, M. A. Mata, J. E. Elias, P. Sarnow, and J. E. Carette. 2016. 'Genetic dissection of Flaviviridae host factors through genome-scale CRISPR screens', *Nature*, 535: 159-63.
- Martin, K., and A. Helenius. 1991. 'Transport of incoming influenza virus nucleocapsids into the nucleus', *J Virol*, 65: 232-44.
- McKenzie, I. F., J. Gardiner, M. Cherry, and G. D. Snell. 1977. 'Lymphocyte antigens: Ly-4, Ly-6, and Ly-7', *Transplant Proc*, 9: 667-9.
- McNab, F., K. Mayer-Barber, A. Sher, A. Wack, and A. O'Garra. 2015. 'Type I interferons in infectious disease', *Nat Rev Immunol*, 15: 87-103.
- Meertens, L., X. Carnec, M. P. Lecoin, R. Ramdasi, F. Guivel-Benhassine, E. Lew, G. Lemke, O. Schwartz, and A. Amara. 2012. 'The TIM and TAM families of phosphatidylserine receptors mediate dengue virus entry', *Cell Host Microbe*, 12: 544-57.
- Meri, S., B. P. Morgan, A. Davies, R. H. Daniels, M. G. Olavesen, H. Waldmann, and P. J. Lachmann. 1990. 'Human protectin (CD59), an 18,000-20,000 MW complement lysis restricting factor, inhibits C5b-8 catalysed insertion of C9 into lipid bilayers', *Immunology*, 71: 1-9.
- Mitchell, R. S., C. Katsura, M. A. Skasko, K. Fitzpatrick, D. Lau, A. Ruiz, E. B. Stephens, F. Margottin-Goguet, R. Benarous, and J. C. Guatelli. 2009. 'Vpu antagonizes BST-2-mediated restriction of HIV-1 release via beta-TrCP and endo-lysosomal trafficking', *PLoS Pathog*, 5: e1000450.
- Miwa, J. M., I. Ibanez-Tallon, G. W. Crabtree, R. Sanchez, A. Sali, L. W. Role, and N. Heintz. 1999. 'lynx1, an endogenous toxin-like modulator of nicotinic acetylcholine receptors in the mammalian CNS', *Neuron*, 23: 105-14.
- Miwa, J. M., T. R. Stevens, S. L. King, B. J. Caldarone, I. Ibanez-Tallon, C. Xiao, R. M. Fitzsimonds, C. Pavlides, H. A. Lester, M. R. Picciotto, and N. Heintz. 2006. 'The prototoxin lynx1 acts on nicotinic acetylcholine receptors to balance neuronal activity and survival in vivo', *Neuron*, 51: 587-600.
- Moffat, J., D. A. Grueneberg, X. Yang, S. Y. Kim, A. M. Kloepper, G. Hinkle, B. Piqani, T. M. Eisenhaure, B. Luo, J. K. Grenier, A. E. Carpenter, S. Y. Foo, S. A. Stewart, B. R. Stockwell, N. Hacohen, W. C. Hahn, E. S. Lander, D. M. Sabatini, and D. E. Root. 2006. 'A lentiviral RNAi library for human and mouse genes applied to an arrayed viral high-content screen', *Cell*, 124: 1283-98.
- Morchikh, M., A. Cribier, R. Raffel, S. Amraoui, J. Cau, D. Severac, E. Dubois, O. Schwartz, Y. Bennasser, and M. Benkirane. 2017. 'HEXIM1 and NEAT1 Long Non-coding RNA Form a Multi-subunit Complex that Regulates DNA-Mediated Innate Immune Response', *Mol Cell*, 67: 387-99 e5.
- Morizono, K., Y. Xie, T. Olafsen, B. Lee, A. Dasgupta, A. M. Wu, and I. S. Chen. 2011. 'The soluble serum protein Gas6 bridges virion envelope phosphatidylserine to the TAM receptor tyrosine kinase Axl to mediate viral entry', *Cell Host Microbe*, 9: 286-98.

- Neil, S. J., T. Zang, and P. D. Bieniasz. 2008. 'Tetherin inhibits retrovirus release and is antagonized by HIV-1 Vpu', *Nature*, 451: 425-30.
- Neufeldt, C. J., M. Cortese, E. G. Acosta, and R. Bartenschlager. 2018. 'Rewiring cellular networks by members of the Flaviviridae family', *Nat Rev Microbiol*, 16: 125-42.
- Noda, S., A. Kosugi, S. Saitoh, S. Narumiya, and T. Hamaoka. 1996. 'Protection from anti-TCR/CD3-induced apoptosis in immature thymocytes by a signal through thymic shared antigen-1/stem cell antigen-2', *J Exp Med*, 183: 2355-60.
- OhAinle, M., L. Helms, J. Vermeire, F. Roesch, D. Humes, R. Basom, J. J. Delrow, J. Overbaugh, and M. Emerman. 2018. 'A virus-packageable CRISPR screen identifies host factors mediating interferon inhibition of HIV', *Elife*, 7.
- Okumura, A., A. L. Rasmussen, P. Halfmann, F. Feldmann, A. Yoshimura, H. Feldmann, Y. Kawaoka, R. N. Harty, and M. G. Katze. 2015. 'Suppressor of Cytokine Signaling 3 Is an Inducible Host Factor That Regulates Virus Egress during Ebola Virus Infection', *J Virol*, 89: 10399-406.
- Okumura, R., T. Kurakawa, T. Nakano, H. Kayama, M. Kinoshita, D. Motooka, K. Gotoh, T. Kimura, N. Kamiyama, T. Kusu, Y. Ueda, H. Wu, H. Iijima, S. Barman, H. Osawa, H. Matsuno, J. Nishimura, Y. Ohba, S. Nakamura, T. Iida, M. Yamamoto, E. Umemoto, K. Sano, and K. Takeda. 2016. 'Lypd8 promotes the segregation of flagellated microbiota and colonic epithelia', *Nature*, 532: 117-21.
- Olivecrona, G., E. Ehrenborg, H. Semb, E. Makoveichuk, A. Lindberg, M. R. Hayden, P. Gin, B. S. Davies, M. M. Weinstein, L. G. Fong, A. P. Beigneux, S. G. Young, T. Olivecrona, and O. Hernell. 2010. 'Mutation of conserved cysteines in the Ly6 domain of GPIHBP1 in familial chylomicronemia', *J Lipid Res*, 51: 1535-45.
- Owczarek, K., A. Szczepanski, A. Milewska, Z. Baster, Z. Rajfur, M. Sarna, and K. Pyrc. 2018. 'Early events during human coronavirus OC43 entry to the cell', *Sci Rep*, 8: 7124.
- Pache, L., R. Konig, and S. K. Chanda. 2011. 'Identifying HIV-1 host cell factors by genome-scale RNAi screening', *Methods*, 53: 3-12.
- Paddison, P. J., J. M. Silva, D. S. Conklin, M. Schlabach, M. Li, S. Aruleba, V. Balija, A. O'Shaughnessy, L. Gnoj, K. Scobie, K. Chang, T. Westbrook, M. Cleary, R. Sachidanandam, W. R. McCombie, S. J. Elledge, and G. J. Hannon. 2004. 'A resource for large-scale RNA-interference-based screens in mammals', *Nature*, 428: 427-31.
- Pelkmans, L., E. Fava, H. Grabner, M. Hannus, B. Habermann, E. Krausz, and M. Zerial. 2005. 'Genome-wide analysis of human kinases in clathrin- and caveolae/raft-mediated endocytosis', *Nature*, 436: 78-86.
- Perez-Pinera, P., D. D. Kocak, C. M. Vockley, A. F. Adler, A. M. Kabadi, L. R. Polstein, P. I. Thakore, K. A. Glass, D. G. Ousterout, K. W. Leong, F. Guilak, G. E. Crawford, T. E. Reddy, and C. A. Gersbach. 2013. 'RNA-guided gene activation by CRISPR-Cas9-based transcription factors', *Nat Methods*, 10: 973-6.
- Pfaller, C. K., R. C. Donohue, S. Nersisyan, L. Brodsky, and R. Cattaneo. 2018. 'Extensive editing of cellular and viral double-stranded RNA structures accounts

- for innate immunity suppression and the proviral activity of ADAR1p150', *PLoS Biol*, 16: e2006577.
- Platt, R. J., S. Chen, Y. Zhou, M. J. Yim, L. Swiech, H. R. Kempton, J. E. Dahlman, O. Parnas, T. M. Eisenhaure, M. Jovanovic, D. B. Graham, S. Jhunjhunwala, M. Heidenreich, R. J. Xavier, R. Langer, D. G. Anderson, N. Hacohen, A. Regev, G. Feng, P. A. Sharp, and F. Zhang. 2014. 'CRISPR-Cas9 knockin mice for genome editing and cancer modeling', *Cell*, 159: 440-55.
- Pluck, A., and C. Klasen. 2009. 'Generation of chimeras by microinjection', *Methods Mol Biol*, 561: 199-217.
- Pujantell, M., E. Riveira-Munoz, R. Badia, M. Castellvi, E. Garcia-Vidal, G. Sirera, T. Puig, C. Ramirez, B. Clotet, J. A. Este, and E. Ballana. 2017. 'RNA editing by ADAR1 regulates innate and antiviral immune functions in primary macrophages', *Sci Rep*, 7: 13339.
- Purnama, C., S. L. Ng, P. Tetlak, Y. A. Setiagani, M. Kandasamy, S. Baalasubramanian, K. Karjalainen, and C. Ruedl. 2014. 'Transient ablation of alveolar macrophages leads to massive pathology of influenza infection without affecting cellular adaptive immunity', *Eur J Immunol*, 44: 2003-12.
- Qiu, L., T. Wang, Q. Tang, G. Li, P. Wu, and K. Chen. 2018. 'Long Non-coding RNAs: Regulators of Viral Infection and the Interferon Antiviral Response', *Front Microbiol*, 9: 1621.
- Randall, G., M. Panis, J. D. Cooper, T. L. Tellinghuisen, K. E. Sukhodolets, S. Pfeffer, M. Landthaler, P. Landgraf, S. Kan, B. D. Lindenbach, M. Chien, D. B. Weir, J. J. Russo, J. Ju, M. J. Brownstein, R. Sheridan, C. Sander, M. Zavolan, T. Tuschl, and C. M. Rice. 2007. 'Cellular cofactors affecting hepatitis C virus infection and replication', *Proc Natl Acad Sci U S A*, 104: 12884-9.
- Randle, E. S., G. A. Waanders, M. Masciantonio, D. I. Godfrey, and R. L. Boyd. 1993. 'A lymphostromal molecule, thymic shared Ag-1, regulates early thymocyte development in fetal thymus organ culture', *J Immunol*, 151: 6027-35.
- Richardson, R. B., M. B. Ohlson, J. L. Eitson, A. Kumar, M. B. McDougal, I. N. Boys, K. B. Mar, P. C. De La Cruz-Rivera, C. Douglas, G. Konopka, C. Xing, and J. W. Schoggins. 2018. 'A CRISPR screen identifies IFI6 as an ER-resident interferon effector that blocks flavivirus replication', *Nat Microbiol*, 3: 1214-23.
- Rinkenberger, N., and J. W. Schoggins. 2018. 'Mucolipin-2 Cation Channel Increases Trafficking Efficiency of Endocytosed Viruses', *MBio*, 9.
- Saitoh, S., A. Kosugi, S. Noda, N. Yamamoto, M. Ogata, Y. Minami, K. Miyake, and T. Hamaoka. 1995. 'Modulation of TCR-mediated signaling pathway by thymic shared antigen-1 (TSA-1)/stem cell antigen-2 (Sca-2)', *J Immunol*, 155: 5574-81.
- Sancho-Shimizu, V., R. Perez de Diego, E. Jouanguy, S. Y. Zhang, and J. L. Casanova. 2011. 'Inborn errors of anti-viral interferon immunity in humans', *Curr Opin Virol*, 1: 487-96.
- Sancho-Shimizu, V., R. Perez de Diego, L. Lorenzo, R. Halwani, A. Alangari, E. Israelsson, S. Fabrega, A. Cardon, J. Maluenda, M. Tatematsu, F. Mahvelati, M. Herman, M. Ciancanelli, Y. Guo, Z. AlSum, N. Alkhamis, A. S. Al-Makadma, A.

- Ghadiri, S. Boucherit, S. Plancoulaine, C. Picard, F. Rozenberg, M. Tardieu, P. Lebon, E. Jouanguy, N. Rezaei, T. Seya, M. Matsumoto, D. Chaussabel, A. Puel, S. Y. Zhang, L. Abel, S. Al-Muhsen, and J. L. Casanova. 2011. 'Herpes simplex encephalitis in children with autosomal recessive and dominant TRIF deficiency', *J Clin Invest*, 121: 4889-902.
- Sanjana, N. E., O. Shalem, and F. Zhang. 2014. 'Improved vectors and genome-wide libraries for CRISPR screening', *Nat Methods*, 11: 783-84.
- Savidis, G., W. M. McDougall, P. Meraner, J. M. Ferreira, J. M. Portmann, G. Trincucci, S. P. John, A. M. Aker, N. Renzette, D. R. Robbins, Z. Guo, S. Green, T. F. Kowalik, and A. L. Brass. 2016. 'Identification of Zika Virus and Dengue Virus Dependency Factors using Functional Genomics', *Cell Rep*, 16: 232-46.
- Schmid, E. T., I. K. Pang, E. A. Carrera Silva, L. Bosurgi, J. J. Miner, M. S. Diamond, A. Iwasaki, and C. V. Rothlin. 2016. 'AXL receptor tyrosine kinase is required for T cell priming and antiviral immunity', *Elife*, 5.
- Schneider, C., S. P. Nobs, A. K. Heer, M. Kurrer, G. Klinke, N. van Rooijen, J. Vogel, and M. Kopf. 2014. 'Alveolar macrophages are essential for protection from respiratory failure and associated morbidity following influenza virus infection', *PLoS Pathog*, 10: e1004053.
- Schneider, W. M., M. D. Chevillotte, and C. M. Rice. 2014. 'Interferon-stimulated genes: a complex web of host defenses', *Annu Rev Immunol*, 32: 513-45.
- Schoggins, J. W., M. Dorner, M. Feulner, N. Imanaka, M. Y. Murphy, A. Ploss, and C. M. Rice. 2012. 'Dengue reporter viruses reveal viral dynamics in interferon receptor-deficient mice and sensitivity to interferon effectors in vitro', *Proc Natl Acad Sci U S A*, 109: 14610-5.
- Schoggins, J. W., D. A. MacDuff, N. Imanaka, M. D. Gainey, B. Shrestha, J. L. Eitson, K. B. Mar, R. B. Richardson, A. V. Ratushny, V. Litvak, R. Dabelic, B. Manicassamy, J. D. Aitchison, A. Aderem, R. M. Elliott, A. Garcia-Sastre, V. Racaniello, E. J. Snijder, W. M. Yokoyama, M. S. Diamond, H. W. Virgin, and C. M. Rice. 2014. 'Pan-viral specificity of IFN-induced genes reveals new roles for cGAS in innate immunity', *Nature*, 505: 691-5.
- Schoggins, J. W., and C. M. Rice. 2011. 'Interferon-stimulated genes and their antiviral effector functions', *Curr Opin Virol*, 1: 519-25.
- Schoggins, J. W., S. J. Wilson, M. Panis, M. Y. Murphy, C. T. Jones, P. Bieniasz, and C. M. Rice. 2011. 'A diverse range of gene products are effectors of the type I interferon antiviral response', *Nature*, 472: 481-5.
- Schwartz, R. M., and M. O. Dayhoff. 1979. 'Protein and nucleic Acid sequence data and phylogeny', *Science*, 205: 1038-9.
- Seo, J. Y., R. Yaneva, E. R. Hinson, and P. Cresswell. 2011. 'Human cytomegalovirus directly induces the antiviral protein viperin to enhance infectivity', *Science*, 332: 1093-7.
- Shalem, O., N. E. Sanjana, E. Hartenian, X. Shi, D. A. Scott, T. Mikkelsen, D. Heckl, B. L. Ebert, D. E. Root, J. G. Doench, and F. Zhang. 2014. 'Genome-scale CRISPR-Cas9 knockout screening in human cells', *Science*, 343: 84-87.

- Shan, X., A. Bourdeau, A. Rhoton, D. E. Wells, E. H. Cohen, B. E. Landgraf, and R. G. Palfree. 1998. 'Characterization and mapping to human chromosome 8q24.3 of Ly-6-related gene 9804 encoding an apparent homologue of mouse TSA-1', *J Immunol*, 160: 197-208.
- Sharma, S., S. K. Patnaik, R. T. Taggart, E. D. Kannisto, S. M. Enriquez, P. Gollnick, and B. E. Baysal. 2015. 'APOBEC3A cytidine deaminase induces RNA editing in monocytes and macrophages', *Nat Commun*, 6: 6881.
- Shimojima, M., Y. Ikeda, and Y. Kawaoka. 2007. 'The mechanism of Axl-mediated Ebola virus infection', *J Infect Dis*, 196 Suppl 2: S259-63.
- Sievers, F., A. Wilm, D. Dineen, T. J. Gibson, K. Karplus, W. Li, R. Lopez, H. McWilliam, M. Remmert, J. Soding, J. D. Thompson, and D. G. Higgins. 2011. 'Fast, scalable generation of high-quality protein multiple sequence alignments using Clustal Omega', *Mol Syst Biol*, 7: 539.
- Silva, J. M., M. Z. Li, K. Chang, W. Ge, M. C. Golding, R. J. Rickles, D. Siolas, G. Hu, P. J. Paddison, M. R. Schlabach, N. Sheth, J. Bradshaw, J. Burchard, A. Kulkarni, G. Cavet, R. Sachidanandam, W. R. McCombie, M. A. Cleary, S. J. Elledge, and G. J. Hannon. 2005. 'Second-generation shRNA libraries covering the mouse and human genomes', *Nat Genet*, 37: 1281-8.
- Skarnes, W. C., B. Rosen, A. P. West, M. Koutsourakis, W. Bushell, V. Iyer, A. O. Mujica, M. Thomas, J. Harrow, T. Cox, D. Jackson, J. Severin, P. Biggs, J. Fu, M. Nefedov, P. J. de Jong, A. F. Stewart, and A. Bradley. 2011. 'A conditional knockout resource for the genome-wide study of mouse gene function', *Nature*, 474: 337-42.
- Smit, J. M., B. Moesker, I. Rodenhuis-Zybert, and J. Wilschut. 2011. 'Flavivirus cell entry and membrane fusion', *Viruses*, 3: 160-71.
- Smith, K. A., P. E. Baker, S. Gillis, and F. W. Ruscetti. 1980. 'Functional and molecular characteristics of T-cell growth factor', *Mol Immunol*, 17: 579-89.
- Spangrude, G. J., Y. Aihara, I. L. Weissman, and J. Klein. 1988. 'The stem cell antigens Sca-1 and Sca-2 subdivide thymic and peripheral T lymphocytes into unique subsets', *J Immunol*, 141: 3697-707.
- Sparrer, K. M., and M. U. Gack. 2015. 'Intracellular detection of viral nucleic acids', *Curr Opin Microbiol*, 26: 1-9.
- Spindler, K. R., A. R. Welton, E. S. Lim, S. Duvvuru, I. W. Althaus, J. E. Imperiale, A. I. Daoud, and E. J. Chesler. 2010. 'The major locus for mouse adenovirus susceptibility maps to genes of the hematopoietic cell surface-expressed LY6 family', *J Immunol*, 184: 3055-62.
- Stier, M. T., and K. R. Spindler. 2012. 'Polymorphisms in Ly6 genes in Msq1 encoding susceptibility to mouse adenovirus type 1', *Mamm Genome*, 23: 250-8.
- Stothard, P. 2000. 'The sequence manipulation suite: JavaScript programs for analyzing and formatting protein and DNA sequences', *Biotechniques*, 28: 1102, 04.
- Subramanian, G., T. Kuzmanovic, Y. Zhang, C. B. Peter, M. Veleparambil, R. Chakravarti, G. C. Sen, and S. Chattopadhyay. 2018. 'A new mechanism of interferon's antiviral action: Induction of autophagy, essential for paramyxovirus

- replication, is inhibited by the interferon stimulated gene, TDRD7', *PLoS Pathog*, 14: e1006877.
- Sun, L., J. Wu, F. Du, X. Chen, and Z. J. Chen. 2013. 'Cyclic GMP-AMP synthase is a cytosolic DNA sensor that activates the type I interferon pathway', *Science*, 339: 786-91.
- Suzuki, Y., W. X. Chin, Q. Han, K. Ichiyama, C. H. Lee, Z. W. Eyo, H. Ebina, H. Takahashi, C. Takahashi, B. H. Tan, T. Hishiki, K. Ohba, T. Matsuyama, Y. Koyanagi, Y. J. Tan, T. Sawasaki, J. J. Chu, S. G. Vasudevan, K. Sano, and N. Yamamoto. 2016. 'Characterization of RyDEN (C19orf66) as an Interferon-Stimulated Cellular Inhibitor against Dengue Virus Replication', *PLoS Pathog*, 12: e1005357.
- Taguwa, S., K. Maringer, X. Li, D. Bernal-Rubio, J. N. Rauch, J. E. Gestwicki, R. Andino, A. Fernandez-Sesma, and J. Frydman. 2015. 'Defining Hsp70 Subnetworks in Dengue Virus Replication Reveals Key Vulnerability in Flavivirus Infection', *Cell*, 163: 1108-23.
- Takaoka, A., Z. Wang, M. K. Choi, H. Yanai, H. Negishi, T. Ban, Y. Lu, M. Miyagishi, T. Kodama, K. Honda, Y. Ohba, and T. Taniguchi. 2007. 'DAI (DLM-1/ZBP1) is a cytosolic DNA sensor and an activator of innate immune response', *Nature*, 448: 501-5.
- Tang, N. L., P. K. Chan, C. K. Wong, K. F. To, A. K. Wu, Y. M. Sung, D. S. Hui, J. J. Sung, and C. W. Lam. 2005. 'Early enhanced expression of interferon-inducible protein-10 (CXCL-10) and other chemokines predicts adverse outcome in severe acute respiratory syndrome', *Clin Chem*, 51: 2333-40.
- Tekinay, A. B., Y. Nong, J. M. Miwa, I. Lieberam, I. Ibanez-Tallon, P. Greengard, and N. Heintz. 2009. 'A role for LYNX2 in anxiety-related behavior', *Proc Natl Acad Sci U S A*, 106: 4477-82.
- The UniProt, Consortium. 2018. 'UniProt: the universal protein knowledgebase', *Nucleic Acids Res*.
- Tobler, L. H., M. J. Cameron, M. C. Lanteri, H. E. Prince, A. Danesh, D. Persad, R. S. Lanciotti, P. J. Norris, D. J. Kelvin, and M. P. Busch. 2008. 'Interferon and interferon-induced chemokine expression is associated with control of acute viremia in West Nile virus-infected blood donors', *J Infect Dis*, 198: 979-83.
- Tripathi, S., M. O. Pohl, Y. Zhou, A. Rodriguez-Frandsen, G. Wang, D. A. Stein, H. M. Moulton, P. DeJesus, J. Che, L. C. Mulder, E. Yanguez, D. Andenmatten, L. Pache, B. Manicassamy, R. A. Albrecht, M. G. Gonzalez, Q. Nguyen, A. Brass, S. Elledge, M. White, S. Shapira, N. Hacohen, A. Karlas, T. F. Meyer, M. Shales, A. Gatorano, J. R. Johnson, G. Jang, T. Johnson, E. Verschueren, D. Sanders, N. Krogan, M. Shaw, R. Konig, S. Stertz, A. Garcia-Sastre, and S. K. Chanda. 2015. 'Meta- and Orthogonal Integration of Influenza "OMICs" Data Defines a Role for UBR4 in Virus Budding', *Cell Host Microbe*, 18: 723-35.
- Tsetlin, V. I. 2015. 'Three-finger snake neurotoxins and Ly6 proteins targeting nicotinic acetylcholine receptors: pharmacological tools and endogenous modulators', *Trends Pharmacol Sci*, 36: 109-23.

- Tumpey, T. M., A. Garcia-Sastre, J. K. Taubenberger, P. Palese, D. E. Swayne, M. J. Pantin-Jackwood, S. Schultz-Cherry, A. Solorzano, N. Van Rooijen, J. M. Katz, and C. F. Basler. 2005. 'Pathogenicity of influenza viruses with genes from the 1918 pandemic virus: functional roles of alveolar macrophages and neutrophils in limiting virus replication and mortality in mice', *J Virol*, 79: 14933-44.
- Unterholzner, L., S. E. Keating, M. Baran, K. A. Horan, S. B. Jensen, S. Sharma, C. M. Sirois, T. Jin, E. Latz, T. S. Xiao, K. A. Fitzgerald, S. R. Paludan, and A. G. Bowie. 2010. 'IFI16 is an innate immune sensor for intracellular DNA', *Nat Immunol*, 11: 997-1004.
- van Bragt, M. P., N. Ciliberti, W. L. Stanford, D. G. de Rooij, and A. M. van Pelt. 2005. 'LY6A/E (SCA-1) expression in the mouse testis', *Biol Reprod*, 73: 634-8.
- Van Damme, N., D. Goff, C. Katsura, R. L. Jorgenson, R. Mitchell, M. C. Johnson, E. B. Stephens, and J. Guatelli. 2008. 'The interferon-induced protein BST-2 restricts HIV-1 release and is downregulated from the cell surface by the viral Vpu protein', *Cell Host Microbe*, 3: 245-52.
- van der Ree, M. H., J. M. de Vree, F. Stelma, S. Willemse, M. van der Valk, S. Rietdijk, R. Molenkamp, J. Schinkel, A. C. van Nuenen, U. Beuers, S. Hadi, M. Harbers, E. van der Veer, K. Liu, J. Grundy, A. K. Patick, A. Pavlicek, J. Blem, M. Huang, P. Grint, S. Neben, N. W. Gibson, N. A. Kootstra, and H. W. Reesink. 2017. 'Safety, tolerability, and antiviral effect of RG-101 in patients with chronic hepatitis C: a phase 1B, double-blind, randomised controlled trial', *Lancet*, 389: 709-17.
- Varble, A., A. A. Benitez, S. Schmid, D. Sachs, J. V. Shim, R. Rodriguez-Barrueco, M. Panis, M. Crumiller, J. M. Silva, R. Sachidanandam, and B. R. tenOever. 2013. 'An in vivo RNAi screening approach to identify host determinants of virus replication', *Cell Host Microbe*, 14: 346-56.
- Waanders, G. A., D. I. Godfrey, and R. L. Boyd. 1989. 'Modulation of T-cell differentiation in murine fetal thymus organ cultures', *Thymus*, 13: 73-82.
- Wack, A., E. Terczynska-Dyla, and R. Hartmann. 2015. 'Guarding the frontiers: the biology of type III interferons', *Nat Immunol*, 16: 802-9.
- Waithman, J., D. Zanker, K. Xiao, S. Oveissi, B. Wylie, R. Ng, L. Togel, and W. Chen. 2013. 'Resident CD8(+) and migratory CD103(+) dendritic cells control CD8 T cell immunity during acute influenza infection', *PLoS One*, 8: e66136.
- Wakim, L. M., N. Gupta, J. D. Mintern, and J. A. Villadangos. 2013. 'Enhanced survival of lung tissue-resident memory CD8(+) T cells during infection with influenza virus due to selective expression of IFITM3', *Nat Immunol*, 14: 238-45.
- Wandrer, F., C. S. Falk, K. John, B. Skawran, M. P. Manns, K. Schulze-Osthoff, and H. Bantel. 2016. 'Interferon-Mediated Cytokine Induction Determines Sustained Virus Control in Chronic Hepatitis C Virus Infection', *J Infect Dis*, 213: 746-54.
- Wang, H., H. Yang, C. S. Shivalila, M. M. Dawlaty, A. W. Cheng, F. Zhang, and R. Jaenisch. 2013. 'One-step generation of mice carrying mutations in multiple genes by CRISPR/Cas-mediated genome engineering', *Cell*, 153: 910-8.
- Wang, L. N., M. H. Gao, B. Wang, B. B. Cong, and S. C. Zhang. 2018. 'A role for GPI-CD59 in promoting T-cell signal transduction via LAT', *Oncol Lett*, 15: 4873-81.

- Wang, P., S. Zhu, L. Yang, S. Cui, W. Pan, R. Jackson, Y. Zheng, A. Rongvaux, Q. Sun, G. Yang, S. Gao, R. Lin, F. You, R. Flavell, and E. Fikrig. 2015. 'Nlrp6 regulates intestinal antiviral innate immunity', *Science*, 350: 826-30.
- Wei, Y., M. Lukashev, D. I. Simon, S. C. Bodary, S. Rosenberg, M. V. Doyle, and H. A. Chapman. 1996. 'Regulation of integrin function by the urokinase receptor', *Science*, 273: 1551-5.
- Wei, Y., D. A. Waltz, N. Rao, R. J. Drummond, S. Rosenberg, and H. A. Chapman. 1994. 'Identification of the urokinase receptor as an adhesion receptor for vitronectin', *J Biol Chem*, 269: 32380-8.
- Weischenfeldt, J., and B. Porse. 2008. 'Bone Marrow-Derived Macrophages (BMM): Isolation and Applications', *CSH Protoc*, 2008: pdb prot5080.
- White, J. M., and G. R. Whittaker. 2016. 'Fusion of Enveloped Viruses in Endosomes', *Traffic*, 17: 593-614.
- Wu, J., L. Sun, X. Chen, F. Du, H. Shi, C. Chen, and Z. J. Chen. 2013. 'Cyclic GMP-AMP is an endogenous second messenger in innate immune signaling by cytosolic DNA', *Science*, 339: 826-30.
- Wu, L., M. Antica, G. R. Johnson, R. Scollay, and K. Shortman. 1991. 'Developmental potential of the earliest precursor cells from the adult mouse thymus', *J Exp Med*, 174: 1617-27.
- Wu, M. N., W. J. Joiner, T. Dean, Z. Yue, C. J. Smith, D. Chen, T. Hoshi, A. Sehgal, and K. Koh. 2010. 'SLEEPLESS, a Ly-6/neurotoxin family member, regulates the levels, localization and activity of Shaker', *Nat Neurosci*, 13: 69-75.
- Wu, M., C. A. Puddifoot, P. Taylor, and W. J. Joiner. 2015. 'Mechanisms of inhibition and potentiation of alpha4beta2 nicotinic acetylcholine receptors by members of the Ly6 protein family', *J Biol Chem*, 290: 24509-18.
- Wu, M., J. E. Robinson, and W. J. Joiner. 2014. 'SLEEPLESS is a bifunctional regulator of excitability and cholinergic synaptic transmission', *Curr Biol*, 24: 621-9.
- Xu, X., C. Qiu, L. Zhu, J. Huang, L. Li, W. Fu, L. Zhang, J. Wei, Y. Wang, Y. Geng, X. Zhang, W. Qiao, and J. Xu. 2014. 'IFN-stimulated gene LY6E in monocytes regulates the CD14/TLR4 pathway but inadequately restrains the hyperactivation of monocytes during chronic HIV-1 infection', *J Immunol*, 193: 4125-36.
- Yan, N., and Z. J. Chen. 2012. 'Intrinsic antiviral immunity', *Nat Immunol*, 13: 214-22.
- Yoshimura, A., T. Naka, and M. Kubo. 2007. 'SOCS proteins, cytokine signalling and immune regulation', *Nat Rev Immunol*, 7: 454-65.
- Yu, J., R. Abagyan, S. Dong, A. Gilbert, V. Nussenzweig, and S. Tomlinson. 1997. 'Mapping the active site of CD59', *J Exp Med*, 185: 745-53.
- Yu, J., C. Liang, and S. L. Liu. 2017. 'Interferon-inducible LY6E Protein Promotes HIV-1 Infection', *J Biol Chem*, 292: 4674-85.
- Yu, X., Y. Yu, B. Liu, K. Luo, W. Kong, P. Mao, and X. F. Yu. 2003. 'Induction of APOBEC3G ubiquitination and degradation by an HIV-1 Vif-Cul5-SCF complex', *Science*, 302: 1056-60.
- Zammit, D. J., S. P. Berzins, J. W. Gill, E. S. Randle-Barrett, L. Barnett, F. Koentgen, G. W. Lambert, R. P. Harvey, R. L. Boyd, and B. J. Classon. 2002. 'Essential role for

- the lymphostromal plasma membrane Ly-6 superfamily molecule thymic shared antigen 1 in development of the embryonic adrenal gland', *Mol Cell Biol*, 22: 946-52.
- Zamore, P. D. 2006. 'RNA interference: big applause for silencing in Stockholm', *Cell*, 127: 1083-6.
- Zhang, H., B. Yang, R. J. Pomerantz, C. Zhang, S. C. Arunachalam, and L. Gao. 2003. 'The cytidine deaminase CEM15 induces hypermutation in newly synthesized HIV-1 DNA', *Nature*, 424: 94-8.
- Zhang, R., J. J. Miner, M. J. Gorman, K. Rausch, H. Ramage, J. P. White, A. Zuiani, P. Zhang, E. Fernandez, Q. Zhang, K. A. Dowd, T. C. Pierson, S. Cherry, and M. S. Diamond. 2016. 'A CRISPR screen defines a signal peptide processing pathway required by flaviviruses', *Nature*, 535: 164-8.
- Zhang, S. Y., E. Jouanguy, S. Ugolini, A. Smahi, G. Elain, P. Romero, D. Segal, V. Sancho-Shimizu, L. Lorenzo, A. Puel, C. Picard, A. Chapgier, S. Plancoulaine, M. Titeux, C. Cognet, H. von Bernuth, C. L. Ku, A. Casrouge, X. X. Zhang, L. Barreiro, J. Leonard, C. Hamilton, P. Lebon, B. Heron, L. Vallee, L. Quintana-Murci, A. Hovnanian, F. Rozenberg, E. Vivier, F. Geissmann, M. Tardieu, L. Abel, and J. L. Casanova. 2007. 'TLR3 deficiency in patients with herpes simplex encephalitis', *Science*, 317: 1522-7.
- Zhang, Y. H., Y. Zhao, N. Li, Y. C. Peng, E. Giannoulatou, R. H. Jin, H. P. Yan, H. Wu, J. H. Liu, N. Liu, D. Y. Wang, Y. L. Shu, L. P. Ho, P. Kellam, A. McMichael, and T. Dong. 2013. 'Interferon-induced transmembrane protein-3 genetic variant rs12252-C is associated with severe influenza in Chinese individuals', *Nat Commun*, 4: 1418.
- Zhao, H., W. Lin, K. Kumthip, D. Cheng, D. N. Fusco, O. Hofmann, N. Jilg, A. W. Tai, K. Goto, L. Zhang, W. Hide, J. Y. Jang, L. F. Peng, and R. T. Chung. 2012. 'A functional genomic screen reveals novel host genes that mediate interferon-alpha's effects against hepatitis C virus', *J Hepatol*, 56: 326-33.
- Zhao, X., F. Guo, F. Liu, A. Cuconati, J. Chang, T. M. Block, and J. T. Guo. 2014. 'Interferon induction of IFITM proteins promotes infection by human coronavirus OC43', *Proc Natl Acad Sci U S A*, 111: 6756-61.
- Zhao, X., M. Sehgal, Z. Hou, J. Cheng, S. Shu, S. Wu, F. Guo, S. J. Le Marchand, H. Lin, J. Chang, and J. T. Guo. 2018. 'Identification of Residues Controlling Restriction versus Enhancing Activities of IFITM Proteins on Entry of Human Coronaviruses', *J Virol*, 92.
- Zhu, S., S. Ding, P. Wang, Z. Wei, W. Pan, N. W. Palm, Y. Yang, H. Yu, H. B. Li, G. Wang, X. Lei, M. R. de Zoete, J. Zhao, Y. Zheng, H. Chen, Y. Zhao, K. A. Jurado, N. Feng, L. Shan, Y. Kluger, J. Lu, C. Abraham, E. Fikrig, H. B. Greenberg, and R. A. Flavell. 2017. 'Nlrp9b inflammasome restricts rotavirus infection in intestinal epithelial cells', *Nature*, 546: 667-70.
- Zust, R., L. Cervantes-Barragan, T. Kuri, G. Blakqori, F. Weber, B. Ludewig, and V. Thiel. 2007. 'Coronavirus non-structural protein 1 is a major pathogenicity factor:

implications for the rational design of coronavirus vaccines', *PLoS Pathog*, 3: e109.